Model Order Reduction for Prediction of Turbine Engine Rotor Vibration Response in Presence of Parametric Uncertainties

Vladislav Ganine

Department of Electrical & Computer Engineering
McGill University
Montreal, Canada

February 2010

A thesis submitted to McGill University in partial fulfillment of the requirements for the Degree of Doctor of Philosophy.

Abstract

Statistical inhomogeneity of material properties, variations in nominal geometry, manufacturing tolerances, operational wear lead to uncertainties in the parameters associated with FE models of turbine engine rotors and consequently to uncertainties in their vibration response. Reliable assessment of the rotor system behavior cannot be made unless the effects of such uncertainties are understood and quantified. In practical situations the parametric probabilistic approach is the first choice to employ in that context yielding efficient algorithms with feasible implementations. A set of measured or estimated experimentally random parameters is repeatedly propagated through rotor models in Monte-Carlo simulations, which would pose a formidable computational task if the full order high-fidelity finite element (FE) models were utilized. The objective of this dissertation is to decrease the expense of analyzing systems modified in the parametric space by developing accurate model reduction computational techniques suitable for repeated analysis, in particular addressing the problem of large variations in nominal geometry. The first part of the dissertation is concerned with the structural blade mistuning problem. The existing projection based model order reduction techniques capable to numerically characterize variations in nominal geometry of periodic structures are examined, a method generating very compact reduced order models (ROM) based on correction, as opposed to expansion, of the modal subspace is selected and its limitations are analyzed. A new algorithm drawing on optimal preconditioned iterative methods for generalized eigenvalue problem is introduced to address its deficiencies. Both techniques are combined in a stochastic simulation framework to analyze the effect of random mistuning on geometrically modified bladed disks, where random parameter variation in blade properties is introduced in modal space at component level. A family of benchmark problems on an industrial scale bladed disk model are utilized in a comparative study assessing the amount of computational effort and storage, scalability and accuracy as well as providing insight on underlying physical phenomena. In the second part of dissertation a new computational technique is proposed focusing on prediction of the effects of uncertainty in rotor assembly inter-stage geometry on

global vibration response. The algorithm stands apart from the traditional modal projection based framework employing harmonic truncation only. It is shown that decent performance can be achieved due to reliance on sparse matrix linear algebra and sampling of small parametric space. Particular emphasis is given to the computational efficiency of ROM update. Accuracy and performance of the technique is illustrated with representative simulation examples over a practical range of geometrical parameter variations and operational conditions.

Abrégé

La prise en compte des effets des incertitudes est un élément fondamental pour une conception fiable des machines tournantes. Les inhomogénéités matérielles, les variations de géométrie, les tolérances de fabrication ou encore les phénomènes d'usure en service comptent parmi les nombreuses sources de variabilité des paramètres de modélisation qui conduisent, au niveau de la réponse dynamique des structures, à des incertitudes qu'il est nécessaire de quantifier.

En pratique, l'approche probabiliste paramétrique est souvent privilégiée pour sa facilité des mise en œuvre ainsi que pour l'efficacité des algorithmes utilisables. Dans le cadre de simulations de Monte-Carlo, qui consistent à évaluer de façon répétée un modèle en fonction d'un grand nombre de réalisations de paramètres aléatoires (déterminés expérimentalement ou estimés), les coûts de calcul peuvent s'avérer prohibitifs si des modèles éléments-finis de haute fidélité sont utilisés. L'objectif de cette thèse est de diminuer l'effort nécessaire à l'évaluation de la réponse de systèmes incertains en développant des techniques de réduction de modèles adaptées à des analyses répétées et permettant, en particulier, la prise en compte de grandes variations géométriques.

La première partie de cette dissertation concerne le problème du désaccordage structurel des roues aubagées. Les techniques existantes de réduction de modèles basées des projections qui permettent de caractériser les variations de géométrie de structures périodiques sont dans un premier temps revues. Une méthode amenant un modèle réduit très compact, basée sur la correction et non l'expansion du sous-espace modal est ensuite sélectionnée et ses limitations sont analysées. Un nouvel algorithme, inspiré des méthodes itératives de pré-conditionnement optimal pour les problèmes aux valeurs propres généralisés, est ensuite introduit pour palier ces insuffisances. Les deux techniques sont combinées dans le cadre de simulations stochastiques pour analyser les effets désaccordage aléatoire et de modifications géométriques pour les roues aubagées. Les variations aléatoires sont introduites en tant que paramètres des aubes dans l'espace modal. Une étude comparative est ensuite présentée en s'appuyant sur un modèle de taille industrielle. Les coûts de

calcul, les possibilités d'extension ou encore la précision des méthodes sont examinés et des aspects phénoménologiques sont discutés.

Dans la second partie de cette dissertation, une nouvelle approche numérique est proposée pour la quantification des effets d'incertitudes géométriques dans les assemblages inter-étages des rotors. L'algorithme se distingue des approches traditionnelles basées sur des projections en cela que seule une troncature harmonique est considérée. Des performances satisfaisantes peuvent être obtenues grâce à des opérations d'algèbre linéaire sur des matrices creuses ainsi qu'à l'échantillonnage d'un espace paramétrique minimal. En particulier, l'efficacité numérique de la mise à jour du modèle réduit sera mise en évidence. Enfin, la précision et le performance de cette méthode seront illustrées au moyen d'exemples représentatifs tant en termes de variations de paramètres géométriques que de conditions de fonctionnement.

Acknowledgments

I would like to express my gratitude to my first advisor, Prof. Christophe Pierre, for introducing me to a new exciting area and proposing the dissertation's topic. I would like to thank him for his invaluable support, for giving me outstanding academical freedom, providing interesting applications of my research and interaction with industry. Furthermore, I would like to thank Prof. Hannah Michalska, my second advisor. This dissertation would not be possible without her excellent research advice. My gratitude also goes to Professors Luc Mongeau and Michael Paidoussis, for serving on my examination committee and for their comments. I am grateful to my colleagues at Structural Dynamic and Vibration Lab. To Denis Laxalde for numerous great discussions and help, due to his patience and availability the majority of sentences in this dissertation contain verbs and articles. I owe thanks to Mathias Legrand, who lent his research expertise and who supplied lots of creativity and energy to my thesis working his magic with LaTeX. Shahram Tabandeh and Melita Hadzagic, my colleagues at CIM, deserve to be mentioned for their support and encouragement. Finally, I would like to acknowledge Pratt & Whitney Canada for their financial and technical support of the second part of this research.

Contents

List of Figures

List of Tables

List of Acronyms

BLAS	Basic Linear Algebra Subroutines
CMM	Component Mode Mistuning
DFT	Discrete Fourier Transform
DOD	Domestic Object Damage
DOF	Degree Of Freedom
EO	Engine Order
FE	Finite Element
FOD	Foreign Object Damage
FRF	Frequency Response Function
GMRES	Generalized Minimum Residual
IDFT	Inverse Discrete Fourier Transform
ILU	Incomplete LU
JD	Jacobi-Davidson
LU	Lower and Upper triangular matrix decomposition
MAM	Modal Acceleration Method
MAC	Modal Assurance Criterion
MC	Monte-Carlo
PDF	Probability Density Function
ROM	Reduced Order Model
SMC	Static Mode Compensation
SPAI	Sparse Approximate Inverse

Chapter 1

Introduction

1.1 Motivation

With the current trends towards increased operating speeds and lighter more, flexible structures the effects of uncertainty are of growing concern in the design of turbine engines. Practical experience suggests that even with very sophisticated and detailed numerical FE models the predicted results do not always coincide with experimental data due to unavoidable and inherent randomness of complex structural components. The ability to accurately account for all relevant physical effects that lead to variability in the vibration response implies increased safety, reliability, performance, "robustness" and cost-effectiveness of turbine engine designs which, in turns, minimize their life-cycle costs of development, manufacturing and maintenance. Hence there is a pressing need for more efficient and accurate predictive computational tools that allow the effects of random uncertainty to be included in the analysis.

The problems of uncertainty quantification are complicated by the underlying growth of modeling complexity: the models of high cost aerospace components are becoming larger and more complicated due to both the increased demand for complex components and desire for increased level of detail and accuracy. That complexity leads to higher analysis costs, typically, the order of system matrices easily exceeds 10^6 or even higher. Regardless of available computer resources, in order to analyze these large-scale linear dynamical systems, there is a need for reduced-order models

of much smaller size. It is obvious that such methods must approximate the behavior of the original model while preserving its important characteristics, at least for the frequency or time range of interest. An important issue is how a model order reduction algorithm can be welded into uncertainty quantification framework in such a way that the resulting ROM is valid and easily updatable over a range of uncertain parameters. Such problems cannot be solved efficiently with the existing general-purpose solvers, which calls for novel approaches. Fortunately, many techniques have become computationally feasible with the increasing computer power of parallel multi-core platforms and with the current state of the art linear algebra algorithms. Many benefits are to be gained from the exploitation of sparse and domain dependent structured problems, leading to reduced computational times, reduced storage requirements, improved accuracy of prediction, etc.

1.2 Uncertainty in structural analysis

Uncertainty is inherent in any analysis process. The errors of discretization in FE, non-linear interactions in linear models, inaccurate modeling of boundary conditions, uncertainties in loading, variability in structural properties and geometrical imperfections, are all aspects which contribute to the discrepancy between predicted and measured results. While *epistemic* uncertainties in mechanical modeling due to lack of knowledge are reducible by incorporating additional information compensating for insufficient modeling, *aleatory*, i.e., intrinsic physical uncertainties are irreducible and thus require rational treatment.

Uncertainties, either epistemic or aleatory, are commonly modeled within two somewhat conflicting views: *probabilistic* or *possibilistic*. In non-deterministic analysis with possibilistic view the uncertain properties are assumed to lie in certain ranges. Two approaches have dominated the current literature, interval analysis and fuzzy FE [1]. The methods are deemed to be appropriate when imprecise or rather vague information is available on system parameters, whereas the statistical data cannot be easily obtained or the uncertainty is not of random nature. However, the methods are criticized for being overly conservative and for not providing accu-

rate predictions at higher frequencies. Additionally, only academic models with very limited order and complexity have been reported.

Therefore, in most practical situations stochastic modeling techniques are applied, where the uncertainties variation in time and/or in space is described in terms of stochastic processes and/or random fields defined as follows.

Definition 1. *Let* $(\Theta, \mathfrak{F}, \mathbb{P})$ *be a complete probability space, where* Θ *is the sample space,* $\mathbb{P}$ *is the probability measure and* $\mathfrak{F}$ *is a* σ*-algebra associated with* Θ*. A random variable (resp. vector) is a mapping* $(\Theta, \mathfrak{F}, \mathbb{P}) \to \mathbb{R}^m$ *if* $m = 1$ *(resp.* $m > 1$*).*

Definition 2. *Let* $T \subseteq \mathbb{R}^n$ *be a set. A random field is defined as a mapping* $H(\boldsymbol{\theta}, \mathbf{u}) : \Theta \times T \to \mathbb{R}^m$ *such that* $H(\boldsymbol{\theta}, \mathbf{u})$ *is a random variable or a random vector for each* $u \in T$*. If* $n = 1$ *it is a random process, if* $n > 1$ *and* $m = 1$ *it is a scalar random field; for* $m > 1$ *it is a vector random field.*

Within the probabilistic modeling view one can distinguish parametric and non-parametric approaches, methods employing statistical Gaussian models and those based on non-Gaussian distributions [2]. The methods of computational stochastic mechanics employed for evaluating the global probabilistic structure of random response are based on stochastic FEM, i.e., solution of stochastic static or dynamic problems involving finite elements with random properties. Generally, the analysis involves the following basic steps:

- Modeling of random uncertainties.
- Propagation of the uncertainties through stochastic FEM.
  - Discretization of stochastic processes and fields.
  - Formulation of stochastic FE matrices.
  - Calculation of system response statistics.
- Postprocessing of the statistical results.

The starting point is the assignment of probability distribution to continuous spatially correlated random fluctuations in material or geometric properties. Normally, due to lack of relevant experimental measurement data assumptions must be made regarding the distribution choice; most common and convenient is the Gaussian distribution assumption. The next step begins with the discretization, i.e. approximation of a continuous random field with a finite set of random variables grouped in a random vector. The main issue is to define the the best approximation with respect to some estimation of error using the *minimal* number of random variables. Various discretization techniques are available in the literature, by and large they can be divided into three groups: point discretization, averaging, and series expansion.

The point discretization results in a discrete set of values of the stochastic field at specified points of the domain, whereas the averaging type methods yield weighted integrals of the stochastic field over each finite element. For illustration, we consider random variation in the elasticity modulus in a stiffness matrix. Applying weighted integral method, the elementary stiffness matrix can then be expressed as

$$\mathbf{K}^{(e)}(\theta) = \mathbf{K}_0^{(e)} + \int_{D^{(e)}} H(\theta, u)\mathbf{B}^T\mathbf{D}_0\mathbf{B}\mathrm{d}D^{(e)} \tag{1.1}$$

where $\mathbf{K}_0^{(e)}$ denotes the mean value of an elementary stiffness matrix, $\mathbf{B}$ is the matrix relating components of stress to the nodal displacements and $\mathbf{D}_0$ stands for the elasticity matrix. The difficulties in those approaches involve the choice of a stochastic mesh, that is mainly dictated by the variability of a random field. Often the correlation length does not correspond to the FE mesh defined by geometry leading to the usage of different meshes.

The series expansion represents a random field as a series involving random variables and deterministic spatial functions. Approximation is obtained as a truncation of the series. The most widely used is Karhunen-Loève expansion of a random field [2, 3, 4]. It is based on the spectral decomposition of the random field autocovariance function $C_{HH}(\mathbf{u}, \mathbf{u}') = \sigma(\mathbf{u})\sigma(\mathbf{u})\rho(\mathbf{u}, \mathbf{u}')$, where $\sigma(\mathbf{u})$ and $\rho(\mathbf{u}, \mathbf{u}')$ are the variance and the correlation function. The orthogonal deterministic functions are chosen as the eigenfunctions of the Fredholm integral equation with the autocovari-

ance function as the kernel

$$\int_D C_{HH}(\mathbf{u},\mathbf{u}')\phi_i(\mathbf{u}')\mathrm{d}D_{\mathbf{u}'} = \lambda_i\phi_i(\mathbf{u}) \tag{1.2}$$

where λ_i and ϕ_i are eigenvalues and eigenvectors of the autocovariance function $C_{HH}(\mathbf{u},\mathbf{u}')$. Any realization of a random field $H(\boldsymbol{\theta},\mathbf{u})$ can be expanded over this basis as follows

$$H(\boldsymbol{\theta},\mathbf{u}) = \mu(\mathbf{u}) + \sum_{i=1}^{M}\sqrt{\lambda_i}\xi_i(\theta)\phi_i(\mathbf{u}) \tag{1.3}$$

where $\mu(\mathbf{u})$ is the mean of the field, ξ_i is a set of uncorrelated random variables, M is the number of retained Karhunen-Loève terms. For strongly correlated random fields only a few terms corresponding to the M largest eigenvalues are required. Again employing the random elasticity modulus example, the stochastic elementary stiffness matrix becomes

$$\mathbf{K}^{(e)}(\theta) = \mathbf{K}_0^{(e)} + \mathbf{K}_i^{(e)}\xi_i(\theta) \tag{1.4}$$

where $\mathbf{K}_0^{(e)}$ is the mean value of $\mathbf{K}_i^{(e)}(\theta)$, and $\mathbf{K}_i^{(e)}$ are deterministic matrices defined as

$$\mathbf{K}_i^{(e)} = \sqrt{\lambda_i}\int_{D^{(e)}}\phi_i(\mathbf{u})\mathbf{B}^T\mathbf{D}_0\mathbf{B}dD_{\mathbf{u}}^{(e)} \tag{1.5}$$

Clearly, the method does not require a random field mesh and is by far more efficient in terms of the number of random variables required for a given accuracy. However, Karhunen-Loève series expansion are mainly valid for Gaussian random fields. The most serious of its drawbacks is the fact that the integral eigenvalue problem Eq. (1.2) has to be solved numerically, in most practical situations leading to very large scale dense problems.

In addition to Karhunen-Loève there are some other methods for series expansion of random fields, such as Optimal Linear Estimation or Polynomial Chaos Expansion. The interested reader is referred to [2, 3, 5] for a recent and detailed review of the methods and for a discussion of their applicability and shortcomings.

Upon assembly of the global random matrices the following discretized stochastic

equation of motion is obtained

$$\mathbf{M}(\boldsymbol{\theta})\ddot{\mathbf{x}}(\boldsymbol{\theta},t) + \mathbf{C}(\boldsymbol{\theta})\dot{\mathbf{x}}(\boldsymbol{\theta},t) + \mathbf{K}(\boldsymbol{\theta})\mathbf{x}(\boldsymbol{\theta},t) = \mathbf{f}(t) \tag{1.6}$$

Arguably, two of the most popular methods employed to assess the response variability within the stochastic FEM framework in current literature are perturbation methods and Monte-Carlo simulation. The perturbation based approach [6, 7, 8] involves first or second order Taylor series expansions of the response vector in terms of the basic input random parameters and application of standard stochastic operators to obtain the first two moments of the response statistics. Two major limitations of that method stem from the assumption that both the uncertainty of random parametric input and the non-linearity of random solution with respect to random input must be small. In this context, it is generally recognized that the Monte-Carlo simulation approach, where the deterministic system Eq. (1.6) is solved a large number of times by generating random parameters $\boldsymbol{\theta}$, remains the most general and versatile method to propagate random uncertainties. In many cases it is even impossible to compute the statistical response by other means than Monte Carlo simulations, which is often used in the literature as the reference method to assess accuracy of other approaches. As pointed out in [2, 9, 10], the Monte-Carlo method is superior to other approaches exhibiting slower computational expense growth for large scale problems. Complex nonlinear behavior and large uncertainty variation do not complicate the procedure or deteriorate its accuracy. Finally, the numerical implementations are easily parallelizable, many acceleration techniques are available such as importance sampling, etc.

Random field discretization procedure followed by the solution of a system of stochastic differential equations, such as that described above, results in approximation of the response as a random vector of nodal displacements $\mathbf{x}$, each component being a random variable x_i to be statistically characterized. Instead of sampling of input parametric space followed by random response propagation, the spectral FE methods [2, 3, 5, 10] aim at more efficient sampling of response probabilistic space. The input Gaussian random field is represented as truncated Karhunen-Loève expan-

sion, presented earlier, while the response is expanded in a series of random Hermite polynomials $\Psi_j(\theta) = (-1)^j e^{\frac{1}{2}\theta^T\theta} \frac{\delta^j}{\delta\theta_{i1}\ldots\delta\theta_{ij}} e^{-\frac{1}{2}\theta^T\theta}$

$$\mathbf{x}(\boldsymbol{\theta}) = \sum_{j=1}^{P} \mathbf{x}_j \Psi_j(\theta) \tag{1.7}$$

where P is finite. The Galerkin projection approach applied to the static problem or similarly to a time-dependent problem transformed to the frequency domain leads to a system of linear algebraic equations of order Pn.

$$\left(\sum_{i=1}^{M} \mathbf{K}_i \xi_i(\theta)\right)\left(\sum_{j=1}^{P} \mathbf{x}_j \Psi_j(\theta)\right) - \mathbf{F} = 0 \tag{1.8}$$

where $\mathbf{K}_i$ is assembled deterministic matrices defined in Eq. (1.5) corresponding to M kept Karhunen-Loève terms and $\mathbf{F}$ is a deterministic loading vector. Clearly, the computational complexity depends directly on the number of P terms retained. Application of the method is practically limited to linear systems with smooth solutions [2].

The key issues of prohibitive computational cost associated with uncertainty propagation that plague large scale systems, reduction of the parametric space to most important random parameters and lack of statistical measurement data to quantify spatially varying random properties can also be effectively addressed by introducing random uncertainty through perturbation of selected modal parameters [7, 11]. Needless to mention that since the parameters of the system are described in a probabilistic sense, the eigenvectors and eigenvalues are random too. However, with a simple and practical approach of neglecting the uncertainty in mode shapes, great computational savings can be achieved with reduced order dynamics analysis. The lack of high-resolution measurements in physical space is overcome because experimental quantification of the eigenvalues and their statistics are easily measurable and fairly straightforward to obtain. Moreover simulation of randomness in the modal space can account for all sources of uncertainties, parametric and non-parametric, in both mass and stiffness matrices at the same time.

1.3 Model order reduction

Consider a second order linear time-invariant system of the type

$$\begin{cases} \mathbf{M}\ddot{\mathbf{x}}(t) + \mathbf{C}\dot{\mathbf{x}}(t) + \mathbf{K}\mathbf{x}(t) = \mathbf{B}\mathbf{f}(t) \\ \mathbf{y}(t) = \mathbf{D}\mathbf{x}(t) \end{cases} \tag{1.9}$$

where $\mathbf{f}(t) \in \mathbb{R}^m$, $\mathbf{y}(t) \in \mathbb{R}^p$, $\mathbf{q}(t) \in \mathbb{R}^n$, $\mathbf{B} \in \mathbb{R}^{n\times m}$, $\mathbf{D} \in \mathbb{R}^{p\times n}$, $\mathbf{M}, \mathbf{C}, \mathbf{K} \in \mathbb{R}^{n\times n}$. The symmetric matrices $\mathbf{M}, \mathbf{C}, \mathbf{K}$ in mechanical systems represent respectively mass, stiffness and damping.

In complex aerospace structures the dimension n is so high that in many analysis situations the system cannot be solved in a reasonable time. The goal of model order reduction is to replace a large scale model of a physical system by a model of lower dimension $k \ll n$

$$\begin{cases} \hat{\mathbf{M}}\ddot{\hat{\mathbf{x}}}(t) + \hat{\mathbf{C}}\dot{\hat{\mathbf{x}}}(t) + \hat{\mathbf{K}}\hat{\mathbf{x}}(t) = \hat{\mathbf{B}}\mathbf{f}(t) \\ \hat{\mathbf{y}}(t) = \hat{\mathbf{D}}\hat{\mathbf{x}}(t) \end{cases} \tag{1.10}$$

where $\hat{\mathbf{x}}(t) \in \mathbb{R}^k$, $\hat{\mathbf{B}} \in \mathbb{R}^{k\times m}$, $\hat{\mathbf{D}} \in \mathbb{R}^{p\times k}$, $\hat{\mathbf{M}}, \hat{\mathbf{C}}, \hat{\mathbf{K}} \in \mathbb{R}^{k\times k}$. The resulting ROM is expected to exhibit similar behavior, typically measured in terms of its frequency or time response characteristics. Depending on the application area the following properties are to be satisfied [12]:

- The approximation error is small (the error function is application dependent).
- Relevant to application area system properties are preserved, like second order structure, stability, passivity, etc.
- The procedure is computationally stable and efficient.

Model order reduction schemes can be broadly classified as either projection based or derived by optimizing some performance criteria. Reduction of very large-scale systems is addressed exclusively within the projection framework. The latter involves representation of the state vector $\mathbf{x}$ as a linear combination of $k \ll n$ basis vectors (Galerkin projection)

$$\hat{\mathbf{x}}(t) = \mathbf{V}\mathbf{x}(t) \tag{1.11}$$

where projected system matrices become

$$\hat{\mathbf{M}} = \mathbf{V}^T\mathbf{M}\mathbf{V}, \quad \hat{\mathbf{C}} = \mathbf{V}^T\mathbf{C}\mathbf{V} \quad \hat{\mathbf{K}} = \mathbf{V}^T\mathbf{K}\mathbf{V}, \quad \hat{\mathbf{B}} = \mathbf{V}^T\mathbf{B} \quad \text{and} \quad \hat{\mathbf{D}} = \mathbf{D}\mathbf{V} \tag{1.12}$$

It appears that there are only two kinds of projection based methods [13]. The first involves two essential steps, transformation into a form where the coordinates can be ranked according to some measure of importance and subsequent truncation of less important ones. The methods that fall into this setting, which are relevant to structural dynamics problems, include modal truncation [14], balanced truncation [15], truncation of spatial harmonics, and a plethora of domain decomposition methods [16].

In modal projection approach, applied usually to systems dominated by resonance behavior, the transformation matrix is composed of orthogonal undamped eigenvectors $\mathbf{V} \in \mathbb{R}^{n\times n}$

$$\mathbf{V}^T\mathbf{K}\mathbf{V} = \mathbf{\Lambda} \quad \text{and} \quad \mathbf{V}^T\mathbf{M}\mathbf{V} = \boldsymbol{I} \tag{1.13}$$

By truncating the projection matrix $\mathbf{V} \in \mathbb{R}^{n\times k}$, where the retained eigenvectors correspond to $\lambda_i \in \mathbb{B}$ in analyzed frequency band $\mathbb{B} = [\omega_1, \omega_2]$, the resulting projected ROM retains the ability to accurately capture dynamics of the original model at resonance frequencies in $\mathbb{B}$, where the maximum amplitude of response is expected.

Similarly, systems featuring cyclic symmetry [17], can be rendered into pseudo-block diagonal form with subsequent truncation of less important spatial frequencies

$$\mathbf{V}^T\mathbf{K}\mathbf{V} = \underset{h=1,\ldots,H}{\text{Bdiag}}\,[\mathbf{K}_h] \quad \text{and} \quad \mathbf{V}^T\mathbf{M}\mathbf{V} = \underset{h=1,\ldots,H}{\text{Bdiag}}\,[\mathbf{M}_h] \tag{1.14}$$

where $\mathbf{V} = (\mathbf{F} \otimes \boldsymbol{I})$ and $\mathbf{F}$ is real discrete Fourier transform matrix.

The domain decomposition methods are based essentially on the same principle, which can be illustrated with the following simple example of Guyan condensation

method [16]. Let the system stiffness matrix be partitioned as

$$\mathbf{K} = \begin{bmatrix} \mathbf{K}_{ss} & \mathbf{K}_{sm} \\ \mathbf{K}_{ms} & \mathbf{K}_{mm} \end{bmatrix} \tag{1.15}$$

where subscripts m and s denote master and slave degrees of freedom, i.e. more and less important coordinates in the nodal space. Then the transformation $\mathbf{V}$ renders it into the form with two uncoupled blocks

$$\mathbf{V}^T\mathbf{K}\mathbf{V} = \begin{bmatrix} \mathbf{K}_{ss} & \mathbf{0} \\ \mathbf{0} & \hat{\mathbf{K}} \end{bmatrix} \tag{1.16}$$

where

$$\mathbf{V} = \begin{bmatrix} \boldsymbol{I} & -\mathbf{K}_{ss}^{-1}\mathbf{K}_{sm} \\ \mathbf{0} & \boldsymbol{I} \end{bmatrix} \tag{1.17}$$

is the Gaussian eliminator and the uncoupled projected matrix that we retain after truncation $\hat{\mathbf{K}} = \mathbf{K}_{mm} - \mathbf{K}_{ms}\mathbf{K}_{ss}^{-1}\mathbf{K}_{sm}$ is the Schur complement of $\mathbf{K}_{ss}$.

Finally, the most popular projection based method in control applications of the first type is probably the truncated balanced realization [12, 16, 15]. Consider related to the system Eq. (1.9) two continuous time Lyapunov equations

$$\mathbf{A}\mathcal{P} + \mathcal{P}\mathbf{A}^T + \mathbf{B}\mathbf{B}^T = 0 \quad \text{and} \quad \mathbf{A}^T\mathcal{Q} + \mathcal{Q}\mathbf{A} + \mathbf{D}^T\mathbf{D} = 0 \tag{1.18}$$

where the augmented system matrices in the state space are

$$\mathbf{A} = \begin{bmatrix} \mathbf{0} & \boldsymbol{I} \\ -\mathbf{K} & -\mathbf{C} \end{bmatrix}, \quad \mathbf{B} = \begin{bmatrix} \mathbf{0} \\ \mathbf{B} \end{bmatrix}, \quad \mathbf{D} = \begin{bmatrix} \mathbf{D} & \mathbf{0} \end{bmatrix} \tag{1.19}$$

Under the assumptions of asymptotic stability and minimality of the system, the equations have unique symmetric positive definite solutions $\mathcal{P}, \mathcal{Q} \in \mathbb{R}^{2n\times 2n}$ called controllability and observability Gramians. The Hankel singular values are defined

as square roots of the eigenvalues of the product $\mathcal{PQ}$

$$\sigma_i(\mathbf{G}(s)) = \sqrt{\lambda_i(\mathcal{PQ})} \tag{1.20}$$

and they are clearly basis independent. The system is called Lyapunov balanced if

$$\mathcal{P} = \mathcal{Q} = \mathbf{\Sigma} = \text{diag}(\sigma_i) \tag{1.21}$$

The balancing transformation is determined simply by calculating the eigenvectors of $\mathcal{PQ}$

$$\mathcal{PQ} = \mathbf{V}\text{diag}(\sigma_i^2)\mathbf{V}^{-1} \tag{1.22}$$

The reduced order model is achieved by truncating the states with small Hankel singular values, which deletes less observable and less controllable states.

The desirable feature of the balanced truncation method is a guaranteed error of approximation, the norm of the approximation error is bounded by the sum of the Hankel singular values not retained in ROM

$$\|\mathbf{G}(s) - \hat{\mathbf{G}}(s)\|_{\mathcal{H}_\infty} \leq 2(\sigma_{k+1}, \ldots, \sigma_n) \tag{1.23}$$

where $\mathbf{G}(s)$ the transfer function associated with the system Eq. (1.9) in the Laplace domain. The method is not practical for very large scale systems due to computational complexity involved in calculation of Gramians, i.e. solution of the Lyapunov equations.

The second type of projection methods arising due to other considerations, namely transfer function interpolation or moment matching, utilize Krylov subspace iterative techniques. Application of Krylov subspace projection methods to second order undamped or proportionally damped systems is reported in [18, 19, 20, 21, 22]. Let the transfer function associated with the system Eq. (1.9) in the Laplace domain is given by

$$\mathbf{G}(s) = \mathbf{D}(\mathbf{M}s^2 + \mathbf{C}s + \mathbf{K})^{-1}\mathbf{B} \tag{1.24}$$

With proportional damping assumption the approach is to generate projection vec-

tors $\mathbf{V}$ spanning a regular first order Krylov subspace.

$$\mathbf{V} = \text{span}\{\mathbf{K}^{-1}\mathbf{B}, \ldots, (\mathbf{K}^{-1}\mathbf{M})^{r-1}\mathbf{K}^{-1}\mathbf{B}\} \tag{1.25}$$

The goal of Krylov-based model reduction techniques is to find a reduced-order dynamical system by projecting Eq. (1.24) in such a way that projected $\hat{\mathbf{G}}(s)$ interpolates $\mathbf{G}(s)$. Thus, given the original transfer function that is expanded in a Taylor series around a given point $s_0 \in \mathbb{C}$

$$\mathbf{G}(s_0 + \sigma) = \eta_0 + \eta_1\sigma + \eta_2\sigma^2 + \eta_3\sigma^3 + \ldots \tag{1.26}$$

where η_i are the moments, find a reduced order systems

$$\hat{\mathbf{G}}(s_0 + \sigma) = \hat{\eta}_0 + \hat{\eta}_1\sigma + \hat{\eta}_2\sigma^2 + \hat{\eta}_3\sigma^3 + \ldots \tag{1.27}$$

such that $k \ll n$ moments are matched.

$$\hat{\eta}_i = \eta_i, \quad i = 1, \ldots, k \tag{1.28}$$

Reliable and stable algorithm implementations are reported using classical Lanczos or Arnoldi processes. The weak points of all Krylov subspace based projection methods include lack of general strategy for approximation error control, stopping condition and suboptimality.

If the linear projection based model reduction techniques have reached their maturity, they are well understood and have stable reliable algorithm implementations, their extensions to parameter-dependent models are still underdeveloped due to intrinsic complexity [23]. Let a parameter-dependent linear time-invariant system be

$$\begin{cases} \mathbf{M}(\mathbf{p})\ddot{\mathbf{x}}(t) + \mathbf{C}(\mathbf{p})\dot{\mathbf{x}}(t) + \mathbf{K}(\mathbf{p})\mathbf{x}(t) = \mathbf{B}\mathbf{f}(t) \\ \mathbf{y}(t) = \mathbf{D}\mathbf{x}(t) \end{cases} \tag{1.29}$$

where $\mathbf{p} \in \mathbb{R}^m$ is a parameter vector. The goal of a parametric model order reduction is to compute a ROM that preserves the parameter-dependency, thus allowing a

variation of any of the parameters without the need to repeat the ROM construction step.

$$\begin{cases} \hat{\mathbf{M}}(\mathbf{p})\ddot{\hat{\mathbf{x}}}(t) + \hat{\mathbf{C}}(\mathbf{p})\dot{\hat{\mathbf{x}}}(t) + \hat{\mathbf{K}}(\mathbf{p})\hat{\mathbf{x}}(t) = \hat{\mathbf{B}}\mathbf{f}(t) \\ \hat{\mathbf{y}}(t) = \hat{\mathbf{D}}\hat{\mathbf{x}}(t) \end{cases} \tag{1.30}$$

Two general requirements must be met here, the computational procedure of ROM construction should be sufficiently efficient to offset full model analysis, the update and evaluation of the reduced-order model should be sufficiently efficient either.

The simplest approach is to build a sufficiently robust projection space $\mathbf{V}(\mathbf{p}_0)$ that can be used for models with slightly perturbed parameters $\mathbf{p}$ around a nominal local operating point $\mathbf{p}_0$ [24].

$$\hat{\mathbf{M}}(\mathbf{p}) = \mathbf{V}^T(\mathbf{p}_0)\mathbf{M}(\mathbf{p})\mathbf{V}(\mathbf{p}_0) \quad \text{and} \quad \hat{\mathbf{K}}(\mathbf{p}) = \mathbf{V}^T(\mathbf{p}_0)\mathbf{K}(\mathbf{p})\mathbf{V}(\mathbf{p}_0) \tag{1.31}$$

The method being obviously computationally efficient is limited in small parameter variation assumption.

Several flavors of perturbation based techniques are reported in [23, 25, 26], where the basis vectors are expanded in Taylor series. The general procedure involves drawing several samples form parameter space, for each sample gradients and projection matrix are calculated; fitting is applied to determine the coefficients of a parameter dependent projection matrix. Once the basis is approximated for a parameter change, a reduced linear dynamic analysis can be performed to obtain the parameter dependent output.

A multidimensional multivariate Krylov subspace moment matching technique is reported in [27]. The projection $\mathbf{V}$ is calculated such, that the reduced model not only matches some of the first moments of the transfer function $\mathbf{G}(s)$ with respect to s, but also with respect to the parameters $\mathbf{p}$. The method suffers from "the dimensionality curse" where the order of ROM grows exponentially with the number of parameters.

Another well-known approach is to calculate local projection matrices for several points $\mathbf{p}$ in the parametric space, merge them together, and then apply a common order reducing projection to the original parametric model [28, 29, 26], which in

the last reference is referred to Extended Projection ROM. This method, likewise, rapidly leads to a high order ROM.

Several attempts have been made to decrease the computational effort and the dimension of a resulting parametric ROM by exploiting interpolation and/or a soft switching between the reduced order transfer functions of different non-parametric models [30, 31, 32].

1.4 Objectives

The goal of this dissertation is to develop low order high fidelity models which are suitable for incorporation into uncertainty quantification framework. The target application area is restricted to linear vibration analysis of large-scale FE models of turbine engine rotors. Two types of applications, bladed disks structural mistuning and stacked rotor assemblies misalignment, are considered in particular. Certainly, not the first endeavor in this area, this dissertation will explore the extension of modern linear algebra solvers to the application domain in a systematic way, providing clear statement of the problems to be addressed, a spectrum of model reduction methods as well as a range of tools implementing those methods. Due to the emphasis on the uncertainty effect analysis, each of the algorithms presented in this dissertation is specifically aimed and related to its ability to address large parameter variation.

1.5 Contributions

- Extension, thorough accuracy and numerical efficiency analysis and implementation of SMC algorithm for reduced order modeling of bladed disks subject to large variations in blade geometry [33, 34].

- Development of an original sparse preconditioned iterative technique for reduced order modeling of bladed disks with large variations in blade geometry addressing the accuracy and performance shortcomings of SMC method [34].

- Development and implementation of a stochastic simulation framework combining two aforementioned techniques with CMM method [35].
- First probabilistic assessment of the joint effects of large magnitude deterministic and small random perturbations on vibration response of bladed disks [35].
- Development and efficient implementation of an original parametric model reduction technique for vibration analysis of misaligned stacked disks rotor assemblies [36].
- Provision of some insight and understanding of the effects of misalignment and origins of the additional harmonic content in vibration response [36].

1.6 Thesis organization and outline

This chapter is concluded with a brief outline of the material in the remainder of dissertation.

Chapter 2 presents the problem of large geometrical mistuning of bladed disks and motivates the development of new compact reduced order models. A survey of the existing literature and solution approaches is provided. An important modeling technique based on direct methods, Static Mode Compensation, is extended to the multiple mistuned blades case. It is examined in the context of the perturbed generalized eigenvalue problem by taking the viewpoint of a system of nonlinear equations. Suggestions are made for which cases it should work reasonably well, in situations where it would not fit, a more sophisticated iterative algorithm is introduced based on Jacobi-Davidson scheme adapted to block-circulant systems under a limited class of perturbations. Both algorithms are compared with regard to their efficiency, accuracy and memory requirements using a practical industrial scale FE model of a bladed disk with realistic geometry.

Chapter 3 presents application of the algorithms discussed in previous chapter in stochastic simulation framework to analyze the effect of small random mistuning on geometrically modified bladed disks. A hybrid technique is proposed where

small random parameter variation in blade properties are modeled with Component Mode Mistuning method. The approach is motivated by the ability to retain complexity and level of detail in both the mechanical and stochastic modeling, access to perturbed system modes, realistic physical geometry variation and nonuniform random variations of individual blades at component level, at the same time providing accuracy of approximation and computational efficiency. The performance and precision of the method is verified against results obtained using a full reference model. Statistical analysis of random mistuning effects on geometrically modified rotor is performed. A a set of mesh morphing patterns is applied to a nominal blade geometry approximating some common blade damage scenarios. Some conclusions and observations are offered regarding the mutual effects of large deterministic and small random mistuning on the vibration response.

In Chapter 4 a novel reduced order modeling procedure is developed for vibration response approximation of a misaligned stacked disks rotor assembly. Motivation is provided for more accurate 3D solid FE modeling of modern flexible rotors with complex geometries. Model order reduction approach is rationalized at length built upon truncation of higher order harmonics and efficient introduction of misalignment uncertainty in Fourier domain with sparse BLAS. Radical reduction of the parametric space is achieved by modeling the interstage geometry variation with a small set of tilt and offset parameters. It is shown numerically that with the assumption of small in norm perturbations and rotational periodicity of individual stages, the flexural behavior of misaligned rotor can be accurately approximated by retaining only first three harmonics. Insight and argumentation are provided on the issue of the origins of the additional vibration content in response of a misaligned system. A computational strategy of reducing large condition number of nominal uncoupled system is discussed, that significantly simplifies and accelerates repeated solution of the perturbed system. Statistical Monte-Carlo investigations are employed to showcase the efficiency of algorithm implementation exposing varying sensitivity of global response to uncertainty at individual rotor stages.

Finally, in Chapter 5 conclusions and recommendations for future work are presented.

Chapter 2

Reduced Order Modeling of Geometrically Mistuned Bladed Disks

2.1 Overview

Structural blade mistuning constitutes a difficult problem in turbomachinery applications. Typically, the vibration analysis of rotationally periodic structures is performed on an elementary sector model, from which the dynamics of a whole structure is reconstructed by exploiting the cyclic symmetry [17]. However, manufacturing tolerances, operational usage and inhomogeneities in materials of individual blades create uncertainties in system response. They involve potentially hazardous increases in amplitude of vibration and stresses as opposed to results predicted by a nominal symmetrical model. Structural mistuning is also known to have a dramatic effect on high cycle fatigue, since it can lead to spatial localization of vibration energy around one or few blades [37, 38].

The problem has been studied extensively in the literature [39]. A number of efficient and accurate predictive computational tools has been reported where mistuned rotor forced response is predicted using reduced models having order of number of el-

ementary sectors built from large scale parent FEM [40, 41, 42, 43, 44, 45, 46]. Most of the reduction methods involve projection into a lower order subspace spanned by a small number of nominal system modes corresponding to a contiguous set of eigenvalues in the frequency band of interest. Note that the projection is done on a subspace of the same dimension m as the number of eigenvectors one wants to approximate. Extraction of approximations of perturbed eigenpairs $(\widehat{\lambda}_i, \widehat{\mathbf{v}}_i)$, $i = 1, \ldots, m$ from a low-order subspace $\mathcal{V} \in \mathbb{R}^m$ is essentially the Rayleigh-Ritz procedure. Let $(\mathbf{K}, \mathbf{M})$ correspond to nominal symmetric indefinite stiffness and symmetric positive definite mass matrices with $(\Delta\mathbf{K}, \Delta\mathbf{M})$ denoting perturbations to these matrices due to mistuning. In its practical less expensive form (if $(\mathbf{M} + \Delta\mathbf{M})$-orthonormalization of $\mathbf{V}$ is omitted) the procedure leads to a projected generalized eigenvalue problem and goes as follows:

1. Let the set of nominal modes $\mathbf{V}$ form a basis of $\mathcal{V}$.
2. Compute $\mathbf{H} = \mathbf{V}^T(\mathbf{K} + \Delta\mathbf{K})\mathbf{V}$ and $\mathbf{G} = \mathbf{V}^T(\mathbf{M} + \Delta\mathbf{M})\mathbf{V}$.
3. Find eigenpairs $(\mu_i, \mathbf{z}_i)$ of the matrix pair $(\mathbf{H}, \mathbf{G})$.
4. Accept $(\mu_i, \mathbf{V}\mathbf{z}_i)$ as an approximate eigenpair $(\widehat{\lambda}_i, \widehat{\mathbf{v}}_i)$ of the matrix pair $(\mathbf{K} + \Delta\mathbf{K}, \mathbf{M} + \Delta\mathbf{M})$.

While effective, such approximation is limited in one basic assumption that the perturbation to nominal matrices do not significantly change the eigenspace from which we extract the perturbed eigenpairs. For an accurate approximation the angle between eigenvector $\widehat{\mathbf{v}}_i$ and subspace $\mathcal{V}$ must be sufficiently small. This assumption enables great computational efficiencies but clearly does not hold true for large magnitude perturbations such as geometric mistuning. The smaller angles can be achieved in two ways. One may build a search subspace $\mathcal{V}$ of higher dimension by including more nominal eigenvectors. In practice, that results in subspaces of a very high-order rendering them computationally impractical during repeated statistical Monte-Carlo or design optimization analysis.

Considerable effort has been applied in recent years towards development of algorithms addressing the large geometry variation. Application of domain decom-

position methods to large mistuning problem is reported in [46, 47, 48], but they suffer from similar complexity limitations to be employed efficiently in a repetitive analysis. Sinha [49] recently formulated a projection-based method by building a richer extended set of basis vectors that covers larger parametric space based on measured spatial statistics of a perturbed geometry. However the computational burden grows with the number of retained principal components. Petrov et al. [50] used the Sherman-Morrison-Woodbury formula to calculate the inverse of perturbed FRF. Yet that algorithm yields a limited access to spacial information in the results.

An alternative approach suitable to be employed effectively within repetitive simulation framework is to correct the set of nominal eigenvectors [51]. The SMC method inspired by modal acceleration technique generates accurate approximates of perturbed eigenpairs under large geometric mistuning perturbation extracted from a very compact subspace. The main goal of this chapter is to analyze the SMC method by taking the viewpoint of the perturbed generalized eigenvalue problem as a nonlinear system of equations. We will consider the cases for which the method should work reasonably well, in situations where it would not fit, we will propose a more sophisticated algorithm to correct nominal modes by adopting a Newton-type framework. The Jacobi-Davidson scheme [52], the Trace Minimization method [53] and a number of related algorithms all fall in that category. Our algorithm is essentially an adaptation of the Jacobi-Davidson scheme to the block-circulant system under a limited class of perturbations. We will see that since the algorithm is based on an iterative linear solver, it is more memory efficient and independent from the structure of perturbation as compared to SMC. With the selected class of perturbations the method should converge significantly faster to a target eigenspace than any general purpose iterative eigensolver that does not exploit the structure of the system.

2.2 Static Mode Compensation method

Throughout this study we consider the harmonic steady state response of an undamped mistuned bladed disk finite element model. In the absence of excitation in

frequency domain the equation of motion can be written as:

$$\big((\mathbf{K}+\Delta\mathbf{K})-\widehat{\lambda}_i(\mathbf{M}+\Delta\mathbf{M})\big)\widehat{\mathbf{v}}_i=0 \tag{2.1}$$

where $\widehat{\mathbf{v}}_i$ is i-th mistuned mode, $\sqrt{\widehat{\lambda}_i}$ is i-th natural frequency, $(\mathbf{K},\mathbf{M})$ are real symmetric nominal mass and stiffness matrices, $\mathbf{K}\in\mathbb{R}^{n\times n}$ nonnegative definite and $\mathbf{M}\in\mathbb{R}^{n\times n}$ positive definite, $(\Delta\mathbf{K},\Delta\mathbf{M})$ are symmetric perturbations due to geometric mistuning with the sparsity pattern (zero entries structure) $\mathcal{S}(\Delta\mathbf{K},\Delta\mathbf{M})\subset\mathcal{S}(\mathbf{K},\mathbf{M})$. The defining feature of rotationally periodic structures is the fact that in a cylindrical coordinate system matrices $\mathbf{M},\mathbf{K}\in\mathcal{BC}(M,N)$ are block-circulant. Here M denotes the number of degrees of freedom of an elementary sector, N is number of elementary sectors. It follows that Eq. (2.1) can be decoupled into $N/2$ smaller problems by applying the discrete Fourier transform

$$\begin{aligned}\widetilde{\mathbf{M}}&=(\mathbf{W}^*\otimes I)\mathbf{M}(\mathbf{W}\otimes I)\\ \widetilde{\mathbf{K}}&=(\mathbf{W}^*\otimes I)\mathbf{K}(\mathbf{W}\otimes I)\end{aligned} \tag{2.2}$$

where

$$\mathbf{W}=\frac{1}{\sqrt{N}}\begin{bmatrix}1 & 1 & \cdots & 1\\ 1 & e^{-\mathrm{j}\frac{2\pi}{N}} & \cdots & e^{-\mathrm{j}\frac{2(N-1)\pi}{N}}\\ 1 & e^{-\mathrm{j}\frac{4\pi}{N}} & \cdots & e^{-\mathrm{j}\frac{4(N-1)\pi}{N}}\\ \vdots & \vdots & \ddots & \vdots\\ 1 & e^{-\mathrm{j}\frac{2(N-1)\pi}{N}} & \cdots & e^{-\mathrm{j}\frac{2(N-1)(N-1)\pi}{N}}\end{bmatrix} \tag{2.3}$$

and $\otimes$ denotes Kronecker product.

For parts of the discussion we will make assumptions on the class of perturbations owing to the special structure of the nominal system. It is natural to consider the perturbation matrices due to geometric mistuning structured as subset of nominal symmetric block-circulant structure. If we denote any vector norm and corresponding subordinate matrix norm as $\|\cdot\|$, the perturbations satisfying $\|\Delta\mathbf{K}\|<\epsilon\|\mathbf{K}\|$ for small enough ϵ are referred to as low magnitude perturbations. The influence of the structure of perturbation on the behavior of perturbed eigenpairs is reflected by the

rank. Thus $\Delta\mathbf{K}$ localized to one or few blocks of a block-circulant structure with $\text{rank}\{\Delta\mathbf{K}\} \ll \text{rank}\{\mathbf{K}\}$ is referred to as low rank localized perturbation.

The main idea behind the SMC method, originally presented in Lim et al. [51], is based on the classical MAM [54] used to reduce the modal truncation error of an expanded in modal space FRF. Consider the frequency response of the mistuned system expanded in the truncated modal space under arbitrary excitation $\mathbf{f}(\omega)$:

$$\mathbf{v}(\omega) = \sum_{i=1}^{m} \frac{\widehat{\mathbf{v}}_i^T \mathbf{f}(\omega)}{\widehat{\lambda}_i - \omega^2} \widehat{\mathbf{v}}_i \tag{2.4}$$

If we apply MAM it becomes:

$$\mathbf{v}(\omega) = \big((\mathbf{K} + \Delta\mathbf{K}) - {\omega_c}^2(\mathbf{M} + \Delta\mathbf{M})\big)^{-1}\mathbf{f}(\omega) + \sum_{i=1}^{m} \left(\frac{\omega^2 - {\omega_c}^2}{\widehat{\lambda}_i - {\omega_c}^2}\right) \frac{\widehat{\mathbf{v}}_i^T \mathbf{f}(\omega)}{\widehat{\lambda}_i - \omega^2} \widehat{\mathbf{v}}_i \tag{2.5}$$

where the eigenvalue shift is usually selected in the middle of the ROM frequency band ${\omega_c}^2 = 0.5(\widehat{\lambda}_1 + \widehat{\lambda}_m)$, or zero if low frequency modes are not truncated. Lim proposed to use the first term on the right hand side to correct the set of system nominal mode shapes $\mathbf{v}_j$ such that they approximately span the same subspace as the perturbed eigenvectors $\widehat{\mathbf{v}}_i$:

$$\mathbf{v}_j(\omega_j) - \Delta\mathbf{v}_j = \sum_{i=1}^{m} \left(\frac{\omega_j^2 - {\omega_c}^2}{\widehat{\lambda}_i - {\omega_c}^2}\right) \frac{\widehat{\mathbf{v}}_i^T \mathbf{f}(\omega_j)}{\widehat{\lambda}_i - \omega_j^2} \widehat{\mathbf{v}}_i \tag{2.6}$$

where the correction terms $\Delta\mathbf{v}_j$ called quasi-static modes are:

$$\Delta\mathbf{v}_j = \big((\mathbf{K} + \Delta\mathbf{K}) - {\omega_c}^2(\mathbf{M} + \Delta\mathbf{M})\big)^{-1}\mathbf{f}(\omega_j) \tag{2.7}$$

Notice that in this setting ω_j^2 corresponds to a nominal system eigenvalue λ_j, while $\mathbf{f}(\omega_j)$ is an equivalent to geometric mistuning forcing excitation such that the motion of perturbed system excited at each of the unperturbed natural frequencies corre-

sponds to the nominal eigenvector $\mathbf{v}_j$ at that frequency:

$$\mathbf{f}(\omega_j) = \big((\mathbf{K}+\Delta\mathbf{K}) - \lambda_j(\mathbf{M}+\Delta\mathbf{M})\big)\mathbf{v}_j = \big(\Delta\mathbf{K} - \lambda_j\Delta\mathbf{M}\big)\mathbf{v}_j \tag{2.8}$$

In effect, the forcing terms $\mathbf{f}(\omega_j)$ form a matrix of residual vectors

$$\mathbf{R} = \big(\Delta\mathbf{K} - \mathbf{\Lambda}\Delta\mathbf{M}\big)\mathbf{V} \tag{2.9}$$

Rather than solving a linear system of full order, the correction terms are computed by exploiting the zero structure of perturbation $(\Delta\mathbf{K}, \Delta\mathbf{M})$ together with the block-circulant nature of the nominal matrix pair $(\mathbf{K}, \mathbf{M})$.

$$\big(\widehat{\mathbf{K}} - \omega_c^2\widehat{\mathbf{M}}\big)^{-1}\mathbf{R} = \mathbf{\Phi}_{n,p}\big(I_{p,p} + (\Delta\mathbf{K}_{p,p} - \omega_c^2\Delta\mathbf{M}_{p,p})\mathbf{\Phi}_{p,p}\big)^{-1}\mathbf{R}_p \tag{2.10}$$

where the subscripts n, p denote the matrix partition of order $\mathbf{\Phi}_{n,p} \in \mathbb{R}^{n\times p}$ with p being equal to the number of degrees of freedom affected by perturbation. The set of so-called quasi-static modes $\mathbf{\Phi}_{n,p}$ can be efficiently precalculated off-line in Fourier domain by solving decoupled linear systems of an elementary sector order

$$\mathbf{\Phi}_{n,p} = (\mathbf{W}\otimes I)\,\widetilde{\mathrm{B}}\mathrm{diag}_{h=1,\dots,H}\big[(\widetilde{\mathbf{K}}_h - \omega_c^2\widetilde{\mathbf{M}}_h)^{-1}_{M,p}\big](\mathbf{W}^*\otimes I) \tag{2.11}$$

where $\widetilde{\mathrm{B}}\mathrm{diag}$ denotes a pseudo block diagonal matrix, h is harmonic number and H is total number of harmonics. Note also that since $\mathbf{\Phi} \in \mathcal{BC}(M,N)$ is hermitian block-circulant, the entire $\mathbf{\Phi}_{n,p}$ can be recreated from only $\frac{N}{2}$ blocks $\mathbf{\Phi}_{M,p}$ of an elementary sector order.

Numerical evidence shows that a straightforward application of the SMC algorithm is not always obvious or even adequate for some very large order models, classes of perturbation and areas of spectrum, unless its convergence properties and other limitations are well understood. First, the algorithm implies the use of fully populated matrices $(\mathbf{K} - {\omega_c}^2\mathbf{M})^{-1}$, this can be done efficiently memory-wise only if the rank of perturbation and the order of the system is sufficiently low. An optimal choice of ω_c also remains to be an issue since it must not cross the nominal and

perturbed system natural frequencies, with the latter unknown a priori, while its effect on convergence properties is yet unclear. The primary reason for calculation of correction terms is generation of very compact yet accurate ROM. However the latter is not always the case even for small rank perturbations affecting limited number of blades. If a simple strategy [33] of augmenting the projection basis by including more corrected nominal modes is adopted to increase the accuracy, it may lead to a very slow convergence while generating high dimensional test subspaces.

In order to better understand the convergence properties of SMC we adopt the viewpoint taken by many subspace-based methods for computing eigenvectors and eigenvalues of large sparse matrices. Assume that we have a set of nominal eigenvectors and corresponding eigenvalues $(\lambda_i, \mathbf{v}_i)$ that only approximate eigenpairs $(\widehat{\lambda}_i, \widehat{\mathbf{v}}_i)$ of the mistuned matrix pair $(\widehat{\mathbf{K}}, \widehat{\mathbf{M}})$. In order to find a way to correct a given approximate eigenpair the generalized eigenvalue problem can be viewed as a nonlinear system of equations:

$$(\widehat{\mathbf{K}} - \widehat{\lambda}_i \widehat{\mathbf{M}})\widehat{\mathbf{v}}_i = 0 \tag{2.12}$$

It is a system of n equations with $n+1$ unknowns, so a constraint should be imposed: usually the eigenvectors are mass-orthonormalized $\|\widehat{\mathbf{v}}_i\|_{\widehat{\mathbf{M}}} = 1$, where the norm $\|.\|_{\widehat{\mathbf{M}}}$ is defined in the inner product space $(\mathbf{v}, \mathbf{y})_{\widehat{\mathbf{M}}} = \mathbf{v}^T \widehat{\mathbf{M}} \mathbf{y}$. Given an approximate nominal eigenpair $(\lambda_i, \mathbf{v}_i)$ find a correction $(\Delta\lambda_i, \Delta\mathbf{v}_i)$ to satisfy the system of nonlinear equations:

$$\begin{aligned} \big((\widehat{\mathbf{K}} - \lambda_i \widehat{\mathbf{M}}) - \Delta\lambda_i \widehat{\mathbf{M}}\big)\big(\mathbf{v}_i + \Delta\mathbf{v}_i\big) &= 0 \\ \|\mathbf{v}_i + \Delta\mathbf{v}_i\|_{\widehat{\mathbf{M}}} &= 1 \end{aligned} \tag{2.13}$$

which can be rewritten as:

$$\begin{aligned} (\widehat{\mathbf{K}} - \lambda_i \widehat{\mathbf{M}})\Delta\mathbf{v}_i &= -(\Delta\mathbf{K} - \lambda_i \Delta\mathbf{M})\mathbf{v}_i + \Delta\lambda_i \widehat{\mathbf{M}}\mathbf{v}_i + \Delta\lambda_i \widehat{\mathbf{M}}\Delta\mathbf{v}_i \\ \|\mathbf{v}_i + \Delta\mathbf{v}_i\|_{\widehat{\mathbf{M}}} &= 1 \end{aligned} \tag{2.14}$$

The correction terms are usually found by solving the linear system that results from

omission of the nonlinear quadratic terms $\Delta\lambda_i\widehat{\mathbf{M}}\Delta\mathbf{v}_i$ as well as the terms $\Delta\lambda_i\widehat{\mathbf{M}}\mathbf{v}_i$:

$$(\widehat{\mathbf{K}} - \lambda_i\widehat{\mathbf{M}})\Delta\mathbf{v}_i = -(\Delta\mathbf{K} - \lambda_i\Delta\mathbf{M})\mathbf{v}_i \tag{2.15}$$

Thus the generalized Davidson method [55] solves the resulting linear system for each eigenvector $\mathbf{v}_i$ as:

$$\Delta\mathbf{v}_i = -\mathbf{T}^{-1}(\Delta\mathbf{K} - \lambda_i\Delta\mathbf{M})\mathbf{v}_i \tag{2.16}$$

with the help of preconditioner $\mathbf{T}^{-1}$ that approximates the inverse $(\widehat{\mathbf{K}} - \lambda_i\widehat{\mathbf{M}})^{-1}$. It is easy to see that the SMC algorithm is equivalent to one iteration of the generalized Davidson method without subspace acceleration, where the same preconditioner $\mathbf{T}^{-1} = (\widehat{\mathbf{K}} - {\omega_c}^2\widehat{\mathbf{M}})^{-1}$ is applied for all corrected eigenvectors. Although qualitative convergence to external eigenpairs analysis of the Davidson method have been developed, the quantitative results seem more difficult to obtain. Still the following remarks are of interest to understanding in which situations SMC method will work. First observe that the omission of the quadratic term is valid only if $\mathbf{v}_i$ is close to an eigenvector $\widehat{\mathbf{v}}_i$ and there exists a small in norm solution to the original nonlinear equation $\Delta\mathbf{v}_i$, such that the quadratic term in it will have relatively small to no influence.

Notice also that the quality of preconditioner $(\widehat{\mathbf{K}}-{\omega_c}^2\widehat{\mathbf{M}})^{-1}$ depends on how close ${\omega_c}^2$ is to currently approximated $\widehat{\lambda}_i$. Suppose that we already know $\widehat{\lambda}_i = \lambda_i$, then both neglected terms in (2.14) would disappear due to $\Delta\lambda_i = 0$ and the equation solved with the ideal preconditioner, the pseudoinverse $(\widehat{\mathbf{K}} - \lambda_i\widehat{\mathbf{M}})^{\dagger}$, would give us the exact correction $\Delta\mathbf{v}_i$ to an approximate eigenvector $\mathbf{v}_i$. Therefore the correction happens mainly in the direction of the perturbed eigenvector with eigenvalue closest to ${\omega_c}^2$, which is also evident if we apply the amplification factor line of thought presented in the following. Practically, should the linearization condition be satisfied, the precision of SMC is acceptable if we either select very narrow bands of nominal eigenpairs to correct or can provide a guess on the area of spectrum where the perturbed eigenvectors with larger angles to nominal eigenspace are most likely to

occur, so that their corresponding eigenvalues would fall close enough to ω_c^2.

2.3 Jacobi-Davidson method for geometrical mistuning problem

The Jacobi-Davidson algorithm, as originally developed by Sleijpen and Van der Vorst in [52], is an alternative more robust approach to calculate correction to a current approximation of an eigenvector that addresses the above-mentioned potential weaknesses of SMC. First, unlike Davidson method, its convergence is guaranteed whenever non-diagonal and non-positive definite preconditioners are used, which is often the case when we approximate the interior of the spectrum. Second, it avoids ill-conditioning of the linear correction equations when we cross the perturbed or nominal eigenvalues and we are not constrained with the choice of ω_c. Moreover, the correction equations can be solved only approximately using an iterative solver such that no fully populated matrices are involved. At the same time controlling the number of inner iterations (the number of iterations of linear solver) can also be used to compensate for lower quality preconditioning. The algorithm goes as follows. After omitting the second-order term in (2.14), i.e. linearizing around $\Delta\mathbf{v}_i = 0$, the correction equation becomes:

$$\begin{aligned} &(\widehat{\mathbf{K}} - \lambda_i\widehat{\mathbf{M}})\Delta\mathbf{v}_i = -\mathbf{r}_i + \Delta\lambda_i\widehat{\mathbf{M}}\mathbf{v}_i \\ &\|\mathbf{v}_i + \Delta\mathbf{v}_i\|_{\widehat{\mathbf{M}}} = 1 \end{aligned} \tag{2.17}$$

where $\mathbf{r}_i$ denotes the residual vector $(\Delta\mathbf{K} - \lambda_i\Delta\mathbf{M})\mathbf{v}_i$. It is a $n+1$ system of equations with $n+1$ unknowns that can be solved on a smaller subspace by invoking an orthogonal projector operator $\mathbf{P} = (I - \mathbf{v}_i\mathbf{v}_i^T\widehat{\mathbf{M}})$. Observing that $\mathbf{P}\mathbf{v}_i = 0$, we obtain a degenerate system:

$$\mathbf{P}^T(\widehat{\mathbf{K}} - \lambda_i\widehat{\mathbf{M}})\Delta\mathbf{v}_i = -\mathbf{P}^T\mathbf{r}_i \tag{2.18}$$

Among all the solutions we seek one $\widehat{\mathbf{M}}$-orthogonal to $\mathbf{v}_i$, i.e. $\Delta\mathbf{v}_i = \mathbf{P}\Delta\mathbf{v}_i$. That yields the linear Jacobi-Davidson correction equation to solve for each approximate eigenvector $\mathbf{v}_i$:

$$\begin{aligned} \mathbf{P}^T(\widehat{\mathbf{K}} - \lambda_i\widehat{\mathbf{M}})\mathbf{P}\mathbf{z}_i &= -\mathbf{P}^T\mathbf{r}_i \\ \Delta\mathbf{v}_i &= \mathbf{P}\mathbf{z}_i \end{aligned} \tag{2.19}$$

It can be solved only approximately using a matrix-free iterative method, usually (if not always) in combination with a projected preconditioner. Unlike SMC, the standard Jacobi-Davidson method makes use of subspace acceleration, i.e. the computed term rather than correcting current approximation of an eigenvector is used for expansion of the test subspace. Each step of subspace expansion, termed outer iteration, is preceded by solution of the correction equation, followed by Rayleigh-Ritz procedure, and so on up until convergence to an eigenpair. The original formulation of Jacobi-Davidson algorithm deals with approximation of individual eigenpairs. If more than one eigenpair is to be corrected at each outer iteration, a more restrictive correction $\Delta\mathbf{v}_i$ is usually used, namely the one $\widehat{\mathbf{M}}$-orthogonal to already converged eigenvectors $\mathbf{q}_1, \ldots, \mathbf{q}_k$ and/or to some clustering Ritz vectors:

$$\begin{aligned} (I - \mathbf{Q}\mathbf{Q}^T\widehat{\mathbf{M}})^T(\widehat{\mathbf{K}} - \lambda_i\widehat{\mathbf{M}})(I - \mathbf{Q}\mathbf{Q}^T\widehat{\mathbf{M}})\mathbf{z}_i &= -(I - \mathbf{Q}\mathbf{Q}^T\widehat{\mathbf{M}})^T\mathbf{r}_i \\ \Delta\mathbf{v}_i &= (I - \mathbf{Q}\mathbf{Q}^T\widehat{\mathbf{M}})\mathbf{z}_i \end{aligned} \tag{2.20}$$

with $\mathbf{Q} = [\mathbf{q}_1, \ldots, \mathbf{q}_k, \mathbf{v}_i]$.

2.3.1 Computational strategies

A direct application of Jacobi-Davidson inner-outer iteration scheme to a periodic system featuring large geometric mistuning could hardly be worth the trouble compared with any modern subspace-based eigensolver if it were not for a host of a priori information available on the structure of the system and perturbation. In this section we propose some heuristic strategies to lower the computational cost of Jacobi-Davidson scheme relevant to typical industrial applications. Thus we con-

sider a FOD event or any kind of local defect to an industrial bladed disk [56] as a target application, which represents a low rank local perturbation of relatively high magnitude. Our arguments are illustrated numerically on a test case model. It is an integrally bladed rotor depicted in Fig. 2.1(a) featuring 29 blades used in the second stage of a compressor. The finite element model was constructed with standard linear brick elements with total 126,846 DOF. The foreign object damage scenario in which one blade suffers severe mistuning, with all other blades being tuned is introduced by significantly changing the blade geometry, as shown in Fig. 2.1(b). The

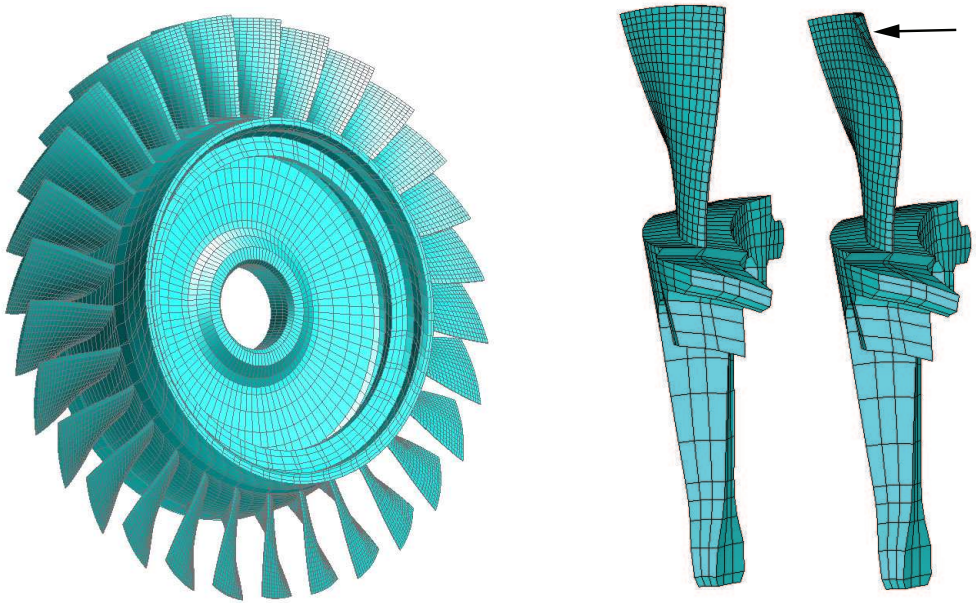

(a) (b)

Figure 2.1 Finite element model of a integrally bladed rotor (a) and geometry of nominal and mistuned blades (b). The mistuning affects 1116 DOF of one blade.

natural frequencies and mode shapes of the nominal system are obtained via cyclic symmetry analysis using a finite element model of a single sector. Fig. 2.2 displays the free vibration natural frequencies of the tuned bladed disk versus the number of nodal diameters, where the frequency band of $34 - 36$ kHz corresponding to $2S$ family of modes is chosen to illustrate the numerical strategies.

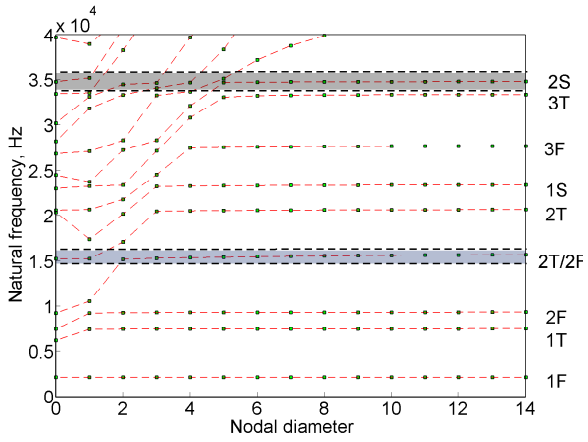

Figure 2.2 Natural frequencies versus nodal diameters. The frequency ranges that include 2S and 2T/2F mode families are marked by horizontal lines.

A priori information on block-circulant systems undergoing structured perturbation

The effect of perturbation on the dynamics of periodic systems has been the subject of a number of theoretical studies [57, 58]. Although commonly the qualitative analysis is carried out on low-order simplified models of periodic systems, we can extend those observations to perturbed eigenstructure of very large scale periodic models. Typically, the eigenvectors of a periodic system are described in terms of nodal diameters (nodal lines across the diameter of a cyclic-symmetrical structure) and nodal circles (nodal lines in the circumferential direction). The number of nodal diameters for an eigenvector corresponds to a certain phase shift between adjacent blocks, given by:

$$\alpha_h = \frac{2\pi h}{N} \tag{2.21}$$

where h is the number of nodal diameters (or harmonic content of an eigenvector), and N is the number of blocks in the system. A periodic system also exhibits repeated natural frequencies for each harmonic, except $h = 0$ and in the case of even N, except $h = N/2$, termed accordingly the doublet and singlet modes. Each member of a doublet has either sinusoidal or co-sinusoidal harmonic content, they are linearly

independent, their absolute orientation is arbitrary due to symmetric nature of the system, while they can be distinguished by relative spatial phase shift. An interesting characteristic of periodic structures is the band structure of natural frequencies, that is the natural frequencies are grouped into narrow bands of mode families, in most cases forming well separated rather stable to perturbation eigenspaces. Since the test case model has no blade-to-blade shrouds, the blade motion dominated modes do not stiffen significantly as the number of nodal diameters increases, so they form lines that are approximately horizontal, which is shown in Fig. 2.2.

When perturbation is introduced into a periodic system, the doublet mode pairs split such that each of the modes have a unique natural frequency. With low magnitude high rank perturbation the natural frequencies are still close in frequency, gradually splitting further apart as the magnitude increases. Low rank high magnitude perturbation limited to one or some blocks significantly affects only few natural frequencies. An example of frequency splitting phenomena for the test case model undergoing FOD event is shown in Fig. 2.3. The eigenvectors with introduction of

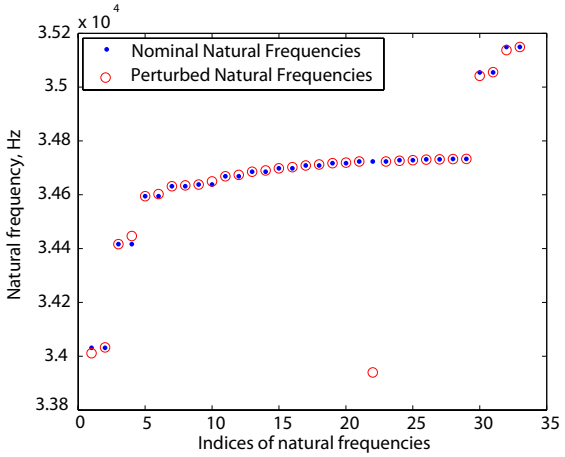

Figure 2.3 Nominal and perturbed natural frequencies for the test case model in $34 - 36$ kHz region. The perturbation brings about a localized mode with natural frequency far away from the unperturbed one. Otherwise, the clustered eigenvalues (all belong to 2S family) seem to be more stable under perturbation.

moderate perturbation would still be recognizable as ones of the nominal system.

Although the perturbation destroys the regular features of mode shapes, they keep their original nodal diameter harmonic content, i.e. overall sinusoidal amplitude envelope, but transition from periodic to almost periodic [57]. As perturbation increases, the mode shapes sustain greater distortion until a sudden transition occurs, after which they become essentially localized around a single sector. However not all modes are equally sensitive to a particular perturbation, and not all of them experience sudden transitions, exhibiting rather a smoother transition from periodic to localized behavior. Fig. 2.4(a) shows the effect of low rank geometrical mistuning on the mode shapes for the test case model in $34-36$ kHz region. The mode distortion is reflected by the canonical angles. Note that the heavily distorted first mistuned mode forms large angles to any of the nominal modes, while one member of nearly each doublet is almost unaffected by perturbation. The combined effect of low-rank geometrical mistuning on an entire subspace spanned by nominal modes can be observed by calculating canonical angles between the corresponding eigenspaces, shown in Fig. 2.4(b). The perturbed eigenspace is very close to the nominal one, except for the five largest canonical angles introduced chiefly by five distorted modes with natural frequencies outside the main cluster, which is why the uncorrected nominal subspace cannot be used in Rayleigh-Ritz procedure. In addition to distortion of the original harmonic content in the mode shapes, perturbation also removes indeterminacy from the absolute orientation [58]. This phenomenon is illustrated in Fig. 2.5 where the norm of residual vector is calculated for the nominal modes subject to different spatial orientation. A nominal mode oriented to minimize the norm would correspond to its perturbed almost periodic counterpart.

Decreasing the number of correction equations to solve

One of our goals in designing a practical reduction technique featuring large mistuning is computational efficiency, and since the major part of computational effort of the Jacobi-Davidson method is spent on solving the correction equations, we must find a way to decrease it. Observe that JD computes an orthogonal correction to an eigenvector that minimizes its residual vector by solving the linear equation (2.15).

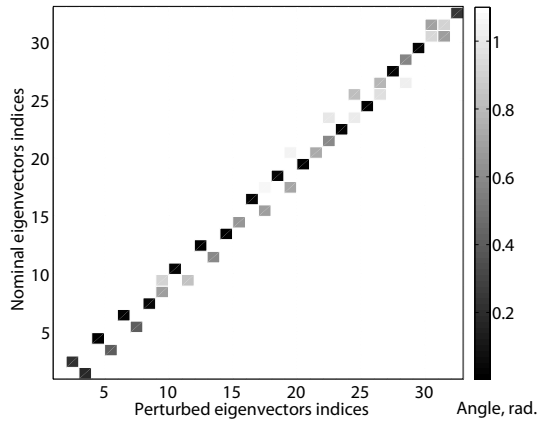

(a)

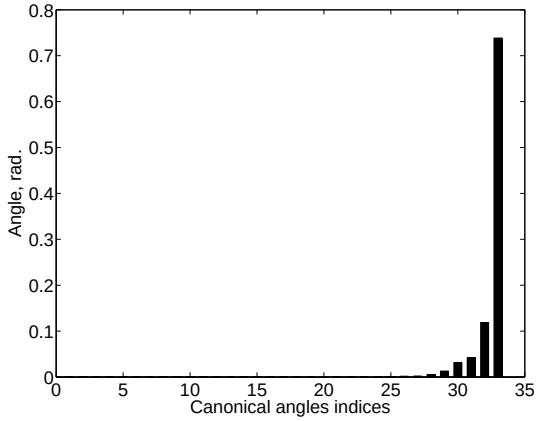

(b)

Figure 2.4 Canonical angles between nominal and perturbed individual eigenvectors (a) and eigenspaces (b) for the test case model in $34 - 36$ kHz region. Note the large angle that makes the first "rogue" localized perturbed mode with any of nominal ones. Also note that one member of almost every nominal doublet keeps its original harmonic content. Plot (b) shows the distance between perturbed and nominal eigenspaces. In order to extract accurate eigenpairs from the nominal eigenspace correction for the five largest canonical angles must be carried out.

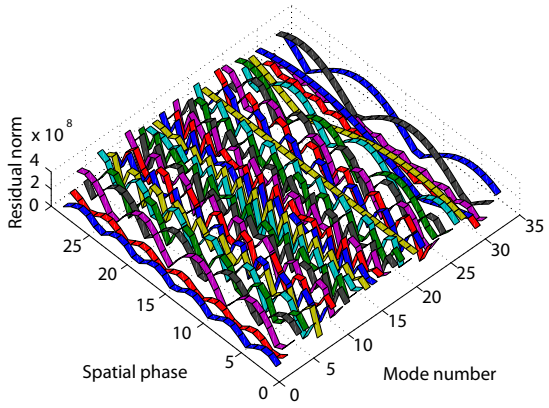

Figure 2.5 Norm of residual vectors calculated for nominal mode shapes in $34 - 36$ kHz region as a function of spatial orientation. The residual norm demonstrates arbitrary orientation and spatial periodicity of nominal eigenvectors. An oriented nominal eigenvector with minimum residual corresponds to its almost periodic perturbed counterpart.

As such, JD correction term is designed to point in the direction of the closest perturbed eigenvector, the one that makes smallest angle with the current approximate eigenvector. Therefore, we can easily avoid computing corrections to both members of a doublet because the corrected eigenvectors would routinely point in the direction of the perturbed eigenvector that keeps maximum of the original harmonic content making smaller angle with both unperturbed nominal eigenvectors. Combined with subspace acceleration, such strategy lowers the computational work almost in half during the first outer iteration without compromising the accuracy of following Rayleigh-Ritz approximation. Out of two members of a doublet we select one with smaller residual based on the following arguments. First, it is expected that we will spare extra matrix vector multiplications of an iterative solver starting with already smaller residual. Valuable observation on the secondary effect of the smaller

residual choice are given in [59]. Consider the exact solution of equation (2.15):

$$\begin{aligned} \Delta\mathbf{v}_i &= \mathbf{v}_i - \epsilon(\widehat{\mathbf{K}} - \lambda_i\widehat{\mathbf{M}})^{-1}\widehat{\mathbf{M}}\mathbf{v}_i \\ \epsilon &= \frac{\mathbf{v}_i^T\widehat{\mathbf{M}}\mathbf{v}_i}{\mathbf{v}_i^T\widehat{\mathbf{M}}(\widehat{\mathbf{K}} - \lambda_i\widehat{\mathbf{M}})^{-1}\widehat{\mathbf{M}}\mathbf{v}_i} \end{aligned} \tag{2.22}$$

If we express $\mathbf{v}_i$ as a linear combination of $\widehat{\mathbf{v}}_j$ it follows that:

$$(\widehat{\mathbf{K}} - \lambda_i\widehat{\mathbf{M}})^{-1}\widehat{\mathbf{M}}\mathbf{v}_i = \sum_j \frac{\alpha_j}{\widehat{\lambda}_j - \lambda_i}\widehat{\mathbf{v}}_j \tag{2.23}$$

Observe that eigenvector components corresponding to eigenvalues closer to λ_i will be amplified more in $(\widehat{\mathbf{K}} - \lambda_i\widehat{\mathbf{M}})^{-1}\widehat{\mathbf{M}}\mathbf{v}_i$ with amplification factors $1/|\widehat{\lambda}_j - \lambda_i|$. It is straightforward to see that due to the $\widehat{\mathbf{M}}$-orthogonalization, as soon as $\mathbf{v}_i$ has large component in the direction of $\widehat{\mathbf{v}}_j$, i.e. smaller angle between them or ultimately smaller residual, the components in the direction of the next closest $\widehat{\mathbf{v}}_{j+1}$ become dominant. Consequently, the correction term computed to turn the first nominal eigenvector with smaller residual in the direction of $\widehat{\mathbf{v}}_j$, if used with subspace acceleration, will inevitably introduce more additional information in the direction of the second perturbed member of the doublet.

Reduction of number of inner iterations

In addition to decreasing the number of correction equations to solve, we can also better exploit the a priori information to reduce the residual norm before applying any iterative solver. In the view of the fact that perturbed modes of periodic systems acquire spatial orientation, as depicted in Fig. 2.5, we can inexpensively find it by computing several residual vectors per double mode. Fig. 2.6 shows the effect of finding spatial orientation on initial residual norm, while Fig. 2.7(a) depicts its effect on the residual convergence history of GMRES linear solver with preconditioning.

The information on how to provide an initial guess vector for iterative solver can be obtained if we argue heuristically as follows. It is a well known fact that if an eigenvalue problem has a cluster of eigenvalues, then the corresponding eigenvectors

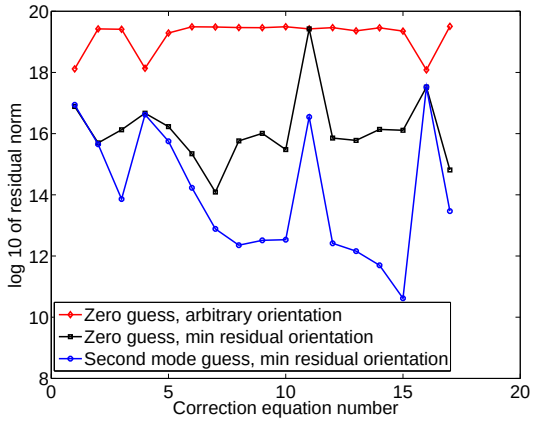

Figure 2.6 Effect of spatial orientation and initial guess vector on initial residual norm for the test case model in $34 - 36$ kHz region. By applying the knowledge about our system one can consistently reduce residual of the linear correction equation before any iterations taken. If spatial orientation strategy is applied, the initial guess reduces residual for 13 correction equations out of 17.

will be extremely ill conditioned, such that even an insignificant perturbation can drastically change the eigenvectors, while spanned by them eigenspace will be relatively well determined and well conditioned [60]. In [61], Theorem 1 implies that the perturbation of an eigenvector corresponding to a multiple eigenvalue will only be unstable in the eigenspace corresponding to this multiple eigenvalue. This fact is also corroborated in [62], where the authors have studied the modal interaction of closely spaced natural modes undergoing perturbation and concluded that the amount of interaction depends on the closeness of natural frequencies. Hence we may very well expect that the orthogonal correction to a nominal eigenvector corresponding to a double eigenvalue, lay, at least in part, in the direction of the second nominal eigenvector corresponding to that eigenvalue. For a single mode we might as well seek the correction in the direction of the closest in spectrum neighbor. Thus we use $\gamma\,\mathbf{v}_{i+1}$ as the initial guess vector for iterative solver of (2.15), where the scaling coefficient γ is chosen such that $\mathbf{P}^T(\widehat{\mathbf{K}} - \lambda_i\widehat{\mathbf{M}})\mathbf{P}\,\gamma\,\mathbf{v}_{i+1}$ is orthogonal to the new residual

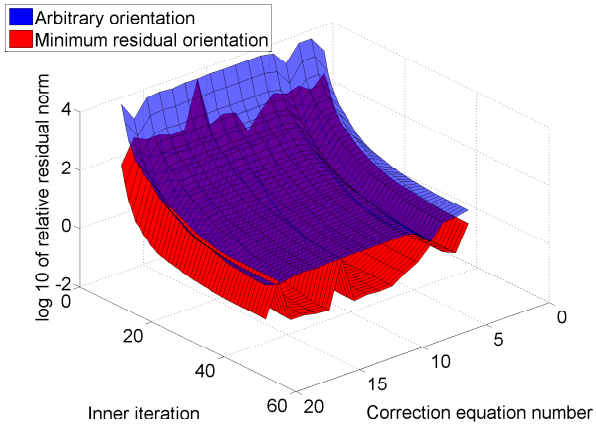

(a)

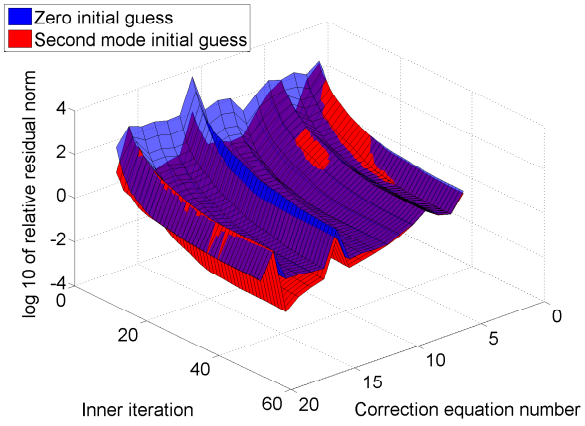

(b)

Figure 2.7 Effect of spatial orientation (a) and initial guess vector with spatially oriented modes (b) on preconditioned GMRES relative residual convergence history for the test case model in $34-36$ kHz region. Faster on average GMRES convergence can be observed in both cases.

$(\mathbf{P}^T(\widehat{\mathbf{K}} - \lambda_i\widehat{\mathbf{M}})\mathbf{P}\,\gamma\,\mathbf{v}_{i+1}) - \mathbf{P}^T\mathbf{r}_i$:

$$\gamma = \frac{(\mathbf{P}^T(\widehat{\mathbf{K}} - \lambda_i\widehat{\mathbf{M}})\mathbf{P}\mathbf{v}_{i+1})^T\mathbf{P}^T\mathbf{r}_i}{(\mathbf{P}^T\mathbf{r}_i)^T\mathbf{P}^T\mathbf{r}_i} \tag{2.24}$$

This strategy has worked well in practice, note the significantly lower initial residual depicted in Fig. 2.5 and relative convergence history after 40 iterations of preconditioned GMRES shown in Fig. 2.7(b).

Preconditioning

In order to accelerate the convergence of iterative sparse linear systems solvers, an auxiliary linear system is solved, which is termed preconditioning. Application of right and left preconditioning schemes to Jacobi-Davidson correction equation is well covered in [52, 63, 59]. In particular, an approximation $\mathbf{T}$ of $(\widehat{\mathbf{K}} - \lambda_i\widehat{\mathbf{M}})$ is used as a preconditioner as long as it is inverted $\widehat{\mathbf{M}}$-orthogonally to the selected subspace. Therefore we apply the projected preconditioner matrix $(I-\mathbf{Q}\mathbf{Q}^T\widehat{\mathbf{M}})^T\mathbf{T}(I-\mathbf{Q}\mathbf{Q}^T\widehat{\mathbf{M}})$, while the associated linear system to be solved can be written as:

$$(I - \mathbf{Q}\mathbf{Q}^T\widehat{\mathbf{M}})^T\mathbf{T}(I - \mathbf{Q}\mathbf{Q}^T\widehat{\mathbf{M}})\mathbf{v} = \mathbf{b} \tag{2.25}$$

with solution given by [63]:

$$\mathbf{v} = (I - \mathbf{K}^{-1}\widehat{\mathbf{M}}\mathbf{Q}(\mathbf{Q}^T\widehat{\mathbf{M}}\mathbf{T}^{-1}\widehat{\mathbf{M}}\mathbf{Q})^{-1}\mathbf{Q}^T\widehat{\mathbf{M}})\mathbf{T}^{-1}\mathbf{b} \tag{2.26}$$

provided that $\mathbf{Q}^T\widehat{\mathbf{M}}\mathbf{T}^{-1}\widehat{\mathbf{M}}\mathbf{Q}$ is non-singular. Then the Jacobi-Davidson correction equation preconditioned from the right can be solved in two steps:

$$\begin{aligned}
&(I - \mathbf{Q}\mathbf{Q}^T\widehat{\mathbf{M}})^T(\widehat{\mathbf{K}} - \lambda_i\widehat{\mathbf{M}})(I - \mathbf{T}^{-1}\widehat{\mathbf{M}}\mathbf{Q}(\mathbf{Q}^T\widehat{\mathbf{M}}\mathbf{T}^{-1}\widehat{\mathbf{M}}\mathbf{Q})^{-1}\mathbf{Q}^T\widehat{\mathbf{M}})\mathbf{T}^{-1}\mathbf{y} = \\
&= -(I - \mathbf{Q}\mathbf{Q}^T\widehat{\mathbf{M}})^T\mathbf{r}_i \\
&\Delta\mathbf{v}_i = (I - \mathbf{T}^{-1}\widehat{\mathbf{M}}\mathbf{Q}(\mathbf{Q}^T\widehat{\mathbf{M}}\mathbf{T}^{-1}\widehat{\mathbf{M}}\mathbf{Q})^{-1}\mathbf{Q}^T\widehat{\mathbf{M}})\mathbf{T}^{-1}\mathbf{y}
\end{aligned} \tag{2.27}$$

One of the most obvious choices for a preconditioner is an ILU factorization of $(\widehat{\mathbf{K}} - \lambda_i \widehat{\mathbf{M}})$. ILU preconditioners have been successful in many general symmetric, indefinite, and nonsymmetric cases [64]. However, as the authors pointed out, if the method is applied to indefinite matrices severe problems can occur, in particular small pivots may lead to unstable inaccurate factorizations as well as the structure of the original matrices may cause unstable triangular solves. The nature of large mistuning problem for periodic systems featuring high modal density and target eigenvalues commonly located in the interior of the spectrum makes $(\widehat{\mathbf{K}} - \lambda_i \widehat{\mathbf{M}})$ highly indefinite and severely ill conditioned once we are close to a target eigenvalue. As a result, we have not succeeded in computing any computationally attractive reasonable quality ILU preconditioner. Zero pivots and extremely ill conditioned LU factors were identified as sources of errors. These results are in part corroborated by [63], where authors observed the necessity for a great deal of fill-in (number of non-zero entries) in order to get efficient preconditioning matrices for interior eigenvalues.

As an alternative, we propose to exploit the block-circulant structure of the unperturbed matrix pair $(\mathbf{K}, \mathbf{M})$ in combination with SPAI algorithm [65]. Recall that a block-circulant matrix is completely block-diagonalized by a Fourier matrix:

$$\underset{h=1,\ldots,H}{\text{Bdiag}}\,[\mathbf{K}_h - \lambda \mathbf{M}_h] = (\mathbf{W}^* \otimes I)(\mathbf{K} - \lambda \mathbf{M})(\mathbf{W} \otimes I) \tag{2.28}$$

We propose to approximate the inverse of each block $(\mathbf{K}_h - \lambda \mathbf{M}_h)^{-1}$ with SPAI algorithm because of its robustness and stability, as compared to ILU. It follows that the application of preconditioner to a vector $\mathbf{v}$ can be carried out by the following steps:

1. $\mathbf{f} = \text{DFT}(\mathbf{v})$
2. $\mathbf{f} = \text{SPAI}(\underset{h=1,\ldots,H}{\text{Bdiag}}\,[\mathbf{K}_h - \lambda \mathbf{M}_h])\mathbf{f}$
3. $\mathbf{y} = \text{IDFT}(\mathbf{f})$

First we decompose $\mathbf{v}$ as a linear combination of the real Fourier basis vectors through DFT, then the real block-Fourier coefficients contained in $\mathbf{f}$ are multiplied by sparse

approximation of the inverse of harmonic blocks $(\mathbf{K}_h - \lambda\mathbf{M}_h)^{-1}$ before they are reassembled by the IDFT to produce the output vector $\mathbf{y}$. The DFT can be implemented efficiently by making use of the fast Fourier transform algorithm with reduced computational complexity. The following set of experiments shows the effect of applying several preconditioners, in particular ILU (0), ILUT and DFT-SPAI, on the convergence behavior of GMRES solver after 40 iterations have been taken. Figs. 2.8(a) and 2.8(b) show that blind application of incomplete factorization is rather unsuccessful as compared to DFT-SPAI preconditioning. In case of structure-based ILU (0) we observe greater inaccuracy due to dropping nonzeros, while unstable triangular solves that may have been caused by very small pivots in addition to $(\mathbf{LU})^{-1}$ high condition number are the main reason of ILUT failure, note in Tab. 2.1 that a relatively large fill-in is done in vain. Apart from SPAI robustness, its success

Table 2.1 Comparison of fill-in in applied preconditioners.

Preconditioner type	Number of non zero entries
ILU(0)	8474496
ILUT	71805692
DFT-SPAI	8461279

can be explained by a very high fill-in of the transformed back from Fourier domain matrix $(\mathbf{W} \otimes I)\mathbf{SPAI}(\underset{h=1,\ldots,H}{\text{Bdiag}}[\mathbf{K}_h - \lambda\mathbf{M}_h])(\mathbf{W}^* \otimes I)$. Note also that the DFT-SPAI preconditioner is independent of perturbation and can be precalculated off-line, while ILUT uses very large amounts of non-zero entries with additional storage requirements and computational effort for factorization each time perturbation changes, thus putting severe limitations on the maximum problem size that can be handled.

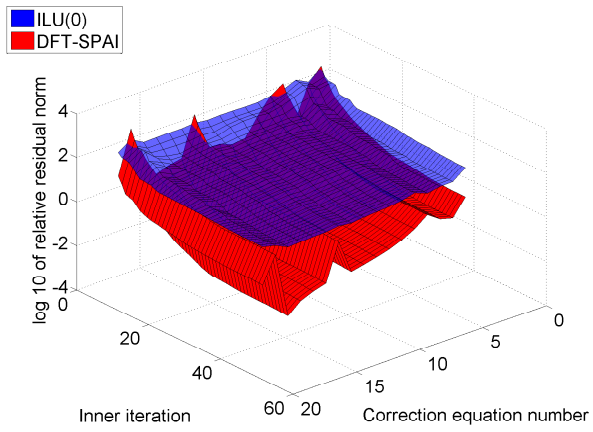

(a)

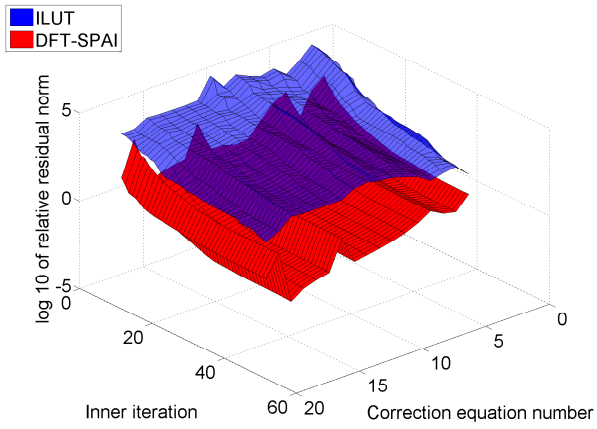

(b)

Figure 2.8 Comparison of GMRES relative residual convergence history with ILU (0) and DFT-SPAI (a), ILUT and DFT-SPAI (b) preconditioners for the test case model in $34 - 36$ kHz region. The DFT-SPAI preconditioner consistently outperforms both structure-based and threshold-based ILU.

2.3.2 Algorithm description

The Jacobi-Davidson method applied to geometric mistuning problem of periodic systems that implements the computational strategies described in the previous sections is outlined in Algorithm 3, Matlab implementation is given in Appendix A. Before applying the main algorithm, a set of preconditioner matrices has to be computed not only with nominal eigenvalues, but also with target values equally covering the frequency band of ROM to have a high-quality preconditioner in case if any localized mode falls in that part of spectrum. The procedure starts with a block of m initial nominal eigenvectors and expands the basis by a block of k vectors. These vectors are approximate solutions of k correction equations, each for one member of double mode with lower residual norm. Note that a more restrictive correction equation (2.20) is implemented, where we are looking for a correction in the space $\widehat{\mathbf{M}}$-orthogonal to the subspace spanned by all selected eigenvectors, each is a member of double mode with smaller residual. This approach, suggested in [53], leads to faster convergence in addition to better conditioned linear correction systems in presence of clustered eigenvalues.

As with all iterative inner-outer processes, we must carefully evaluate the overall computational cost balancing inner solves precision and number of outer iterations. If the correction equations are solved exactly, we may often achieve convergence for all approximated eigenpairs after first Rayleigh-Ritz projection, yet solving inner system to high precision may be very slow and costly. It is generally acknowledged that if a Krylov subspace method is used as linear iterative solver the residual will not decrease substantially up until a large enough subspace is built containing significant spectral information corresponding to omitted parts of the spectrum, which may be prohibitive for very large order systems. Therefore a suitable inner stopping condition scheme must be applied to avoid any superfluous work while computing accurate solutions whenever useful.

As suggested in the literature and based on our experimental observations, the block methods that solve all linear correction equations simultaneously do not consistently improve the overall runtime, unless the eigenpairs are multiple or highly

Algorithm 1 Large Mistuning ROM with Preconditioned Jacobi-Davidson Method

Let $\mathbf{V}^{(0)}$ be an m-column full rank matrix of nominal modes, $k = 1$
for $i = 1, \ldots, m$ **do**
  if $\mathbf{v}_i$ is first member of a double mode **then**
    Find a spatial phase p with minimum norm of residual vector $\mathbf{r}_i = (\widehat{\mathbf{K}} - \lambda_i \widehat{\mathbf{M}})\mathbf{v}_i$
    $\mathbf{u}_k = \text{Rotate}(p, \mathbf{v}_i)$, $\mathbf{v}_k = \text{Rotate}(p, \mathbf{v}_{i+1})$
    $k = k + 1$
  else if $\mathbf{v}_i$ corresponds to a single mode **then**
    $\mathbf{u}_k = \mathbf{v}_i$, set $\mathbf{v}_k$ to the closest in frequency member of double mode
    $k = k + 1$
  end if
end for
$\widehat{\mathbf{M}}$-orthonormalization of $\mathbf{U}$, $\mathbf{Q} = \mathbf{U}/(\mathbf{U}^T\widehat{\mathbf{M}}\mathbf{U})$
Denote $\mathbf{P} = I - \mathbf{Q}\mathbf{Q}^T\widehat{\mathbf{M}}$
for $j = 1, \ldots, k$ **do**
  Denote $\mathbf{Z} = \mathbf{P}^T(\widehat{\mathbf{K}} - \lambda_j\widehat{\mathbf{M}})$
  Denote $\mathbf{T} \approx (\widehat{\mathbf{K}} - \lambda_j\widehat{\mathbf{M}})^{-1}$
  Denote $\mathbf{r}_j = \mathbf{P}^T(\widehat{\mathbf{K}} - \lambda_j\widehat{\mathbf{M}})\mathbf{u}_j$
  Solve the linear system $\mathbf{Z}\Delta_j = \mathbf{r}_j$ by GMRES
  using $\mathbf{Y} = (I - \mathbf{T}\widehat{\mathbf{M}}\mathbf{Q}((\mathbf{T}\widehat{\mathbf{M}}\mathbf{Q})^T\widehat{\mathbf{M}}\mathbf{Q})^{-1}\widehat{\mathbf{M}}\mathbf{Q})\mathbf{T}$ as a preconditioner, and
  $\mathbf{v}_j$ normalized by $(\mathbf{Y}\mathbf{Z}\mathbf{v}_j)^T(\mathbf{Y}\mathbf{r}_j)/(\mathbf{Y}\mathbf{Z}\mathbf{v}_j)^T(\mathbf{Y}\mathbf{Z}\mathbf{v}_j)$ as an initial guess
  $\Delta_j = \mathbf{P}\Delta_j$
end for
$\mathbf{W} = [\mathbf{V}^{(0)}, \Delta]$
$\mathbf{K}' = \mathbf{W}^T\widehat{\mathbf{K}}\mathbf{W}$,$\mathbf{M}' = \mathbf{W}^T\widehat{\mathbf{M}}\mathbf{W}$
Solve the reduced eigenproblem $\mathbf{K}'\mathbf{z} = \theta\mathbf{M}'\mathbf{z}$
for eigenpairs $(\theta_i, \mathbf{z}_i)$
Retain $(\theta_i, \mathbf{W}\mathbf{z}_i)$ $(i = 1, \ldots, l)$ Ritz pairs falling within ROM frequency range
If some Ritz pairs do not converge apply more outer iterations using GMRES with zero initial guess and deflation against converged Ritz pairs

clustered. Therefore from the point of view of performance and efficiency, provided that after first outer iteration the non-converged eigenpairs do not cluster, we choose to solve one correction equation per outer iteration. Moreover, because of the different rates of convergence of each of the approximate eigenvectors, we perform explicit deflation by including them in $\mathbf{Q}$, however, they still have to be present in the basis of the trial subspace of the Rayleigh-Ritz method. After each outer step we may have a number of non-converged eigenpairs in the selected area of spectrum. While only one will be drawn for correction, there is a choice to be made. The most common targeting schemes are: to always select the non-converged eigenvector with eigenvalue closest to a target and to select the one with minimum residual. The rationale for latter is that the selected Ritz pair with minimum residual would converge first to be removed from the following iterations. In the proposed implementation the minimum residual targeting is adopted in order to avoid selecting a spurious Ritz pair, which may be a linear combination of eigenpairs far to the left and to the right of the targeted spectrum.

2.4 Numerical studies

In this section we present a few numerical experiments. We are mainly interested in assessing the speed and accuracy of SMC and JD algorithms in typical situations. The results obtained by ROM will be compared with those of the full FEM reference model of the mistuned bladed disk. Only free response results are computed because if we neglect the modal truncation error, the accuracy of the solution to the forced response problem at resonance frequencies is fully determined by the errors in the approximated natural frequencies and mode shapes. The frequency bands of $34-36$ kHz and $15-16$ kHz corresponding to the blade motion dominated mode families are chosen for analysis and marked by horizontal lines ($2S$ and $2T/2F$ mode families correspondingly) in Fig. 2.2. Their selection is motivated by the fact that they represent two typical situations. In particular, the higher frequency family $2S$ spans a larger frequency range. The frequency veerings can be observed in that region causing some modes belonging to different families to interact. As the result of

generally higher modal density in that area there is less separation between mode families. In fact, as we mentioned earlier, for symmetrical systems the sensitivity of an eigenvector to perturbation depends on the separation of its corresponding eigenvalue from other eigenvalues. Therefore $34-36$ kHz region represents a more difficult to approximate case under equivalent perturbation than that of $15-16$ kHz, or $2T/2F$ mode family, which is well separated from others, in addition to spanning a narrower frequency range.

In our first example we look for 29 perturbed eigenpairs in $15-16$ kHz region. Figs. 2.9(a) and 2.9(b) present nominal and perturbed natural frequencies along with the canonical angles between corresponding eigenvectors. Note the presence of a strongly affected by perturbation eigenpair with eigenvalue separated from the rest of cluster and eigenvector making large angle with all nominal eigenvectors that corresponds to a highly localized mode depicted in Fig. 2.10(a). Figs. 2.11(a) and 2.11(b) show the natural frequency errors on a logarithmic scale and MAC ratio between perturbed mode shapes predicted by SMC and reference model ANSYS modal analysis for the $15-16$ kHz frequency band calculated with $f_c = 15{,}400$ Hz, arbitrarily chosen in the middle of the frequency band. The results show that for this case of relatively narrow well isolated family of modes the correction term calculated with $f_c = 15{,}400$ Hz is still accurate enough to yield approximation for the highly localized 14,965 Hz mode. Thus natural frequency error for all calculated modes is below 0.003% and MAC value above 0.9995. Next we apply our new iterative method for the same problem. We solve the correction equations approximately by using the Matlab built-in GMRES method *gmres.m*, that showed faster convergence on the test case system. We have precalculated a set of SPAI preconditioners with target value covering the frequency region $15-16$ kHz with a step ~ 100 Hz. For all the numerical tests the maximum inner iteration number is set to 500, while the inner iteration tolerance varies. In Fig. 2.12 we show the effect of increasing inner solver accuracy on MAC, $\log 10$ of natural frequency error and number of GMRES iterations for each of the correction equations solved used as a measure of the computational cost. Note that a reasonably accurate estimate of the perturbed eigenpairs can be obtained without applying any further outer iterations, provided that the inner correction

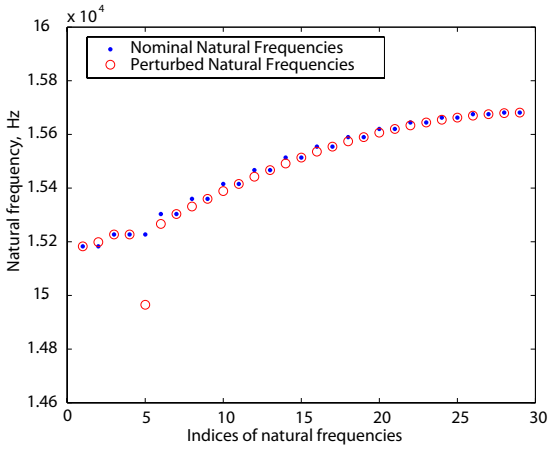

(a)

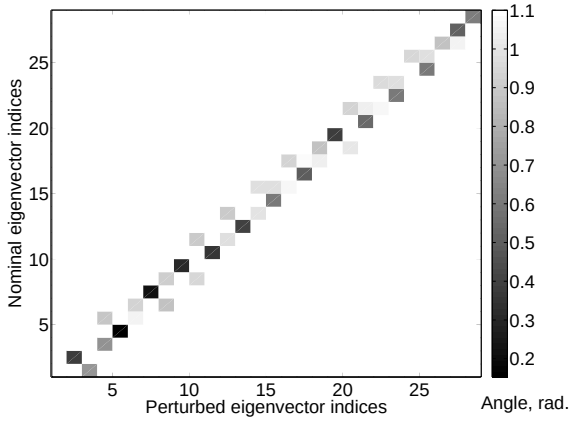

(b)

Figure 2.9 Natural frequencies (a) and canonical angles between eigenvectors (b) of nominal and perturbed test case model in $15 - 16$ kHz region. The "rogue" localized mode can be seen with natural frequency far away from the original cluster and large angle with nominal ones in the lower left corner of plot (b).

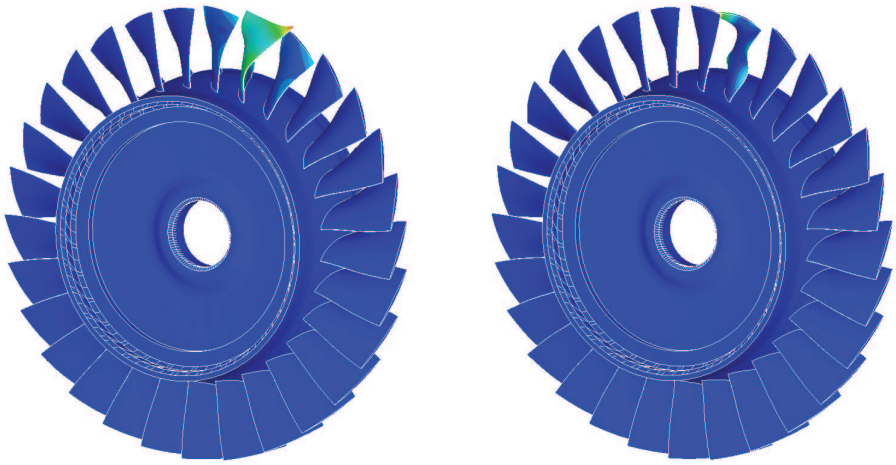

(a) (b)

Figure 2.10 Localized mode shapes corresponding to 14,965 Hz (a) and 33,940 Hz (b).

equations are solved accurately enough. Apparently with 500 steps GMRES and inner relative residual tolerance set to $4 \cdot 10^{-10}$ the correction equations are solved to high enough precision to yield good quality correction terms, and the results are in line with the literature that suggests to apply more accurate inner solves if near convergence. In the current investigation we try to obtain the highest reasonable precision and stop if reach plateau in GMRES convergence. The performance of the method should be tailored by taking into account the overall running time, which in parallel computing environment suggests the strategy of decreasing the number of outer iterations by applying more accurate inner solves. Next we carry out a more severe test to the large geometric mistuning ROM algorithms, that features higher modal density with frequency veering regions corresponding to $2S$ family of modes. The effect of perturbation on nominal modes in that area is shown in Figs. 2.3 and 2.4(a), while Figs. 2.13(a) and 2.13(b) depict the natural frequency errors and MAC ratio in the $34 - 36$ kHz frequency band calculated by SMC with $f_c = 34{,}700$ kHz. Clearly in this case the highly localized mode shown in Fig. 2.10(b) is not properly approximated, with the error in natural frequency more that 0.73% and MAC ratio 0.86. The error could be attributed to the choice of the centering frequency being

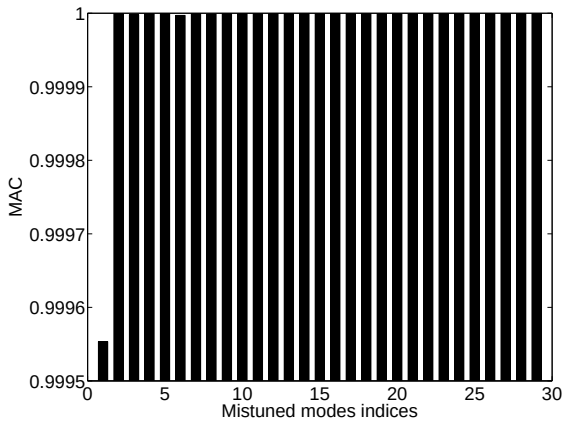

(a)

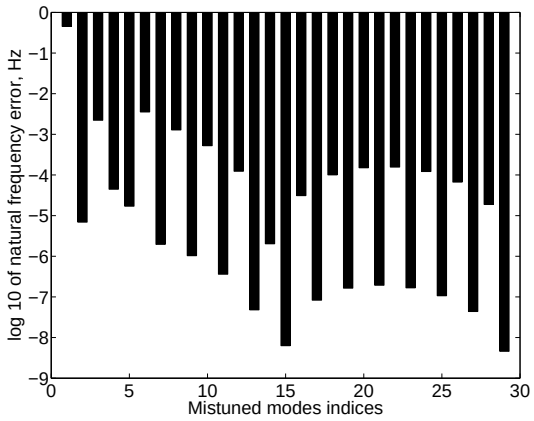

(b)

Figure 2.11 MAC ratio (a) and natural frequency error (b) between reference and approximated by SMC eigenpairs for the test case model in $15 - 16$ kHz region. SMC accurately approximates perturbed eigenpairs in this region, with MAC above 0.9995 and natural frequency error below 0.003%.

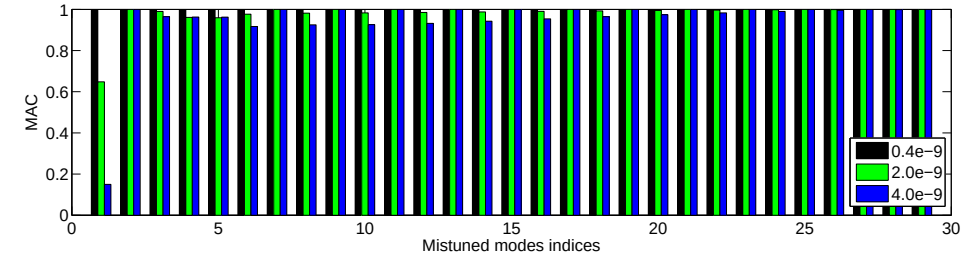

(a)

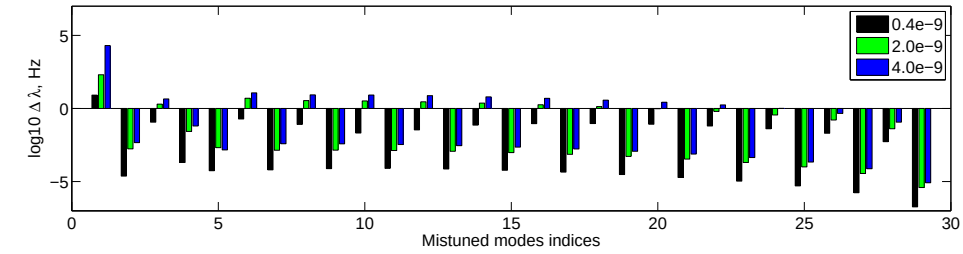

(b)

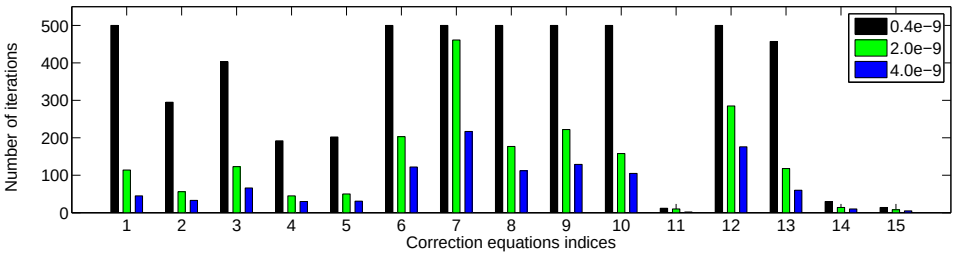

(c)

Figure 2.12 Effect of GMRES relative residual tolerance on MAC (a), natural frequency error (b) and number of inner solves (c) for the test case model in $15 - 16$ kHz region. A reasonable quality solution can be obtained with a single outer iteration by increasing the inner solver accuracy. With a total of 5101 GMRES iterations taken the MAC for all modes is above 0.996 and natural frequency error below 0.05%.

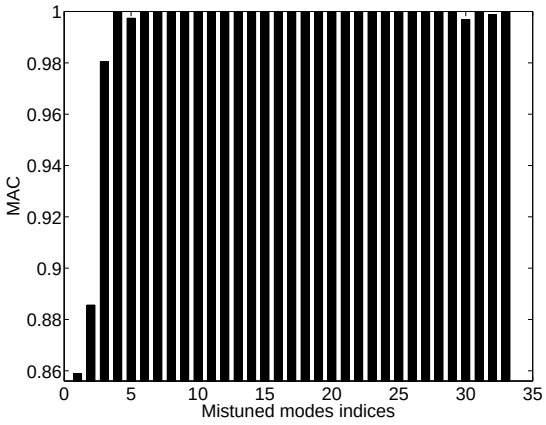

(a)

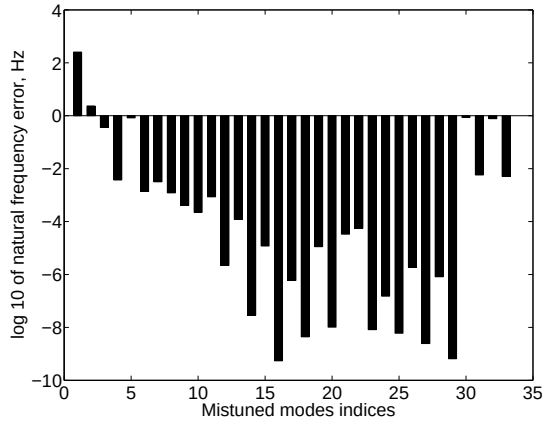

(b)

Figure 2.13 MAC ratio (a) and natural frequency error (b) between reference and approximated by SMC eigenpairs for the test case model in $34 - 36$ kHz region. In this case SMC fails to accurately approximate localized perturbed mode corresponding to 33,940 Hz, which has MAC 0.86 and natural frequency error 0.73% due to poor preconditioning calculated with $f_c = 34{,}700$ Hz.

far from the mode that needs a high quality correction. This example illustrates one of the weak points of SMC method discussed above, i.e. SMC algorithm may not be an optimal choice if applied in the wider areas with high modal density even for

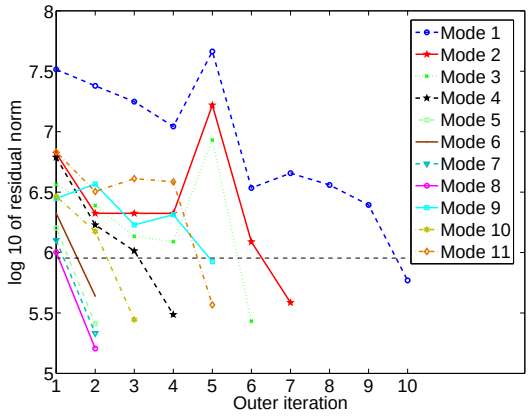

Figure 2.14 Outer loop convergence history of 11 modes after first outer iteration of the preconditioned iterative method in $34 - 36$ kHz region. Each curve shows the convergence of the residual norm of a Ritz pair fallen in $33.9 - 35.2$ kHz region at outer steps. Note that the outer residual tolerance level is marked by the dashed horizontal line.

local low rank perturbations. Now we consider again the $34 - 36$ kHz region and seek 33 perturbed eigenpairs with the iterative method. Here we apply the inner solver settings that yielded acceptable precision in the previous experiment, namely maximum of 500 GMRES iterations with the inner relative residual tolerance set to $4 \cdot 10^{-10}$. After solving 17 correction equations to the selected accuracy level, we find that 11 of approximate eigenparairs do not converge to the outer residual norm tolerance set to $9 \cdot 10^5$. Fig. 2.14 reports the residual convergence history of those eigenpairs that have not converged after first outer iteration, while in Tab. 2.2 the computational cost is provided in terms of number of GMRES solves. Note that even if only one correction equation is solved per outer iteration with the selected targeting strategy, we sometimes observe the convergence of several eigenpairs at a time. The peaks in the convergence behavior of certain eigenpairs are likely to be caused by unstable convergence to internal eigenspaces, which is technically possible but not guaranteed by the theory. The accuracy of approximate eigenpairs after applying 10 outer iterations are presented in Figs. 2.15(a) and 2.15(b).

Summarizing this section, these two examples demonstrate the claim from Sec-

Table 2.2 Computational cost and number of converged eigenpairs per outer iteration.

Outer iteration	Number of GMRES iterations	Number of converged modes
1	7354	22
2	500	4
3	500	1
4	500	1
5	500	2
6	500	1
7	500	1
8	500	0
9	500	0
10	500	1
Total	11854	33

tion 2 that SMC may not yield an accurate approximation when nominal modes selected for ROM are spread over wider areas of spectrum, i.e. in the modal interaction areas, while the iterative preconditioned method consistently produces an accurate reduced-order model. Considering the cases where both methods provide reasonable approximation quality, the preference should be given based on computational time and the ability to scale to larger order industrial models. The algorithmic complexity of SMC depends to a larger extend on the rank of the perturbation (the number of mistuned DOF m) and the order of nominal system n. Essentially, it has the complexity $\mathcal{O}(m^3)$, which mainly accounts for the derivation of compensated basis vectors that incurs the solution of dense linear system of the order m in equation (6) of [33] and a few BLAS3 operations of the same order. The storage requirement roughly amounts to $\mathcal{O}(nm)$ that makes its scaling to larger order models practically infeasible.

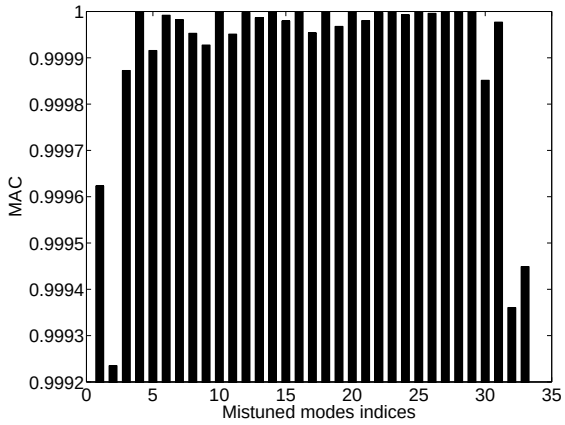

(a)

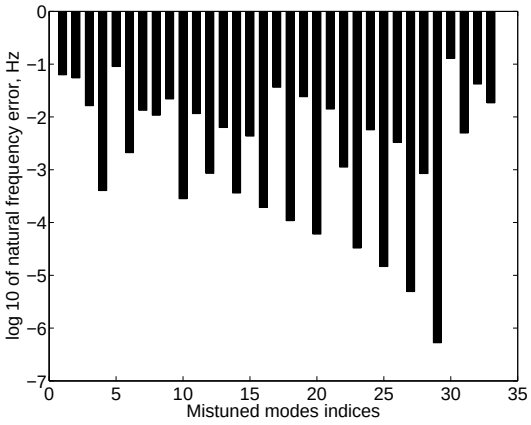

(b)

Figure 2.15 MAC ratio (a) and natural frequency error (b) between reference and approximated by the preconditioned iterative method eigenpairs for the test case model in $34 - 36$ kHz region. MAC ratio for all modes after 10 outer iterations taken is above 0.9992 and natural frequency error below 0.0002%.

Estimation of the computational cost of preconditioned iterative method is a more delicate issue because it concerns the stopping criterion for the inner solver, whose analysis is still an active area of research. Many factors should be considered before setting the optimal condition (cost of preconditioning, relative cost of inner

versus outer iterations, etc.). The performance of such methods is usually evaluated by taking into account the cost of matrix-vector multiplications, which is the most time consuming computation. Since $(\mathbf{K}, \mathbf{M})$ are sparse, the computational cost per one matrix-vector operation will depend on the type of sparsity. But the overall complexity will be essentially proportional to the total number of inner iterations. Therefore if we insure optimal/suboptimal convergence by restricting admissible perturbations it will likely to grow linearly in n. As in any iterative method, the memory requirements are also limited as n grows, they amount to storing one sparse block of $(\mathbf{K}, \mathbf{M})$, its perturbation and a few vectors of order n. Both methods incur some off-line computational effort. A set of nominal quasi-static modes is computed for SMC, those are dense blocks and therefore dependent of the structure of perturbation to be memory efficient. On the contrary, the new method requires a set of sparse preconditioners, which are completely independent of perturbation. It is likely that neither of the methods is a clear winner; SMC may be more efficient for medium size models in many situations.

2.5 Summary

In this chapter we have addressed the problem of quantifying and predicting forced response of geometrically mistuned rotors by building very compact ROM in a computationally efficient way. First we have revisited and analyzed the behavior of SMC method revealing that it is closely related to the generalized Davidson algorithm. There are all indications that from the memory efficiency and accuracy point of view it is a good choice for the moderate order FEM models under low rank localized perturbation if narrow clustered areas of spectrum are analyzed. For very large scale industrial models as well as for the areas of spectrum where multiple mode families interact, a new method is proposed. It stems from the Jacobi-Davidson algorithm implementing a number of simple heuristic strategies based on the block-circulant structure of the nominal system and assumptions on perturbation. In particular, a number of typical industrial applications of ROM are considered such as manufacturing imprecision, erosion or foreign objects damage event that constitute rather

local low rank high amplitude perturbation destroying symmetry. A set of numerical experiments have been conducted on an industrial bladed disk model. In its current form the implementation of the method demonstrates promising numerical results. Our experience indicates that the algorithm combined with proposed preconditioning scheme routinely converges to the perturbed interior eigenspace within reasonable time, provided that the perturbation is localized to a few sectors.

Chapter 3

Statistical Quantification of the Effects of Blade Geometry Modification on Mistuned Disks Vibration

3.1 Overview

The key to incorporating a computationally expensive technique into a stochastic simulation framework is to decrease the expense of analyzing systems modified in the parametric space. In this chapter we will discuss application of the methods capable of generating very compact ROM introduced in the foregoing in the stochastic simulation framework to analyze the effect of random mistuning on geometrically modified bladed disks. Small parameter variation in blade properties is added with Component Mode Mistuning method [46]. Even though the idea of using a set of normal modes of geometrically perturbed bladed disks as a nominal projection basis has been discussed by Yang et al. [41], the methods employed here give us a new tool to calculate them in a computationally efficient way by avoiding costly modal reanalysis of a full order no longer symmetrical structures. In so doing we combine the

ability to retain complexity and level of detail in both the mechanical and stochastic modeling, which involves access to perturbed system modes, realistic physical geometry variation and nonuniform random variations of individual blades at component level, with accuracy and computational efficiency.

Perhaps the best indication of the utility of the proposed analysis framework is that the problem of statistical quantification of random mistuning effects on vibration level of deterministically modified disks has been an area of active research for years. There exists extensive literature investigating the combined effects of intentional and random mistuning that has shown potential in reducing maximum blade response [66, 67, 68, 69, 70]. The results of those studies were still limited in small parameter variation assumption of the numerical tools applied. More recently, a statistical investigation of the effects of intentional and random mistuning was presented by Nikolic et al. [71]. The effect of geometry variation in that study is modeled rather as large variation of a blade component natural frequency, whereas the analysis technique employed [50] yields limited access to spacial information in the results.

In the remainder of the chapter the effectiveness of our approach is demonstrated on FE model of a bladed disk with realistic geometry. As an example, we apply a set of mesh morphing patterns to a nominal blade geometry approximating some common blade damage scenarios. The selected results clearly illustrate the importance of accurate modeling of large geometric mistuning in stochastic simulations. In particular, the geometrical perturbation patterns with similar component natural frequency variation are shown to exhibit quite different magnification levels in random response. The most significant effects of the added deterministic mistuning have been observed in high modal density areas. Perturbation patterns with heavier component mode distortion have caused significant additive magnification levels as well as lower sensitivity to additional random mistuning.

3.2 Hybrid algorithm formulation

In the following we present a computational approach for generating compact parameterized reduced order models to statistically quantify vibrational behavior of

randomly mistuned bladed disks where some blades are geometrically modified.

An important aspect of any model reduction algorithm is balancing the computational complexity of ROM construction and subsequent analysis. Therefore, it is important to make distinction between two types of different in nature perturbations, small random and deterministic geometrical mistuning. Due to the presence of geometrical mistuning our target application requires reduced order models valid over a wide range of large in norm perturbations, which normally leads to higher order models. On the other hand our goal is to achieve extremely compact ROM suitable for repeated evaluation to analyze random parameter dependent performances.

The hybrid approach that we are adopting here is relatively infrequent construction of geometrical perturbation dependent ROM basis vectors at some additional computational cost, still lower than one of a general purpose eigensolver applied to a non cyclic symmetrical full system. The cost can be amortized in later repeated Monte-Carlo simulations, where the large size of the model is more problematic since it directly affects simulation time.

To introduce random uncertainty into geometrically modified FE model we adopt the parametric probabilistic approach. In this setting system matrices can be viewed as functions of a set of random parameters collected in a vector $\boldsymbol{\theta}$. Assuming harmonic excitation the random equation of motion an undamped bladed disk structure around a static equilibrium in frequency domain can be written as

$$\big(-\omega^2\big(\widehat{\mathbf{M}} + \mathbf{M}^{\delta}(\boldsymbol{\theta})\big) + \big(\widehat{\mathbf{K}} + \mathbf{K}^{\delta}(\boldsymbol{\theta})\big)\big)\mathbf{x}(\omega, \boldsymbol{\theta}) = \mathbf{F}(\omega) \tag{3.1}$$

where $\boldsymbol{\theta}$ is a vector of random parameters and superscript δ denotes small random perturbation. Instead of defining explicit dependence of the matrix elements on random parameter vector, uncertainty in FE models is more conveniently represented in the modal space. Assuming small parameter variation around geometrically perturbed state, i.e. $\|\mathbf{K}^{\delta}(\boldsymbol{\theta})\| \ll \|\widehat{\mathbf{K}}\|$, $\|\mathbf{M}^{\delta}(\boldsymbol{\theta})\| \ll \|\widehat{\mathbf{M}}\|$, projected random system matrices can be expressed as

$$\boldsymbol{\mu}' = \widehat{\mathbf{V}}^T\widehat{\mathbf{M}}\widehat{\mathbf{V}} = I, \qquad \boldsymbol{\kappa}' = \widehat{\mathbf{V}}^T\widehat{\mathbf{K}}\widehat{\mathbf{V}} + \boldsymbol{\Lambda}^{\delta}(\boldsymbol{\theta}) = \widehat{\boldsymbol{\Lambda}} + \boldsymbol{\Lambda}^{\delta}(\boldsymbol{\theta}) \tag{3.2}$$

Note that both mass and stiffness matrix variations can be formulated in terms of random natural frequencies. Thus, experimentally measurable random modal parameters can be introduced directly into ROM. Furthermore, significantly reduced parametric space will be sampled during Monte-Carlo simulations.

In this study small random blade-to-blade variations are modeled with CMM method, see [46] for a full development. The random parameters are introduced at individual s-th blade component level using Craig-Bampton basis

$$\mathbf{U}_s = \begin{bmatrix} \widehat{\mathbf{V}}_s^B & \widehat{\mathbf{\Psi}}_s^B \\ \mathbf{0} & I \end{bmatrix} \tag{3.3}$$

where $\mathbf{U}$ is a matrix of component Craig-Bampton basis vectors, subscript b denotes blade DOF partition, superscript B designates cantilevered blade entity and $\mathbf{\Psi}$ is a matrix of boundary basis vectors defined as

$$\widehat{\mathbf{\Psi}}_s^B = -\widehat{\mathbf{K}}_{s,ii}^{-1}\widehat{\mathbf{K}}_{s,ib} \tag{3.4}$$

The blade portion of projection basis vectors $\widehat{\mathbf{V}}_s$ is expressed in the component coordinates as

$$\widehat{\mathbf{V}}_s = \mathbf{U}_s\mathbf{Q}_s \tag{3.5}$$

where modal participation factors are

$$\mathbf{Q}_s = \begin{bmatrix} \widehat{\mathbf{\Lambda}}_s^{B^{-1}}\widehat{\mathbf{V}}_{s,ii}^{B^T}\widehat{\mathbf{K}}_{s,ii}\widehat{\mathbf{V}}_{s,ii} \\ \widehat{\mathbf{V}}_{s,bb} \end{bmatrix} \tag{3.6}$$

where subscript i stands for interior DOF partition. This leads to random reduced order stiffness matrix

$$\boldsymbol{\kappa}' = \widehat{\mathbf{V}}^T\big(\mathbf{K} + \Delta\mathbf{K}\big)\widehat{\mathbf{V}} + \sum_{s=1}^{N}\mathbf{Q}_s^T\mathbf{U}_s^T\mathbf{K}_s^\delta\mathbf{U}_s\mathbf{Q}_s = \widehat{\boldsymbol{\kappa}} + \sum_{s=1}^{N}\mathbf{Q}_s^T\begin{bmatrix} \boldsymbol{\kappa}_{s,VV}^\delta & \boldsymbol{\kappa}_{s,V\Psi}^\delta \\ \boldsymbol{\kappa}_{s,\Psi V}^\delta & \boldsymbol{\kappa}_{s,\Psi\Psi}^\delta \end{bmatrix}\mathbf{Q}_s \tag{3.7}$$

In most practical situations the blade displacements at the boundary are small, therefore contributions of $\boldsymbol{\kappa}_{s,V\Psi}^\delta$ and $\boldsymbol{\kappa}_{s,\Psi\Psi}^\delta$ in equation (4.20) are negligible. Then

the term $\boldsymbol{\kappa}^{\delta}_{s,VV} = \boldsymbol{\Lambda}^{\delta,B}_{s}(\boldsymbol{\theta})$ is conveniently approximated by a diagonal matrix of random parameters

$$\boldsymbol{\kappa}' = \widehat{\boldsymbol{\kappa}} + \sum_{s=1}^{N} \widehat{\mathbf{V}}^{T}_{s,ii} \widehat{\mathbf{K}}^{T}_{s,ii} \widehat{\mathbf{V}}^{B}_{s,ii} \widehat{\boldsymbol{\Lambda}}^{B^{-1}}_{s} \boldsymbol{\Lambda}^{\delta,B}_{s}(\boldsymbol{\theta}) \widehat{\boldsymbol{\Lambda}}^{B^{-1}}_{s} \widehat{\mathbf{V}}^{B^{T}}_{s,ii} \widehat{\mathbf{K}}_{s,ii} \widehat{\mathbf{V}}_{s,ii} \tag{3.8}$$

From the above we may see that since the basis vectors do not change with system random parameters, the entire ROM update amounts to just a few BLAS 3 operations of order m.

Algorithm 2 outlines the proposed steps for the statistical analysis of random mistuning effects on geometrically modified bladed disks.

Algorithm 2 Reduced order simulation framework for statistical analysis of the random mistuning effects on geometrically modified bladed disks.

Let n be a number of geometrical mistuning motifs.
for $i = 1, \ldots, n$ **do**
  Compute corrected basis vectors $\widehat{\mathbf{V}_i}$ using geometrical mistuning pattern $(\Delta\mathbf{K}_i, \Delta\mathbf{M}_i)$.
  Project system matrices $(\mathbf{K} + \Delta\mathbf{K}_i, \mathbf{M} + \Delta\mathbf{M}_i)$ and forcing $\mathbf{F}$.
  For each sector compute participation factors $\mathbf{Q}$, component normal $\widehat{\mathbf{V}}^{B}$ and boundary $\widehat{\boldsymbol{\Psi}}^{B}$ modes.
  Let m be the number of random misalignment realizations.
  for $j = 1, \ldots, m$ **do**
    Generate j-th vector of random parameters $\Lambda^{\delta,B}(\boldsymbol{\theta})$.
    Update the projected stiffness matrix $\boldsymbol{\kappa}'$ according Eq. (4.20).
    Solve the projected system $(\boldsymbol{\kappa}', \boldsymbol{\mu}')$.
  end for
end for

3.3 Numerical examples

In this section we employ a FE model of an integrally bladed disk featuring 29 blades and 126,846 DOF, shown in Fig. 3.1. Modal characteristics of a tuned model are frequently illustrated by plotting natural frequencies versus nodal diameters,

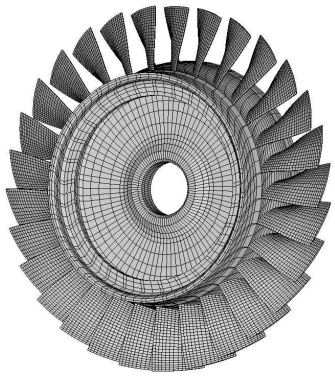

Figure 3.1 Finite element model of bladed disk.

as depicted in Fig. 3.2. In general, tuned cyclic symmetrical bladed disks exhibit

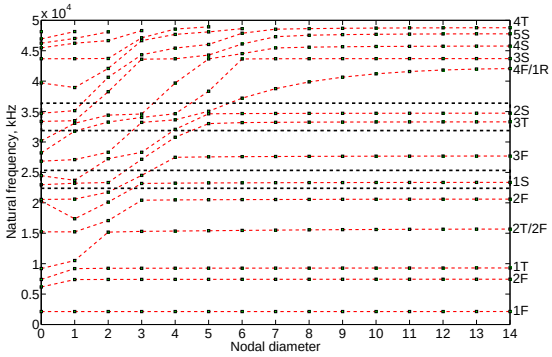

Figure 3.2 Natural frequencies versus nodal diameters.

clusters of closely spaced repeated eigenvalues, forming fundamental mode families. In absence of blade-to-blade shrouds, as in our example, they form nearly horizontal lines of blade motion dominated modes. The mode families are labeled according to blade dominant motion, where F is a flexural mode, T is a torsion mode, S is a stripe or chordwise bending mode, and R denotes a radial elongation mode. The frequency ranges containing particular mode families investigated in statistical studies further in the chapter are marked by dotted horizontal lines.

A set of geometrical mistuning patterns generated by mesh morphing the nominal blade geometry is displayed in Fig. 3.3. They approximate some typical turbine blade

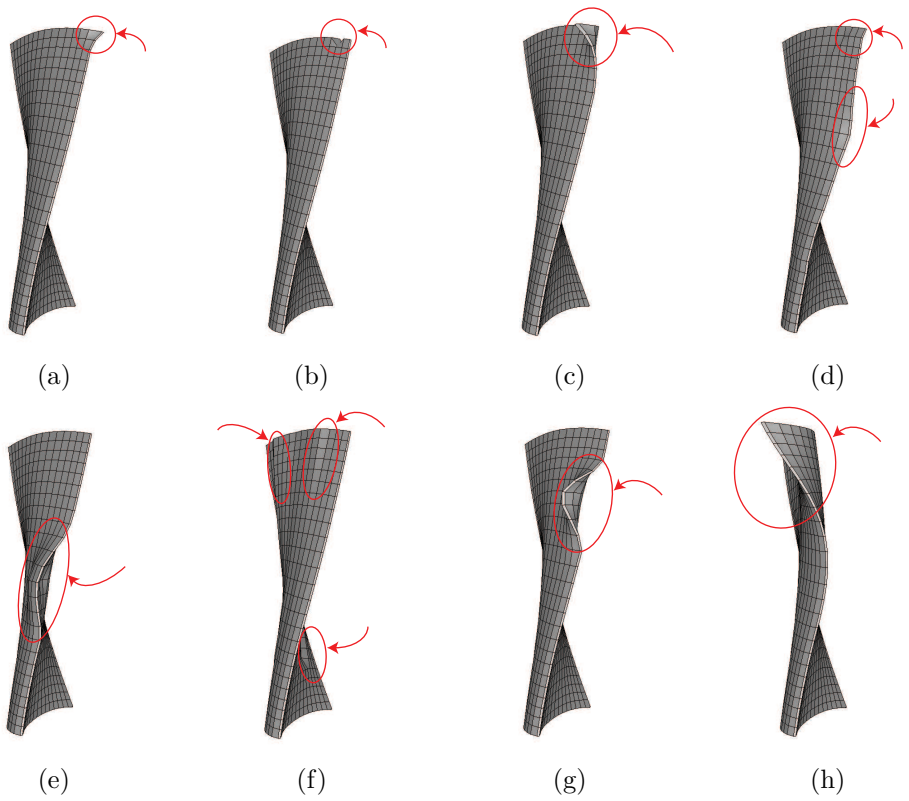

Figure 3.3 Geometrical perturbation patterns representing some typical blade damage scenarios.

distress scenarios, such as airfoil random impact damage due to FOD/DOD event Figs. 3.3(e), 3.3(g) and 3.3(h); leading edge distortion Fig. 3.3(d); blade contour change due to loss and/or build up of material Fig. 3.3(f); blade clang damage - tip curls Figs. 3.3(a), 3.3(c) and V-shaped dent Fig. 3.3(b).

Instead of characterizing the perturbation motifs by norm, rank or sparsity pattern, it is more intuitive to look at their effects on cantilevered blade eigenmodes, which are shown in Fig. 3.4. If we invoke the traveling wave interpretation, the vibra-

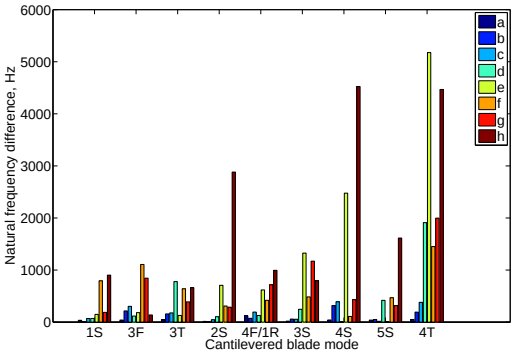

(a)

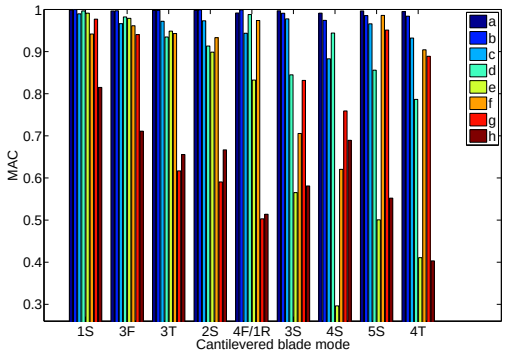

(b)

Figure 3.4 Clamped blade eigenvalue difference (a) and MAC values (b) between nominal and perturbed modes that correspond to selected blade motion dominated families of modes.

tion energy carrying waves propagate through the system in pass bands associated with the fundamental blade motion dominated mode families. Thus, the effect of a

particular perturbation pattern on the global modes within a fundamental family in most cases will be consistent with the corresponding clamped mode shapes degree of distortion and natural frequencies falling outside the pass band causing a global mode to localize around the perturbed blade.

3.3.1 Algorithm accuracy

To validate accuracy of the proposed hybrid model reduction technique free and forced response is compared against the results calculated with a full reference FE model. The nominal geometry of blades 1, 8 and 14 is modified with patterns (g), (f) and (h) correspondingly, whereas the nominal Young's modulus of the n-th blade mistuned as

$$E_n = E_0(1 + \delta_n^e) \tag{3.9}$$

where E_0 is the nominal Young's modulus and δ_n^e is a non-dimensional mistuning value. The specific pattern used in this test case is shown in Tab. 3.1. The modeling technique presented in previous section results in ROM of order 29 DOF in $14.5 - 16.5$ kHz frequency region. Traveling wave point excitation forcing is applied in the direction normal to the surface of a blade, while aerodynamic effects due to modified geometry are neglected. Structural damping loss 0.006 is used throughout all numerical examples. Figs. 3.5 and 3.6 show ROM accuracy in terms natural frequency error and MAC coefficients between normal modes, forced response results are compared in Figs. **??** and **??** in terms of the euclidian norm of maximum responding blade displacement.

Observe that the ROM in both frequency bands provide an accurate representation of mistuned system modes and as a result reliable prediction of the mistuned system's forced response as compared to the results computed by reference FE model.

3.3.2 One damaged blade example

In the following numerical experiments the geometry of a single blade of nominal disk is modified by the perturbation patterns presented in the foregoing. Fig. 3.8 shows the effects of such perturbation on the test model eigenvalues in $22 - 24.5$ kHz

Table 3.1 Eigenvalue mistuning pattern

Blade	δ_n^e	Blade	δ_n^e
1	0.05704	16	0.04934
2	0.01207	17	0.04479
3	0.04670	18	0.03030
4	-0.01502	19	0.00242
5	0.05969	20	0.01734
6	-0.03324	21	0.02919
7	-0.00078	22	-0.00328
8	-0.01688	23	0.00086
9	0.00242	24	-0.03654
10	-0.02747	26	-0.03631
11	-0.03631	26	-0.01665
12	-0.03570	27	0.00783
13	-0.03631	28	-0.01169
14	-0.03631	29	-0.01332
15	0.00242		

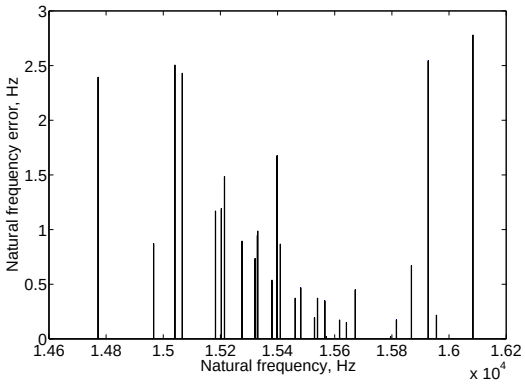

Figure 3.5 Natural frequency errors calculated with reference and ROM models in $14.5 - 16.5$ kHz region.

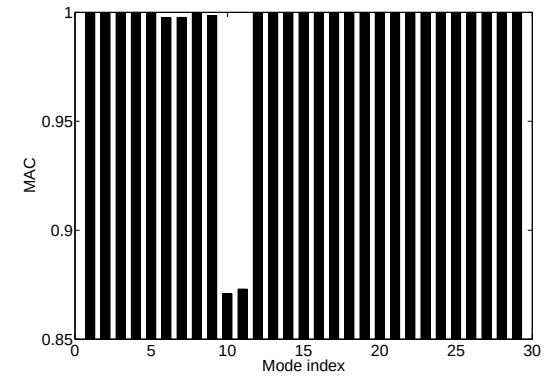

(a)

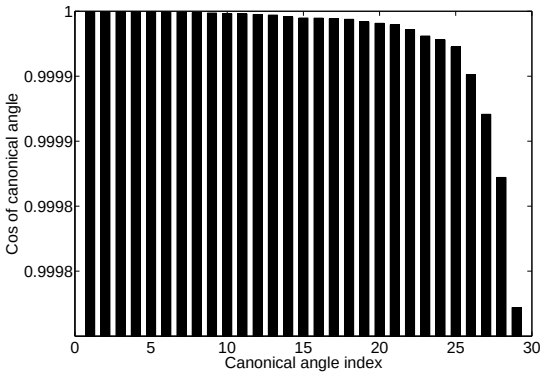

(b)

Figure 3.6 MAC values between modeshapes (a) and cosine of canonical angles between corresponding eigenspaces (b) calculated with reference and ROM models in $14.5 - 16.5$ kHz region. Note that low MAC values is the result of cross contamination of two eigenmodes close in frequency, whereas the entire eigenspace approximated by ROM is accurately predicted as indicated by canonical angles.

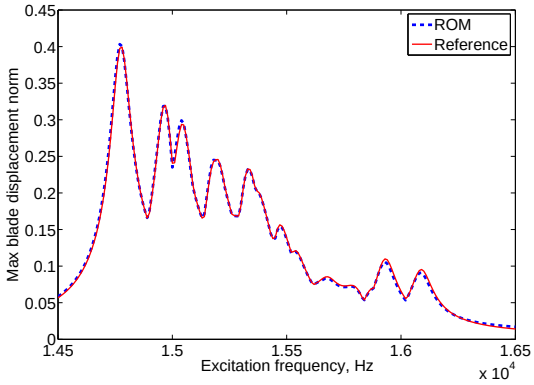

(a)

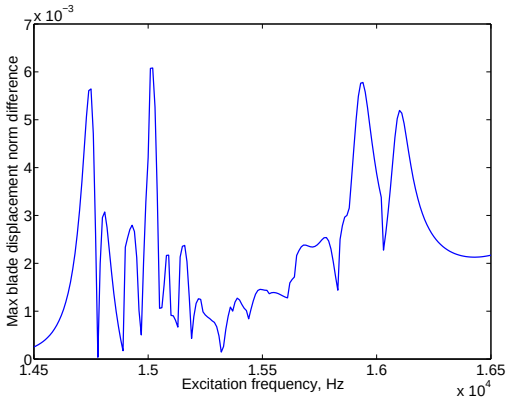

(b)

Figure 3.7 Comparison of envelops of maximum forced response calculated with reference and ROM models obtained with engine order 2 excitation in $14.5 - 16.5$ kHz region (a) and their difference (b).

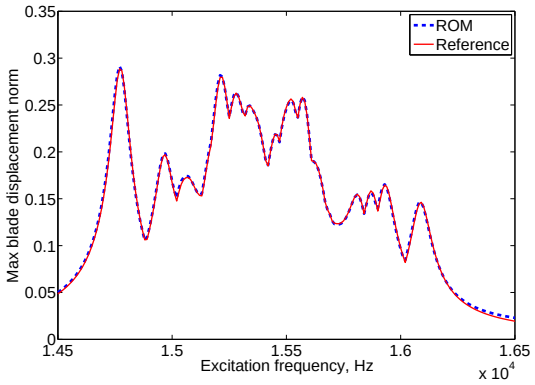

(a)

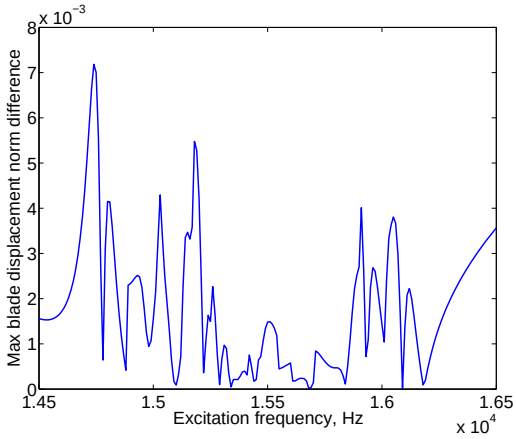

(b)

Figure 3.8 Comparison of envelops of maximum forced response calculated with reference and ROM models obtained with engine order 5 excitation in $14.5 - 16.5$ kHz region (a) and their difference (b).

frequency band. It is interesting to note that large mistuning limited to a single

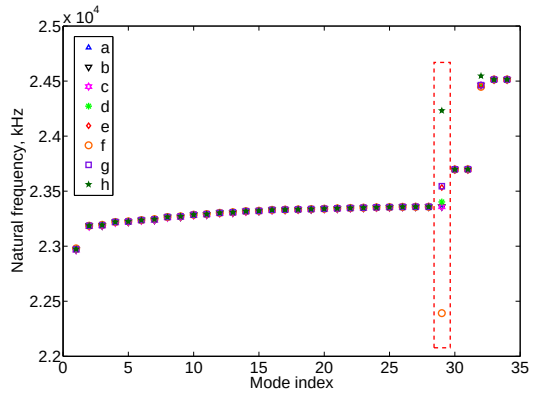

(a)

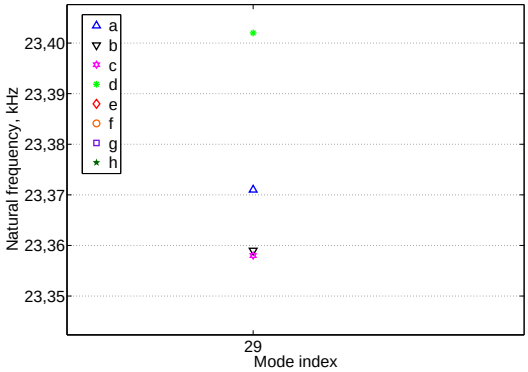

(b)

Figure 3.9 The effect of perturbation of a single blade on system eigenvalues belonging to 1S fundamental mode family (a), detailed view of 29th eigenvalue (b). Note the appearance of "rogue" blade modes, in particular a perturbed member of harmonic 14 23,358 Hz doublet marked by the dashed line box.

blade significantly modifies only few natural frequencies. Thus, every geometrical mistuning pattern except (c) affects 23,358 Hz harmonic 14 eigenmode. The change in eigenvalue is in accordance with the degree of localization of corresponding mode, as shown in Fig. 3.9. The mode shapes corresponding to "rogue" natural frequencies 23,545 Hz, 24,232 Hz and 22,392 Hz of patterns (g), (h) and (f) exhibit the same

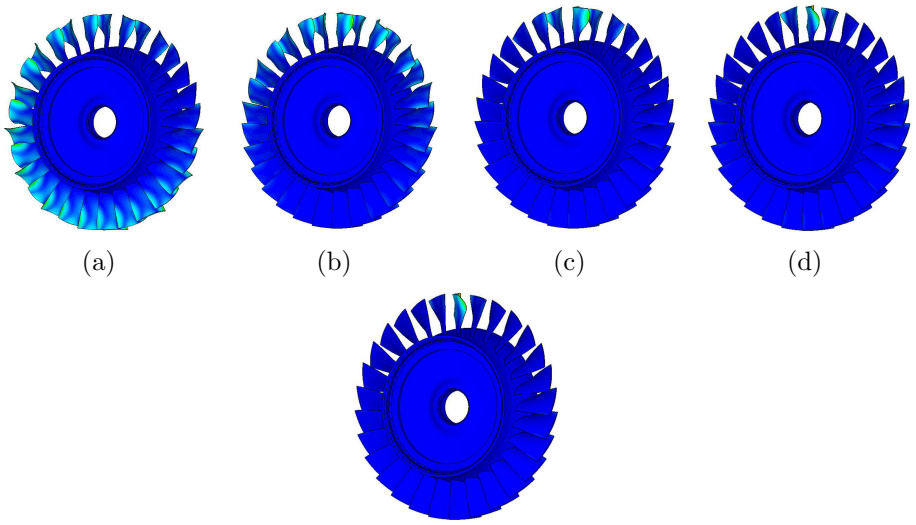

(a) (b) (c) (d)

(e)

Figure 3.10 The effect of perturbation of a single blade on system eigenvector corresponding to harmonic 14 23,358 Hz eigenvalue. Nominal mode shape (a), perturbed mode shape corresponding to 23,359 Hz eigenvalue of pattern Fig. 3.3(b) (b), 23,371 Hz of pattern Fig. 3.3(a) (c), 23,402 Hz of pattern Fig. 3.3(d) (d) and highly localized perturbed mode shape corresponding to 23,532 Hz eigenvalue of patterns Fig. 3.3(e) (e).

strong localized behavior as one depicted in Fig. 3.9(e).

For forced response statistical analysis of geometrically mistuned disks we employ ROM of order 34 DOF in $22 - 24.5$ kHz frequency region and 60 DOF in $32 - 37$ kHz band. The statistical results for all geometrical mistuning patterns are obtained through 100 Monte-Carlo simulations with standard deviation of normally distributed small mistuning parameters ranging from 0.1 to 5 percent applying Weibull hypothesis of response statistics distribution. The latter has been employed by Bladh et al. [45] based on the theory of the statistics of extremes. It has been reasoned that the distribution of the maximum blade amplitudes for a population of mistuned rotors will tend to one of three extreme value distributions, and since the response is bounded, the distribution will asymptotically approach the Weibull distribution.

The 99.9th percentile values and differences of the amplitude magnification factor between nominal disk and geometrically modified ones subject to small random mistuning are shown in Figs. 3.10, 3.11, 3.19 and 3.13 as a function of mistuning strength for three engine order excitation cases. The results indicate that with introduction of blade damage we observe increase in amplification factor at lower standard deviation levels of small random mistuning compared to undamaged randomly mistuned system. As small mistuning level grows, the additive contribution of large deterministic perturbation becomes less pronounced, for some patterns and engine order excitations being negative. Comparing these plots, we also observe that higher engine order excitation response show lower levels of additional amplification. Clearly, the difference around the peak amplitude magnification caused by random mistuning is consistently being below 10 percent of maximum nominal response. In general, the increase in amplification is more or less in agreement with the degree of distortion of corresponding clamped modes. Exceptions are observed for pattern (c) in Figs. 3.11(a) and 3.11(c), as well as for pattern (h) in Fig. 3.13. Figs. 3.14 and 3.15 demonstrate selected random frequency response functions for patterns (c) and (h) in $22 - 22.4$ kHz band under EO1 excitation. Fig. 3.16 depicts random FRF for pattern (h) in $32 - 37$ kHz frequency range excited by EO4. In Fig. 3.14 note that pattern (c) does not generate any highly distorted localized "rogue" mode at 0 per-

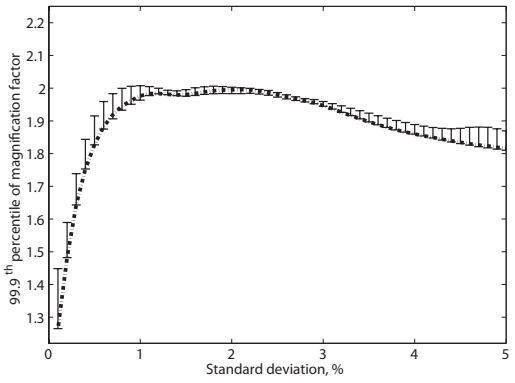

(a)

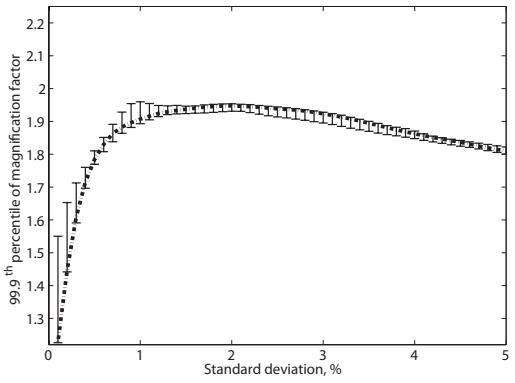

(b)

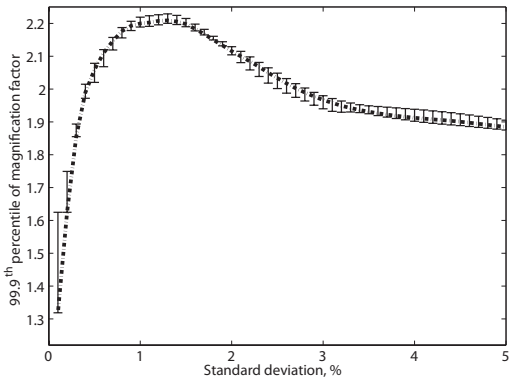

(c)

Figure 3.11 The 99.9th percentile magnification factor of nominal disk in $22-24.5$ kHz band obtained with EO1 (a), EO2 (b) and EO3 (c). The geometrical perturbation contribution to random response (maximum and minimum of all patterns) is marked with error bars.

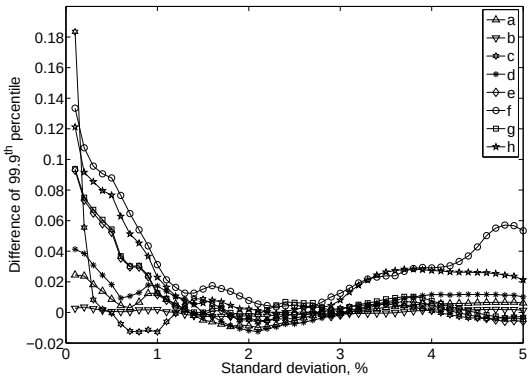

(a)

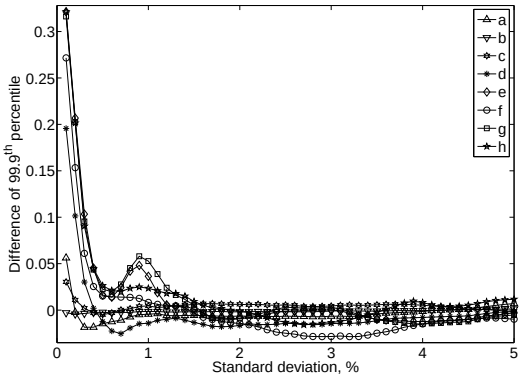

(b)

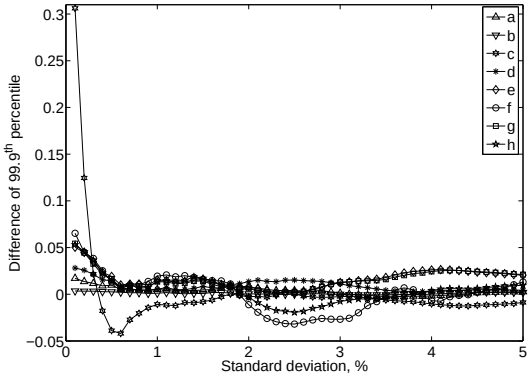

(c)

Figure 3.12 Magnification factor difference (99.9th percentile) between perturbed and nominal disks in $22-24.5$ kHz band obtained with EO1 (a), EO2 (b) and EO3 (c).

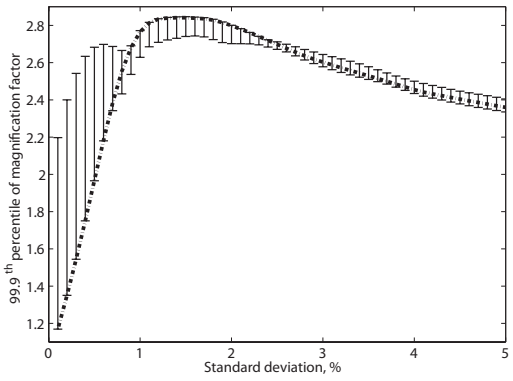

(a)

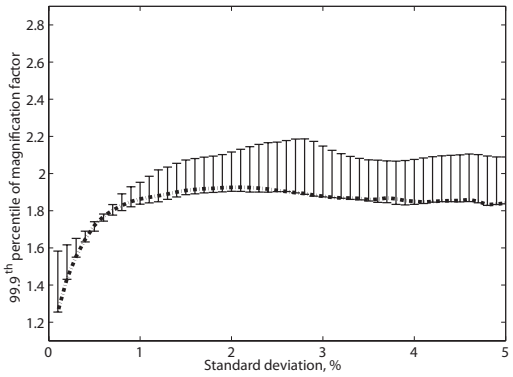

(b)

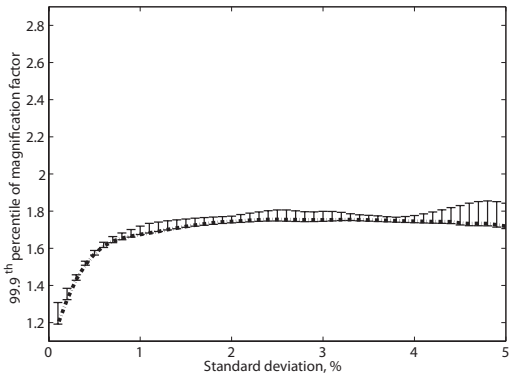

(c)

Figure 3.13 The 99.9th percentile magnification factor of nominal disk in $32-37$ kHz band obtained with EO1 (a), EO4 (b) and EO12 (c). The geometrical perturbation contribution to random response (maximum and minimum of all patterns) is marked with error bars.

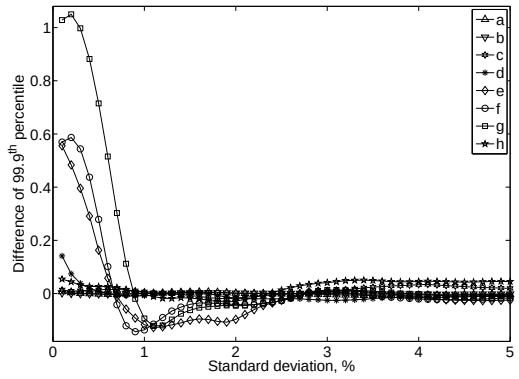

(a)

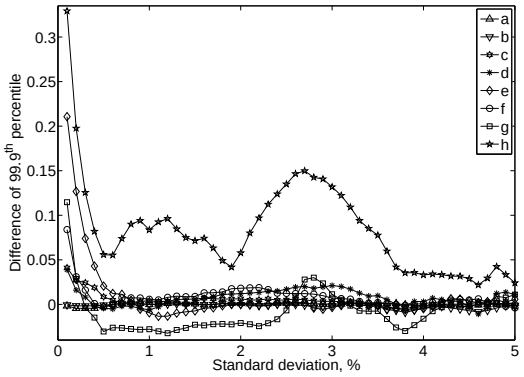

(b)

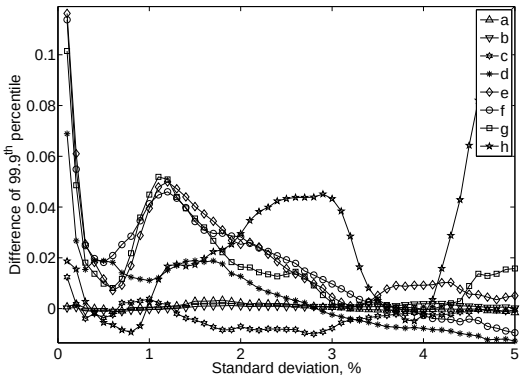

(c)

Figure 3.14 Magnification factor difference (99.9th percentile) between perturbed and nominal disks in $32 - 37$ kHz band obtained with EO1 (a), EO4 (b) and EO12 (c) excitation.

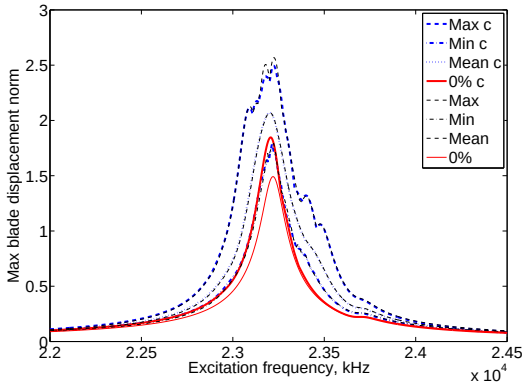

(a)

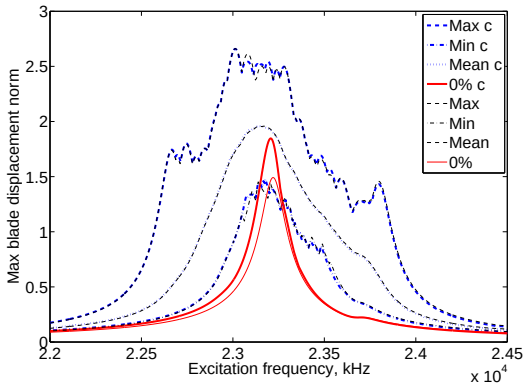

(b)

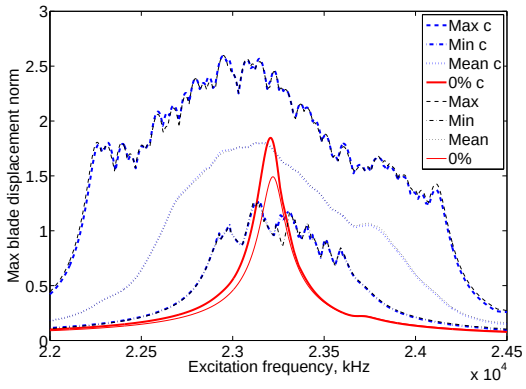

(c)

Figure 3.15 Envelops of maximum forced response obtained with EO1 excitation in $22 - 25.5$ kHz band for geometrically mistuned by pattern Fig. 3.3(c) system subjected to small mistuning with standard deviation δ varying from 0.5% (a), 1.5% (b) to 2.5% (c) showing maximum, mean and minimum response out of 100 random realizations. The system response without geometrical mistuning is depicted in thinner line.

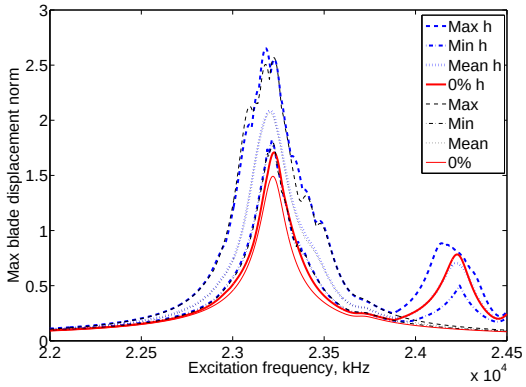

(a)

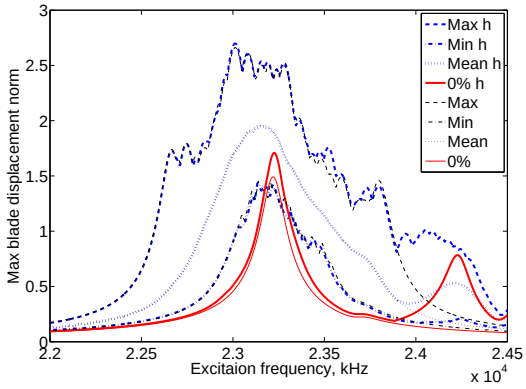

(b)

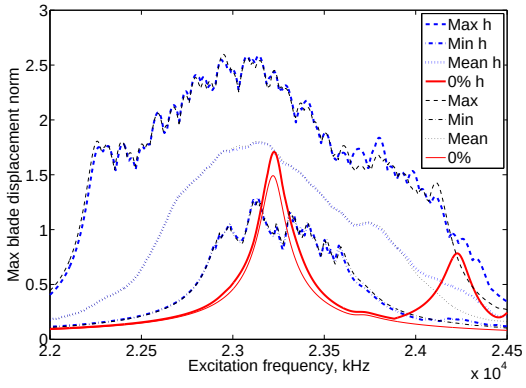

(c)

Figure 3.16 Envelops of maximum forced response obtained with EO1 excitation in $22 - 25.5$ kHz band for geometrically mistuned by pattern Fig. 3.3(h) system subjected to small mistuning with standard deviation δ varying from 0.5% (a), 1.5% (b) to 2.5% (c) showing maximum, mean and minimum response out of 100 random realizations. The system response without geometrical mistuning is depicted in thinner line.

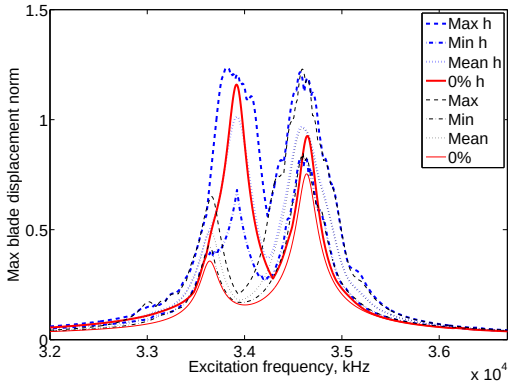

(a)

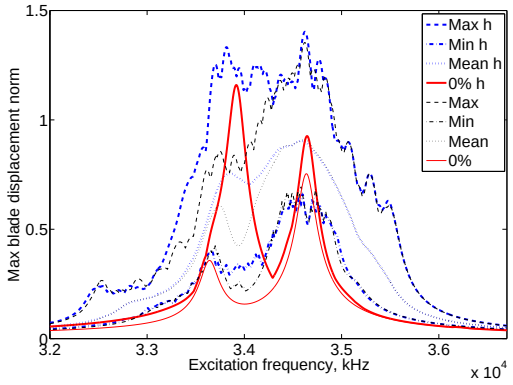

(b)

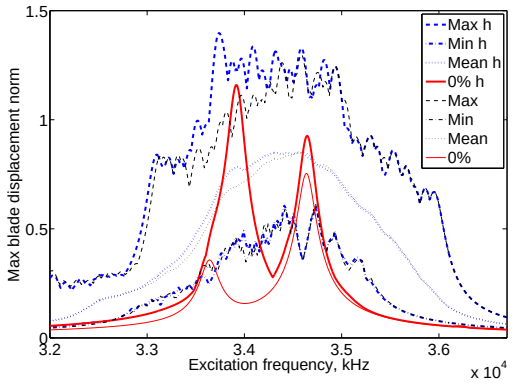

(c)

Figure 3.17 Envelops of maximum forced response obtained with EO4 excitation in $32 - 37$ kHz band for geometrically mistuned by pattern Fig. 3.3(h) system subjected to small mistuning with standard deviation δ varying from 0.5% (a), 1.5% (b) to 2.5% (c) showing maximum, mean and minimum response out of 100 random realizations. The system response without geometrical mistuning is depicted in thinner line.

cent mistuning. All the members of the fundamental family remain quasi-periodic to some degree being contaminated by additional harmonic content, whereas maximum response is observed at main resonance frequency. The pattern incidentally generates highest additive magnitude amplification in $22 - 24.5$ kHz area for EO1 and EO3 at low levels of random mistuning, Figs. 3.11(a) and 3.11(c). The reason for that special behavior is the fact that for EO1 and EO3 this particular frequency region exhibits two eigenfrequency veerings. This implies disk-blade modal interaction and hence better transfer of vibration energy between adjacent blades through the disk at closely clustered nearly unperturbed blade eigenfrequencies. As random mistuning is increased, the FRF curves become visually indistinguishable from geometrically unperturbed case indicating that from 0.3 percent of random mistuning that particular blade damage pattern does not affect the response magnification factor.

Fig. 3.15 shows the random FRF of pattern (h) in the same frequency band. In contrast, more serious damage to blade manifests itself as a heavily distorted localized to that blade mode seen as an extra resonance peak at 24,232 Hz at 0 percent of random mistuning excited by all engine orders. Other perturbed system modes stay quasi-periodic with slight degree of contamination by different wave numbers, which translates into forced response amplification with respect to nominal system, still found at the fundamental family resonance frequency. The remaining perturbation patterns follow similar trend in that frequency area, namely exhibiting an extra resonance peak pending on degree of mode distortion and response amplification around main fundamental family frequency. The effect of damage is visible at all levels of random mistuning as an increase in random response around natural frequency of the highly localized mode.

Finally, Fig. 3.16 depicts random system response to EO4 excitation for pattern (h) in higher modal density $32 - 37$ kHz zone. Exceptional is the fact that the additional resonance peak appeared in the response of the mistuned system around 33,921 Hz at 0 percent of small mistuning is larger than the fundamental family peaks even with growing random mistuning level. Thus, the maximum amplification occur at nearly 1000 Hz lower frequency than nominal mistuned case. Note also that the "rogue" eigenvalue displays higher sensitivity to additional random mistuning

spreading in frequency faster than its fundamental family counterparts.

The variability of magnification factor can also be illustrated by the shape of PDF in Fig. 3.17. PDFs of most patterns and frequency areas where "rogue" mode resonance does not dominate random FRF show higher magnitude and wider distribution at low levels of small mistuning gradually converging to nominal case, as shown in Figs. 3.17(a) and Figs. 3.17(b). Fig. 3.17(c) illustrates the extreme case of pattern (h) in $32 - 37$ kHz band. Note very narrow distribution centered around higher magnitude amplification level from 0.1 to 0.5 percent indicating lower variability and consequently lower sensitivity with respect to additional random mistuning. On the other hand the distribution function significantly widens at 2 to 5 percent levels much greater variability of response levels as opposed to geometrically unmodified mistuned system.

The results demonstrating spatial distribution of maximum responding blade are presented in Figs. 3.18. As anticipated, in the nominal design undergoing random mistuning all blades are more or less equally likely to experience maximum response, whereas even perturbation with pattern (a), which showed minimum additional amplification, brings about spatial deterministic regularity in the random response. Note that some blades, not necessarily the damaged one, are more likely to have larger response than the others. For patterns with heavier component mode distortion we observe that the affected by perturbation blades dominate in maximum response statistics.

3.3.3 Multiple damaged blades test case

In the next study we present the test case where more than one blade sustain significant geometry change. The combinations of patterns can be found in Tab. 3.2. Results shown in Figs. 3.19 and 3.20 correspond to 99.9th percentile values of the magnification factor and differences between nominal disk and geometrically modified ones both subject to various levels of small random mistuning. Comparing these plots to a single blade damage scenario one can observe a noticeable increase in magnification levels. Mistuning combination 3 generates additive magnification

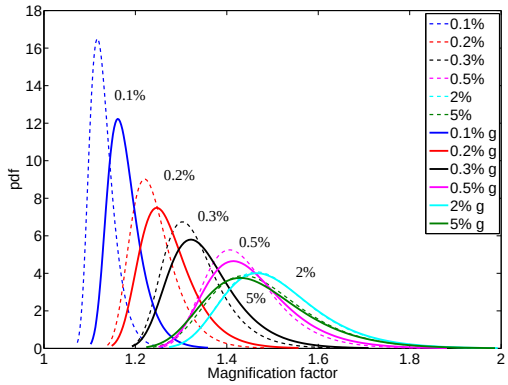

(a)

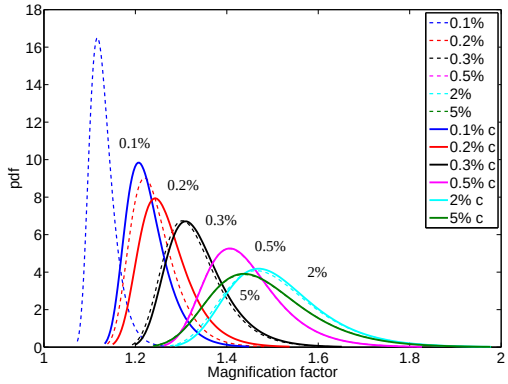

(b)

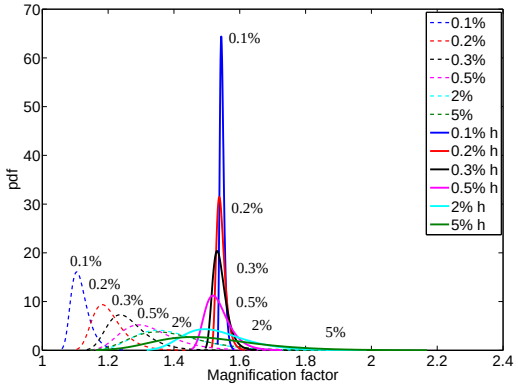

(c)

Figure 3.18 Comparison of probability density functions of magnification factors for perturbed and nominal disks pattern Fig. 3.3(g) in $22-24.5$ kHz with EO1 excitation (a), pattern Fig. 3.3(c) in $22-24.5$ kHz with EO1 excitation (b) and pattern Fig. 3.3(h) in $32-37$ kHz with EO4 excitation (c).

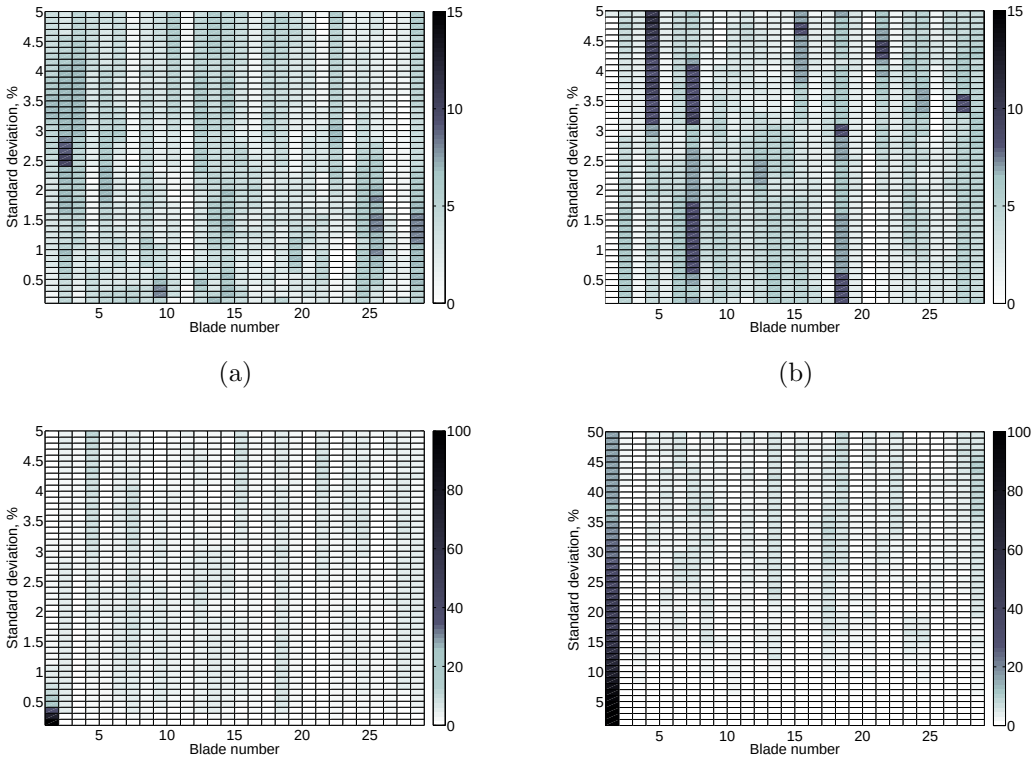

Figure 3.19 Comparison of maximum responding blade histograms in $22-24.5$ kHz region with EO1 excitation: nominal mistuned disk (a), pattern Fig. 3.3(a) (b), pattern Fig. 3.3(c) (c) and pattern Fig. 3.3(h) in $32-37$ kHz region with EO4 excitation (d).

Table 3.2 Combinations of mistuning patterns in multiple blade damage scenario.

Combination	Patterns distribution, sector(pattern)
1	1(h),26(g),27(f)
2	1(g),8(f),14(h)
3	1(h),7(h),12(f),18(e),21(h),26(e)
4	3(h),19(f),23(e)
5	5(h),6(h),16(g),17(e),25(f)

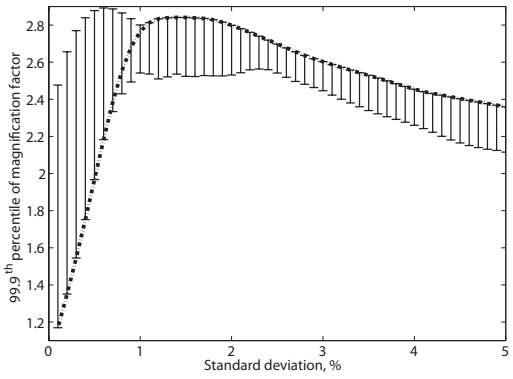

(a)

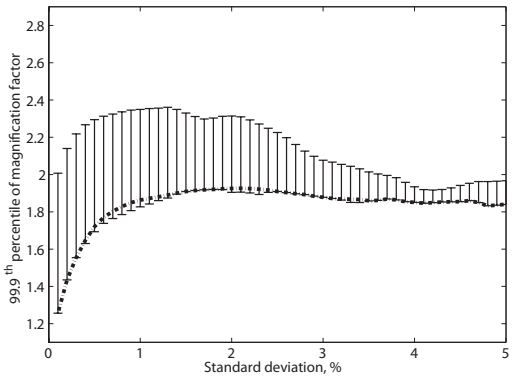

(b)

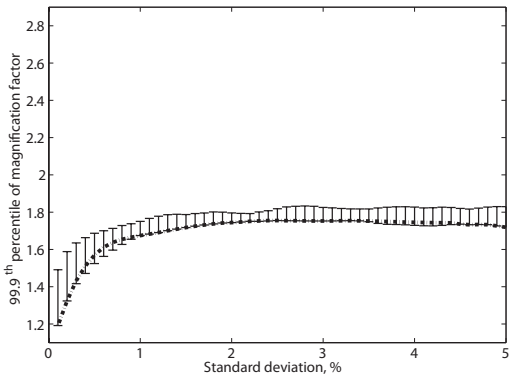

(c)

Figure 3.20 The 99.9th percentile magnification factor of nominal disk in $32-37$ kHz band obtained with EO1 (a), EO4 (b) and EO12 (c). The geometrical perturbation contribution to random response (maximum and minimum of all combinations of patterns) is marked with error bars.

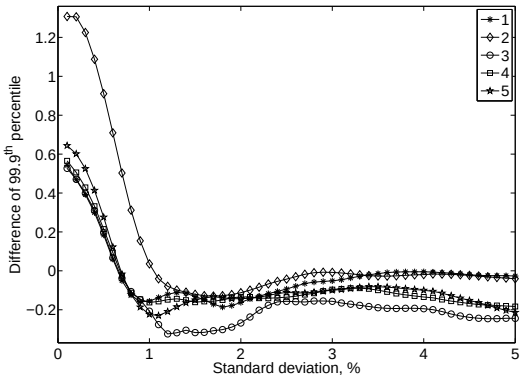

(a)

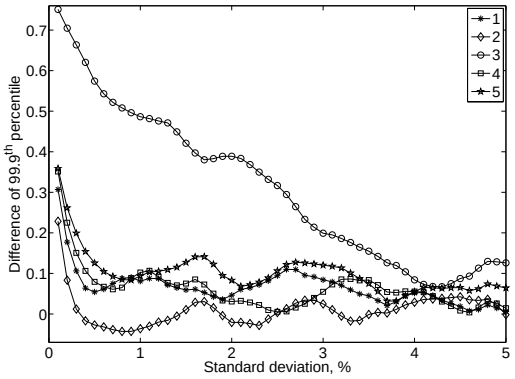

(b)

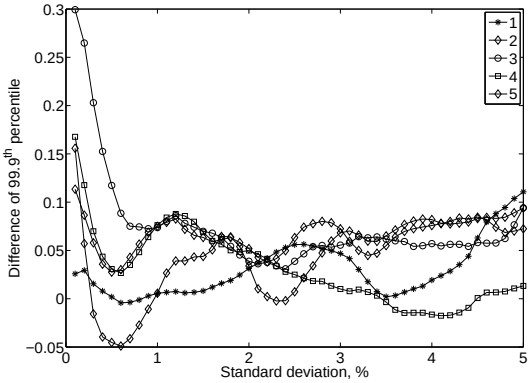

(c)

Figure 3.21 Magnification factor difference (99.9th percentile) between perturbed and nominal disks in $32 - 37$ kHz band obtained with EO1 (a), EO4 (b) and EO12 (c) excitation.

factor over 50 percent of maximum nominal case level under EO4 excitation order. The envelop of maximum random frequency response for that combination is shown in Fig. 3.21. Likewise, we observe an extra resonance peak appeared in the response around 33,900 Hz at 0 percent of mistuning, which dominates over the fundamental family peaks. However, this time several distorted "rogue" localized to damaged blades modes are responsible for that highest peak. In view of Figs. 3.21(b) and 3.21(c) it is significant that the maximum random response of geometrically modified system does not behave the same way as the nominal mistuned case spreading in frequency considerably faster as the random mistuning level grows.

3.4 Summary

This chapter presents a stochastic simulation framework for quantification of random response of geometrically modified bladed disks. The proposed hybrid approach involves relatively infrequent computation of a small set of basis vectors corrected for each deterministic geometry change, which yields a very compact ROM. The latter is used in repetitive Monte-Carlo simulations, where random parameter variation in blade properties is introduced in modal space at a component level. That leads quite naturally to a very attractive numerical tool combining both accuracy and level of detail with computational efficiency. Its effectiveness and precision have been demonstrated through a series of numerical examples on FE model of an industrial bladed disk with some blades featuring significant geometry change due to practical damage patterns. The importance of accurate modeling of geometrical mistuning has been emphasized through a selection of damage patterns with similar component natural frequencies variations that exhibit markedly different response levels. Rather surprisingly, in the majority of the analyzed situations large geometric mistuning has not led to significant additional response magnification beyond very low levels of random mistuning. The worst case has been identified in the high modal density area where "rogue" blade peaks found to be dominant. They are largely responsible for considerable additive magnification factors beyond low levels of random mistuning as compared to nominal case meanwhile exhibiting lower sensitivity to additional

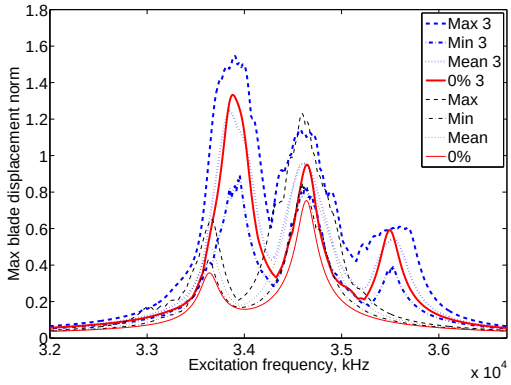

(a)

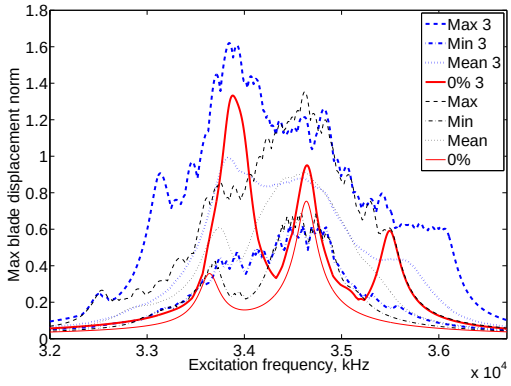

(b)

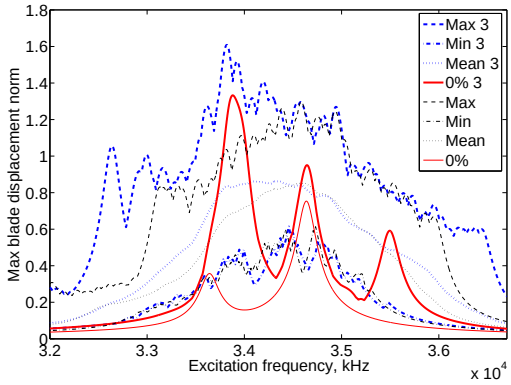

(c)

Figure 3.22 Envelops of maximum forced response obtained with EO4 excitation in 32−37 kHz band for geometrically mistuned by combination 3 system subjected to small mistuning with standard deviation δ varying from 0.5% (a), 1.5% (b) to 2.5% (c) showing maximum, mean and minimum response out of 100 random realizations. The system response without geometrical mistuning is depicted in thinner line.

random mistuning.

Chapter 4

Parameterized Reduced Order Modeling of Misaligned Stacked Disks Rotor Assemblies

4.1 Overview

Flexible rotor-bearing systems show significant sensitivity in overall vibration behavior to system uncertainties. One important issue arising in turbine engine design is quantification of the effects of stacked disks misalignment on the system bending dynamics.

Current trends towards lighter more flexible rotors operating at supercritical speeds require detailed and reliable representation of complex dynamics in order to have a better agreement between simulation and experimental results. $1D$ rotordynamic models enjoy considerable success being simple and accurate in most practical situations. However, as a result of unconventional geometry featuring thin-walled tubular cross sections and flexible bladed disks full three-dimensional modeling of such rotors is unavoidable [72, 73, 74, 75].

For problems of practical interest, the computational effort required to model the rotor continuum using $3D$ FE formulation is substantial. Both the large dimen-

sion of the system and the large computational requirements render such models inadequate for repeated calculations necessary to examine possible combinations of the uncertainties at various operating conditions. Moreover, model parameters are often functions of rotational speed adding considerably to the degree of complexity. To facilitate the analysis, it is essential to have accurate low-order models that are significantly faster to solve than the original full model.

In fact, there is an extensive literature in the area of model order reduction for rotordynamics problems. The application of $2D$ Fourier axisymmetric FE was demonstrated in [76], whereas $3D$ solid FE models featuring cyclic symmetry has been reported in [72, 77]. Both approaches reduce the size of original problem by truncating higher order harmonics. Many reduction techniques are derived using a projection-based framework, in which the system variables and governing equations are projected onto low dimensional subspaces. These methods include balanced truncation [78, 79, 80] and projection into modal space [77, 81, 79, 82, 83]. The modal projection is often combined with Guyan reduction or a component mode synthesis technique.

In the context of parameter-dependent systems, the resulting system is of lower order, but it is not necessarily computationally efficient to update the reduced model once parameters change. The existing techniques developed for non-rotating structures analysis, for the most part, are straightforward extensions of the modal projection based order reduction algorithms [39]. Building a projection space assuming small perturbations around a nominal point is not always appropriate as is the case with uncertainties in geometry [34].

To address the challenges, we introduce a novel procedure suitable for repeated model evaluation that achieves decent approximation properties while retaining computational efficiency. The nominal rotor is discretized with 3D solid FE accounting for rotational inertia effects in body attached frame for a set of selected rotation speeds. Cyclic symmetry approach enables us to manipulate with FE model involving only one elementary sector per stage. At each individual stage the system equations are reduced through truncation of higher order harmonics.

The dynamic effects of disk misalignment are introduced through multiplicative

perturbation to stiffness matrix in Fourier domain accounting for non-isotropic stiffness variation plus centrifugal excitation vector that includes static and dynamic imbalance forces. Both are dependent on a small set of parameters modeling the interstage geometry uncertainties. Perturbation of stiffness matrix is a major difference with reported misalignment modeling methods [84, 85, 86, 87, 88] where "rotor-bow" effects are simulated with equivalent forces and moments applied to the nodes of nominal model.

Practical experience indicates that, with the assumption of small in norm perturbations and rotational periodicity of individual stages, the flexural behavior of misaligned rotor can be studied by retaining only first three harmonics. To couple misaligned bladed disks our algorithm employs the multi-stage cyclic symmetry technique developed in [89]. Finally, we will discuss a computational strategy of reducing large condition number of nominal uncoupled system, which significantly simplifies and accelerates repeated solution of perturbed system.

4.2 Background

4.2.1 3D rotordynamics equations of motion

Consider a FE model of a lightly damped rotating structure. The equations of motion in the body fixed coordinate frame assuming constant angular velocity can be expressed as [72, 74]

$$[\mathbf{K}_E + \mathbf{K}_G(\mathbf{u}_S) - \mathbf{K}_C(\Omega^2)]\mathbf{u}_S = \mathbf{F}_C(\Omega^2) \tag{4.1}$$

$$\mathbf{M}\ddot{\mathbf{u}}_D + \mathbf{C}(\Omega)\dot{\mathbf{u}}_D + [\mathbf{K}_E + \mathbf{K}_G(\mathbf{u}_S) - \mathbf{K}_C(\Omega^2)]\mathbf{u}_D = \mathbf{F} \tag{4.2}$$

where $\mathbf{M} \in \mathbb{R}^{n\times n}$ is a symmetric positive definite mass matrix, $\mathbf{K}_E \in \mathbb{R}^{n\times n}$ is a symmetric semi-definite elastic stiffness matrix. Two rotational aspects are taken into account. The Coriolis forces proportional to the velocities are introduced through a skew-symmetric positive semi-definite pseudo-damping matrix $\mathbf{C} \in \mathbb{R}^{n\times n}$. The centrifugal forces generate spin softening matrix $\mathbf{K}_C(\Omega^2) \in \mathbb{R}^{n\times n}$ and a geometric

stiffness matrix $\mathbf{K}_G(\mathbf{u}_S) \in \mathbb{R}^{n\times n}$ representing stress stiffening effects. $\mathbf{F}_C \in \mathbb{R}^n$ denotes the nodal centrifugal forcing vector, Ω is the rotational speed. $\mathbf{u}_S \in \mathbb{R}^n$ is the static equilibrium position of the structure under centrifugal loading found by solving nonlinear equation (4.1), $\mathbf{u}_D \in \mathbb{R}^n$ is the small dynamic displacement around the static equilibrium and $\mathbf{F} \in \mathbb{R}^n$ is a harmonic excitation vector. Note the dependence of system matrices on rotor speed Ω.

Nominal bladed disks-shaft assemblies at each individual stage feature rotational periodicity that in any cylindrical coordinate system generate block-circulant matrices [17]. Using that property, we can decouple both static Eq. (4.1) and dynamic Eq. (4.2) equations at an individual stage level into $N/2$ smaller problems by applying discrete Fourier transform

$$(\mathbf{W}^* \otimes \boldsymbol{I})[\mathbf{K}_E + \mathbf{K}_G(\mathbf{u}_S) - \mathbf{K}_C(\Omega^2)](\mathbf{W} \otimes \boldsymbol{I})(\mathbf{W}^* \otimes \boldsymbol{I})\mathbf{u}_S = (\mathbf{W}^* \otimes \boldsymbol{I})\mathbf{F}_C(\Omega^2) \quad (4.3)$$

$$\begin{aligned}&(\mathbf{W}^* \otimes \boldsymbol{I})\mathbf{M}(\mathbf{W} \otimes \boldsymbol{I})(\mathbf{W}^* \otimes \boldsymbol{I})\ddot{\mathbf{u}}_D + (\mathbf{W}^* \otimes \boldsymbol{I})\mathbf{C}(\Omega)(\mathbf{W} \otimes \boldsymbol{I})(\mathbf{W}^* \otimes \boldsymbol{I})\dot{\mathbf{u}}_D + \\ &(\mathbf{W}^* \otimes \boldsymbol{I})[\mathbf{K}_E + \mathbf{K}_G(\mathbf{u}_S) - \mathbf{K}_C(\Omega^2)](\mathbf{W} \otimes \boldsymbol{I})(\mathbf{W}^* \otimes \boldsymbol{I})\mathbf{u}_D = (\mathbf{W}^* \otimes \boldsymbol{I})\mathbf{F}\end{aligned} \quad (4.4)$$

where the discrete Fourier transform expressed in matrix form is defined as

$$\mathbf{W} = \frac{1}{\sqrt{N}}\begin{bmatrix} 1 & 1 & \cdots & 1 \\ 1 & e^{-\mathrm{j}\frac{2\pi}{N}} & \cdots & e^{-\mathrm{j}\frac{2(N-1)\pi}{N}} \\ 1 & e^{-\mathrm{j}\frac{4\pi}{N}} & \cdots & e^{-\mathrm{j}\frac{4(N-1)\pi}{N}} \\ \vdots & \vdots & \ddots & \vdots \\ 1 & e^{-\mathrm{j}\frac{2(N-1)\pi}{N}} & \cdots & e^{-\mathrm{j}\frac{2(N-1)(N-1)\pi}{N}} \end{bmatrix}$$

here N denotes the number of elementary sectors. The system equations of motion then become

$$[\widetilde{\mathbf{K}}_{hE} + \widetilde{\mathbf{K}}_{hG}(\tilde{\mathbf{u}}_{hS}) - \widetilde{\mathbf{K}}_{hC}(\Omega^2)]\tilde{\mathbf{u}}_{hS} = \tilde{\mathbf{F}}_{hC}(\Omega^2) \quad (4.5)$$

$$\widetilde{\mathbf{M}}_h\ddot{\tilde{\mathbf{u}}}_{hD} + \widetilde{\mathbf{C}}_h(\Omega)\dot{\tilde{\mathbf{u}}}_{hD} + \left[\widetilde{\mathbf{K}}_{hE} + \widetilde{\mathbf{K}}_{hG}(\tilde{\mathbf{u}}_{hS}) - \widetilde{\mathbf{K}}_{hC}(\Omega^2)\right]\tilde{\mathbf{u}}_{hD} = \tilde{\mathbf{F}}_h \quad (4.6)$$

where subscript h describes the association to a Fourier harmonic. In most practical situations one can strongly reduce the order of the problem by selecting first harmonics $h = 0$ and $h = 1$ ($h = 0$ corresponds to torsion and longitudinal displacements, $h = 1$ to bending). Truncated higher order harmonics are mainly responsible for disk dominated motion or for deformation of shaft cross section having little to no effect on the global bending behavior of the rotor assembly [74].

4.2.2 Modeling of disk misalignment

Consider a multi-stage system of S cyclic symmetrical structures sharing the same axis of rotational symmetry. As it is known, the result of changes due to manufacturing imperfections in the geometry on inter-stage interfaces may result in static or dynamic imbalances in rotor plus non-isotropic variations of stiffness [90]. Assuming that other imperfections of each stage are negligible, i.e. they preserve rotational symmetry, we can describe these effects by orientation and position of an individual stage given by an arbitrary rotation in terms of two Euler angles θ_x, θ_y and two offsets $\Delta x, \Delta y$, as shown in Fig. 4.1.

Thus the perturbed position of a node that belong to n_{th} sector of s_{th} stage in cylindrical coordinate system in which the Z-axis is coincident with the shaft axis of rotation can be computed in three steps as follows

$$\begin{aligned}
\begin{Bmatrix} x \\ y \\ z \end{Bmatrix} &= \mathbf{R}_z \begin{Bmatrix} r \\ \theta \\ z \end{Bmatrix} \\
\begin{Bmatrix} x' \\ y' \\ z' \end{Bmatrix} &= \mathbf{R}_y \mathbf{R}_x \begin{Bmatrix} x + \Delta x \\ y + \Delta y \\ z \end{Bmatrix} \\
\begin{Bmatrix} r' \\ \theta' \\ z' \end{Bmatrix} &= \mathbf{R}_z^T \mathbf{R}'^T_z \begin{Bmatrix} x' \\ y' \\ z' \end{Bmatrix}
\end{aligned} \tag{4.7}$$

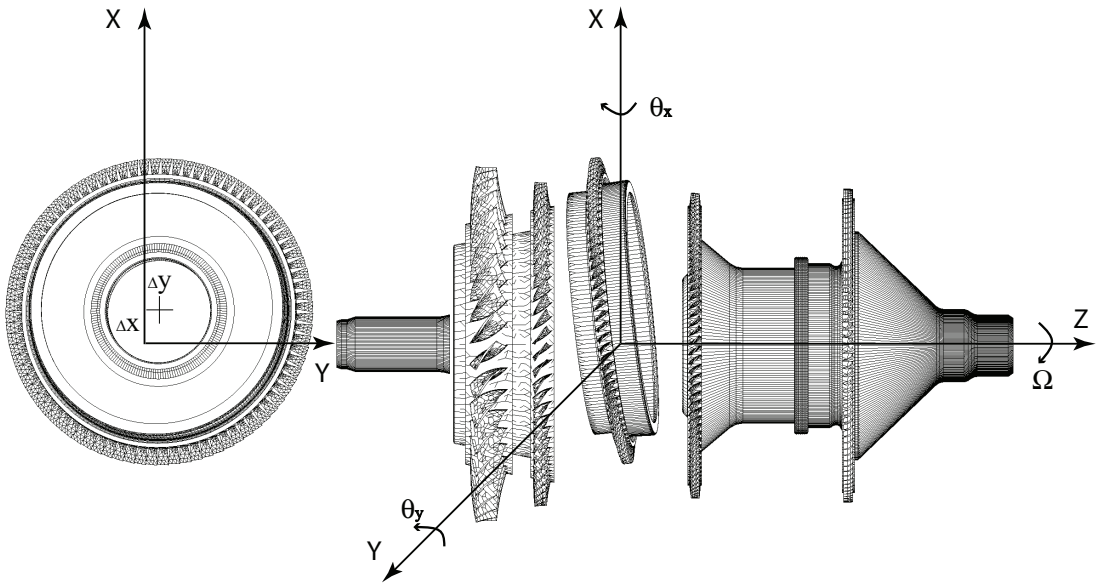

Figure 4.1 Stacked disks assembly misalignment (exaggerated) expressed in terms of two Euler angles θ_x, θ_y and two offsets $\Delta x, \Delta y$.

where the rotation matrices

$$\mathbf{R}_x = \begin{bmatrix} 1 & 0 & 0 \\ 0 & \cos\theta_x & -\sin\theta_x \\ 0 & \sin\theta_x & \cos\theta_x \end{bmatrix}, \mathbf{R}_y = \begin{bmatrix} \cos\theta_y & 0 & \sin\theta_y \\ 0 & 1 & 0 \\ -\sin\theta_y & 0 & \cos\theta_y \end{bmatrix}$$

$$\mathbf{R}_z = \begin{bmatrix} \cos\alpha & -\sin\alpha & 0 \\ \sin\alpha & \cos\alpha & 0 \\ 0 & 0 & 1 \end{bmatrix}, \mathbf{R'}_z = \begin{bmatrix} \cos\Delta\theta_z & -\sin\Delta\theta_z & 0 \\ \sin\Delta\theta_z & \cos\Delta\theta_z & 0 \\ 0 & 0 & 1 \end{bmatrix}$$

$\alpha = 2(n-1)\pi/N$ denotes n_{th} elementary sector rotation angle about the axis of symmetry and $\Delta\theta_z$ is the perturbation of that angle due to rotations and translations in Cartesian coordinate frame.

$$\Delta\theta_z = \arccos(x'/r') - \arccos(x/r) - \alpha \qquad \text{if } \; y' \geq 0$$

$$\Delta\theta_z = \arccos(-x'/r') - \arccos(-x/r) - \alpha + \pi \quad \text{if } \; y' < 0$$

Using the definitions above we can write the equations motion of a misaligned stage in cylindrical coordinate frame

$$[\mathbf{P}^T(\mathbf{K}_E - \mathbf{K}_C(\Omega^2))\mathbf{P} + \widehat{\mathbf{K}}_G(\widehat{\mathbf{u}}_S)]\widehat{\mathbf{u}}_S = \widehat{\mathbf{F}}_C(\Omega^2) \tag{4.8}$$

$$\mathbf{P}^T\mathbf{M}\mathbf{P}\ddot{\widehat{\mathbf{u}}}_D + \mathbf{P}^T\mathbf{C}(\Omega)\mathbf{P}\dot{\widehat{\mathbf{u}}}_D + [\mathbf{P}^T(\mathbf{K}_E - \mathbf{K}_C(\Omega^2))\mathbf{P} + \widehat{\mathbf{K}}_G(\widehat{\mathbf{u}}_S)]\widehat{\mathbf{u}}_D = \mathbf{F} \tag{4.9}$$

here $\mathbf{P} = \underset{i=1,\ldots,n_{nodes}N}{\text{Bdiag}}\{\mathbf{R}_z\mathbf{R'}_z\mathbf{R}_{yx}^T\mathbf{R}_z^T\}$, and n_{nodes} denotes the number of nodes in an elementary sector.

Several basic simplifying assumptions can be taken to reduce computational effort without compromising the accuracy. As pointed out in [91], the form of the mass matrix of $3D$ solid finite elements does not change under orthogonal coordinate transformation, i.e. $\mathbf{P}^T\mathbf{M}\mathbf{P} = \mathbf{M}$. The cost of FE reevaluation of the nodal centrifugal force for each misalignment scenario can be avoided by employing the lumped mass formulation, i.e. the i_{th} nodal centrifugal force can be expressed in the form

$$\widehat{\mathbf{f}}_{iC}(\Omega^2) \approx \Omega^2\mu_i r_i' \tag{4.10}$$

where μ_i is the lumped mass entry, r_i' is perturbed radial coordinate in the cylindrical frame.

Because the deformations due to centrifugal forcing are assumed to be small in this problem due to low rotational speeds Ω and low magnitude of uncertain parameters $(\theta_x, \theta_y, \Delta x, \Delta y)$, the perturbed centrifugal stiffening matrix can be reasonably approximated as the elastic stiffness matrix, i.e. $\widehat{\mathbf{K}}_G(\widehat{\mathbf{u}}_S) = \mathbf{P}^T\mathbf{K}_G(\mathbf{u}_S))\mathbf{P}$. The validity of that assumption will be verified numerically on the industrial scale model later in the dissertation.

Employing these simplifications, the equations of motion of the misaligned stage take form

$$\mathbf{P}^T(\mathbf{K}_E + \mathbf{K}_G(\mathbf{u}_S) - \mathbf{K}_C(\Omega^2))\mathbf{P}\widehat{\mathbf{u}}_S = \widehat{\mathbf{F}}_C(\Omega^2) \tag{4.11}$$

$$\mathbf{M}\ddot{\widehat{\mathbf{u}}}_D + \mathbf{P}^T\mathbf{C}(\Omega)\mathbf{P}\dot{\widehat{\mathbf{u}}}_D + \mathbf{P}^T(\mathbf{K}_E + \mathbf{K}_G(\mathbf{u}_S) - \mathbf{K}_C(\Omega^2))\mathbf{P}\widehat{\mathbf{u}}_D = \mathbf{F} \tag{4.12}$$

Eq. (4.11) can be interpreted simply as follows: the effect of misalignment is intro-

duced by a multiplicative perturbation to stiffness matrix accounting for its non-isotropic variations, plus centrifugal forcing that includes mass imbalance forces.

4.2.3 Misalignment representation in Fourier domain

The preceding discussion was primarily concerned with modeling of misalignment in cylindrical coordinate system. For reduced order model formulation we explore the Fourier domain representation of the multiplicative perturbation matrix $\mathbf{P}$. Let the nominal elastic plus geometric stiffness matrices be partitioned into H harmonic blocks, then we can introduce the misalignment as follows

$$\widehat{\widetilde{\mathbf{K}}} = (\mathbf{W} \otimes \boldsymbol{I})\mathbf{P}^T(\mathbf{W}^* \otimes \boldsymbol{I}) \underset{h=0,\ldots,H}{\widetilde{\mathrm{B}}\mathrm{diag}} \{\widetilde{\mathbf{K}}_{hE} + \widetilde{\mathbf{K}}_{hG} - \widetilde{\mathbf{K}}_{hC}\}(\mathbf{W} \otimes \boldsymbol{I})\mathbf{P}(\mathbf{W}^* \otimes \boldsymbol{I}) \quad (4.13)$$

The DFT of each component of $\mathbf{P}$ can be evaluated separately, moreover one may consider the multiplication $\widetilde{\mathbf{P}} = (\mathbf{W} \otimes \boldsymbol{I})\mathbf{P}(\mathbf{W}^* \otimes \boldsymbol{I})$ as application of the transform $n_{dof}n_{dof}$ times to $N \times N$ matrices, where n_{dof} is the number of degrees of freedom of an elementary sector, N is number of sectors. Clearly, the rotation matrices $\mathbf{R}_x$ and $\mathbf{R}_y$ constant for all sectors are invariant under transform $(\mathbf{W} \otimes \boldsymbol{I})\mathbf{R}_y\mathbf{R}_x(\mathbf{W}^* \otimes \boldsymbol{I}) = \mathbf{R}_y\mathbf{R}_x$.

It can be easily shown that a DFT of a harmonic train that generate cosine and sine entries of the rotational matrices $\mathbf{R}_z$ and $\mathbf{R'}_z$ are of the form [92]

$$\begin{aligned} \cos\left(\frac{2\pi nr}{N}\right)\delta(|n-m|) &\Leftrightarrow \frac{1}{2}\left(\delta(|u-v|-r) + \delta(|u-v|-(N-r))\right) \\ \sin\left(\frac{2\pi nr}{N}\right)\delta(|n-m|) &\Leftrightarrow \frac{1}{2}\left(-j\delta(|u-v|-r) + j\delta(|u-v|-(N-r))\right) \end{aligned} \quad (4.14)$$

where δ is Dirac delta function, $n, m, u, v = 1, \ldots, N$ are row and column indices of an $N \times N$ block and its transform correspondingly. Clearly, the Fourier domain representation of a two dimensional signal

$$x[n,m] = \cos\left(\frac{2\pi rn}{N}\right)\delta(|n-m|)$$

$$n, m = 0, \ldots, N-1$$

can be expressed as

$$x[u,v] = \sum_{m=0}^{N-1}\sum_{n=0}^{N-1} w_N^{-mv} w_N^{nu} \cos\left(\frac{2\pi r n}{N}\right) \delta(|n-m|) =$$

$$= \sum_{m=0}^{N-1} w_N^{-mv}(w_N^{mu} + w_N^{-mu}) \cos\left(\frac{2\pi r m}{N}\right) =$$

$$= \frac{1}{2}\sum_{m=0}^{N-1} w_N^{m(v-u-r)} + \frac{1}{2}\sum_{m=0}^{N-1} w_N^{-m(v-u-r)} + \frac{1}{2}\sum_{m=0}^{N-1} w_N^{m(u-v-r)} + \frac{1}{2}\sum_{m=0}^{N-1} w_N^{-m(u-v-r)} =$$

$$= \frac{1}{2}\delta((v-u)-r) + \frac{1}{2}\delta((v-u)-(N-r)) + \frac{1}{2}\delta((u-v)-r) + \frac{1}{2}\delta((u-v)-(N-r))$$

$$u, v = 0, \ldots, N-1$$

where w_N^{-mv} denotes complex exponential $e^{-\mathrm{j}\frac{2\pi}{N}mv}$. For rotational matrix $\mathbf{R}_z$, where frequency of the harmonic periodic train is $r = 1$, this leads to tri-diagonal matrices of the form

$$\widetilde{\mathbf{R}}_{\cos\alpha} = \begin{pmatrix} 0 & 0.5 & & & & 0.5 \\ 0.5 & \ddots & \ddots & & & \\ & \ddots & \ddots & \ddots & & \\ & & \ddots & \ddots & \ddots & \\ & & & \ddots & \ddots & 0.5 \\ 0.5 & & & & 0.5 & 0 \end{pmatrix}$$

$$\widetilde{\mathbf{R}}_{\sin\alpha} = \begin{pmatrix} 0 & -\mathrm{j}0.5 & & & & \mathrm{j}0.5 \\ \mathrm{j}0.5 & \ddots & \ddots & & & \\ & \ddots & \ddots & \ddots & & \\ & & \ddots & \ddots & \ddots & \\ & & & \ddots & \ddots & -\mathrm{j}0.5 \\ -\mathrm{j}0.5 & & & & \mathrm{j}0.5 & 0 \end{pmatrix}$$

Note that for real conjugate-even sequences with real-valued DFT employed the entries 0.5 and $\pm$j0.5 at $\delta(|u-v|-(N-r))$ locations disappear. It follows readily that the transform $(\mathbf{W}\otimes\boldsymbol{I})\mathbf{R}_z(\mathbf{W}^*\otimes\boldsymbol{I})$ need not be evaluated numerically.

The non-zero structure of the transform of matrix $\mathbf{R}'_z$ is again banded due to nearly harmonic periodic nature of $\Delta\theta_z$ with frequency $r=1$. Therefore the transformed entries $\cos\Delta\theta_z$ will be dominated by double frequency $r=2$ components, while $\sin\Delta\theta_z$ entries will retain the same $r=1$ frequency. Observe, that the exact values of the transformed matrices will be dependent on the phase of the periodic train as a function of misalignment parameters $(\theta_x,\theta_y,\Delta x,\Delta y)$ and thus have to be computed.

With the assumption of small in norm perturbation the product of the nominal block-diagonal stiffness matrix with Fourier domain representation of the misalignment matrix given in Eq. (4.13) will essentially result in a block-banded matrix

$$\widehat{\widetilde{\mathbf{K}}}=\begin{pmatrix} B_0 & B_{0,1} & B_{0,2} & & & & \\ B_{0,1}^T & \ddots & \ddots & \ddots & & & \\ B_{0,2}^T & \ddots & \ddots & \ddots & \ddots & & \\ & \ddots & \ddots & \ddots & \ddots & B_{H-2,H} & \\ & & \ddots & \ddots & \ddots & B_{H-1,H} & \\ & & & B_{H-2,H}^T & B_{H-1,H}^T & B_H & \end{pmatrix}$$

where $2n_{dof}\times 2n_{dof}$ submatrix B_h is an original perturbed harmonic block and $B_{h,h+1}$ is a $2n_{dof}\times 2n_{dof}$ term introduced by pre- and post-multiplication that couples neighboring harmonics, such that $\|B_{h,h+1}\|\ll\|B_h\|$ for small variations of parameters $(\theta_x,\theta_y,\Delta x,\Delta y)$. Then other coupling off-diagonal blocks of higher order are negligible in norm $\|B_{h,h+2}\|\ll\|B_{h,h+1}\|$. In particular, that result implies that one may obtain a reasonable accuracy reduced order system to analyze harmonic one behavior through a simple truncation by retaining first three harmonic blocks with respective coupling terms.

4.2.4 Interstage coupling and assembly

Employing small magnitude perturbation assumption that does not significantly change interstage interface the connection of misaligned adjacent stages can be achieved through multi-stage cyclic symmetry coupling. Consider the displacements compatibility condition between adjacent stages s and $s+1$ defined in physical coordinates by

$$\mathbf{A}\mathbf{u}_b^s - \mathbf{u}_b^{s+1} = 0 \tag{4.15}$$

in which $\mathbf{A}$ is a Boolean connectivity matrix which makes the two interstage meshes compatible. The multi-stage cyclic symmetry coupling procedure defines independent compatibility relations between compatible (in terms of harmonic index) cyclic components of adjacent stages. Accordingly, given a cyclic harmonic of the rotor n, Eq. (4.15) is rewritten using cyclic harmonics $p_s(n)$ and $p_{s+1}(n)$ defined according to aliasing of respective Fourier bases of stage s and $s+1$:

$$(\mathbf{w}^{s+1}_{p_{s+1}(n)}{}^{*} \otimes \mathbf{I})\mathbf{A}(\mathbf{w}^{s}_{p_s(n)} \otimes \mathbf{I})\tilde{\mathbf{u}}^s_{b,p_s(n)} - \tilde{\mathbf{u}}^{s+1}_{b,p_{s+1}(n)} = 0 \tag{4.16}$$

$\mathbf{w}^s_{p_s(n)}$ a column of Fourier transform matrix associated with harmonic $p_s(n) \in [0, N_s]$ of stage s, subscript b denotes degrees-of-freedom on the inter-stage boundary. For further details, please refer to [89]. In order to eliminate the duplicated cyclic components of the interstage boundary of stage $s+1$ a rectangular coupling matrix is defined as

$$\mathcal{T} = \begin{bmatrix} \boldsymbol{I}_{b,s} & \mathbf{0} & \mathbf{0} & \cdots \\ \mathbf{0} & \boldsymbol{I}_{i,s} & \mathbf{0} & \cdots \\ \mathcal{B}_p & \mathbf{0} & \mathbf{0} & \cdots \\ \mathbf{0} & \mathbf{0} & \boldsymbol{I}_{i,s+1} & \cdots \\ \vdots & \vdots & \vdots & \ddots \end{bmatrix} \tag{4.17}$$

where

$$\mathcal{B}_p = (\mathbf{w}^{s+1}_{p_{s+1}(n)}{}^{*} \otimes \mathbf{I})\mathbf{A}(\mathbf{w}^{s}_{p_s(n)} \otimes \mathbf{I})$$

It follows that the equations of motion of the coupled misaligned rotor system,

for $h = 0, \ldots, 2$ can be expressed as

$$\mathcal{T}^T \widetilde{\mathbf{P}}^T [\widetilde{\mathbf{K}}_{hE} + \widetilde{\mathbf{K}}_{hG} - \widetilde{\mathbf{K}}_{hC}] \widetilde{\mathbf{P}} \mathcal{T} \widehat{\tilde{\mathbf{u}}}_{hS} = \widehat{\tilde{\mathbf{F}}}_{hC} \tag{4.18}$$

$$\mathcal{T}^T \widetilde{\mathbf{M}}_h \mathcal{T} \ddot{\tilde{\mathbf{u}}}_{hD} + \mathcal{T}^T \widetilde{\mathbf{P}}^T \widetilde{\mathbf{C}}_h \widetilde{\mathbf{P}} \mathcal{T} \dot{\tilde{\mathbf{u}}}_{hD} + \mathcal{T}^T \widetilde{\mathbf{P}}^T \left[\widetilde{\mathbf{K}}_{hE} + \widetilde{\mathbf{K}}_{hG} - \widetilde{\mathbf{K}}_{hC}\right] \widetilde{\mathbf{P}} \mathcal{T} \widehat{\tilde{\mathbf{u}}}_{hD} = \tilde{\mathbf{F}}_h \tag{4.19}$$

4.2.5 Algorithm for repeated ROM evaluation

The main important result of the proposed method is that the complexity of solving Eqs. (4.18) and (4.19) can be greatly reduced if the linear systems are solved sequentially instead of calculating the matrix product, a highly populated matrix, and then solving it. However, typically the nominal uncoupled system is severely ill-conditioned due to the presence of rigid body modes. To improve the conditioning of nominal uncoupled system we propose to take advantage of the orthogonality properties of Fourier coefficients. If we define a rectangular coupling matrix

$$\mathcal{T}_{0.5} = \mathcal{T} \begin{bmatrix} 0.5\boldsymbol{I}_{b,s} & \mathbf{0} & \mathbf{0} & \cdots \\ \mathbf{0} & \boldsymbol{I}_{i,s} & \mathbf{0} & \cdots \\ \mathbf{0} & \mathbf{0} & \mathbf{0} & \cdots \\ \mathbf{0} & \mathbf{0} & \boldsymbol{I}_{i,s+1} & \cdots \\ \vdots & \vdots & \vdots & \ddots \end{bmatrix} \tag{4.20}$$

the effect of the repeated coupling-uncoupling on the nominal system $\mathcal{T}_{0.5}\mathcal{T}^T\widetilde{\mathbf{K}}_h\mathcal{T}\mathcal{T}_{0.5}^T$ would amount to just averaging of matrix entries on the interstage boundaries having negligible effect on perturbed system global dynamic. Furthermore, its LU factors may be reused for different misalignment realizations. In absence of any perturbation the repeated coupling-uncoupling does not modify the nominal system

$$\mathcal{T}^T \mathcal{T}_{0.5} = \boldsymbol{I} \tag{4.21}$$

The combined results of two preceding section are summarized in Algorithm 3.

Algorithm 3 Reduced order modeling of rotors with stacked disks misalignment effect

Let $\mathbf{\Omega} = [\Omega_1, \ldots, \Omega_m]$ be a set of m discrete rotation frequencies
Let n be a number of misalignment realizations
Extract elementary sector matrices of each stage $\mathbf{K}_E^s, \mathbf{K}_G^s(\Omega_i), \mathbf{K}_C^s(\Omega_i^2)$ with FE software
Form interstage coupling matrices $\mathcal{T}, \mathcal{T}_{0.5}$ for a set of retained harmonics $h = 0, \ldots, 2$
for $i = 1, \ldots, m$ **do**
  Denote $\widetilde{\mathbf{K}}_h = \widetilde{\mathbf{K}}_{hE} + \widetilde{\mathbf{K}}_{hG}(\Omega_i) + \widetilde{\mathbf{K}}_{hC}(\Omega_i^2)$
  Factorize nominal coupled matrix $\mathcal{T}^T \widetilde{\mathbf{K}}_h \mathcal{T}$
  for $j = 1, \ldots, n$ **do**
    Generate parameters $(\theta_x^{j,s}, \theta_y^{j,s}, \Delta x^{j,s}, \Delta y^{j,s})$
    Form $\widetilde{\mathbf{P}}(\theta_x^{j,s}, \theta_y^{j,s}, \Delta x^{j,s}, \Delta y^{j,s})$
    Compute centrifugal forcing $\widehat{\widetilde{\mathbf{F}}}_C(\theta_x^{j,s}, \theta_y^{j,s}, \Delta x^{j,s}, \Delta y^{j,s}, \Omega_i^2)$
    Solve the static problem in three steps:
    $\widetilde{\mathbf{u}} = (\mathcal{T}^T \widetilde{\mathbf{P}} \mathcal{T}_{0.5})^{-1} \widehat{\widetilde{\mathbf{F}}}_C$
    $\widetilde{\mathbf{u}} = (\mathcal{T}^T \widetilde{\mathbf{K}}_h \mathcal{T})^{-1} \widetilde{\mathbf{u}}$
    $\widetilde{\mathbf{u}} = (\mathcal{T}_{0.5}^T \widetilde{\mathbf{P}} \mathcal{T})^{-1} \widetilde{\mathbf{u}}$
  end for
end for

4.3 Numerical examples

In this study we consider a rotor assembly consisting of four high pressure compressor integrally bladed discs composed of 36, 60, 84 and 96 sectors respectively connected to a turbine disk featuring 120 sectors. The finite-element mesh of elementary sectors is depicted in Fig. 4.2. The assembly is analyzed in body attached frame that

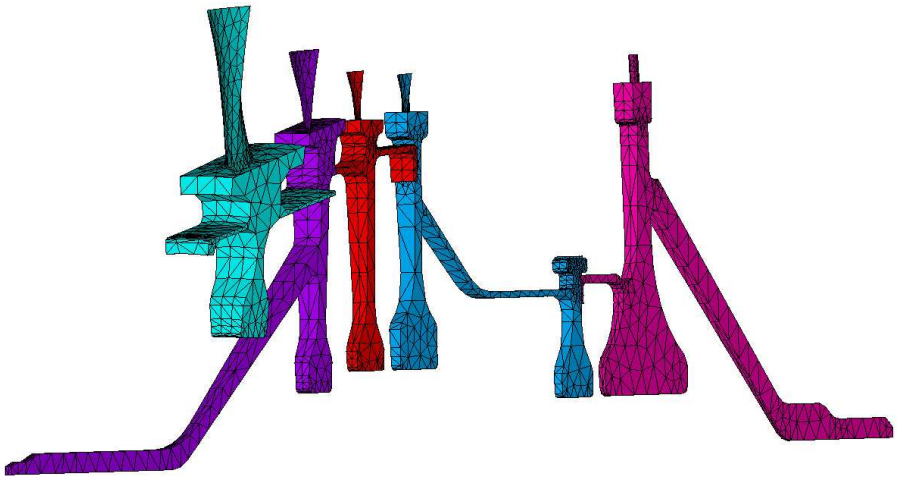

Figure 4.2 Finite element model of the multi-stage assembly.

rotates about the undeformed centerline of the bearings with a constant speed. It is simply supported at the extremities, isotropic stiffness and damping at discrete nodal locations are taken into account. The bearing stiffness and damping coefficients are $k_{xx} = k_{yy} = 4.58\times10^8$ N/m, $k_{xy} = k_{yx} = 7.63\times10^7$ N/m, $c_{xx} = c_{yy} = 1.52\times10^6$ Ns/m correspondingly, while internal rotor material damping is neglected.

Lowest frequency complex eigenmodes are calculated at 60 discrete frequency points 10 Hz $\leq \Omega \leq$ 600 Hz with a step 10 Hz using multi-stage cyclic symmetry approach. The evolution of complex natural frequencies in rotating frame is given in Fig. 4.3(a). Same frequencies in inertial frame are depicted in Fig. 4.3(b), where the relationship between the frames is defined as $\omega_{rotating} = \omega_{fixed} \pm h\Omega$ with h denoting the nodal diameter with sign depending on the traveling wave direction. Note that synchronous and 2X whirls plotted to locate critical speeds are marked with

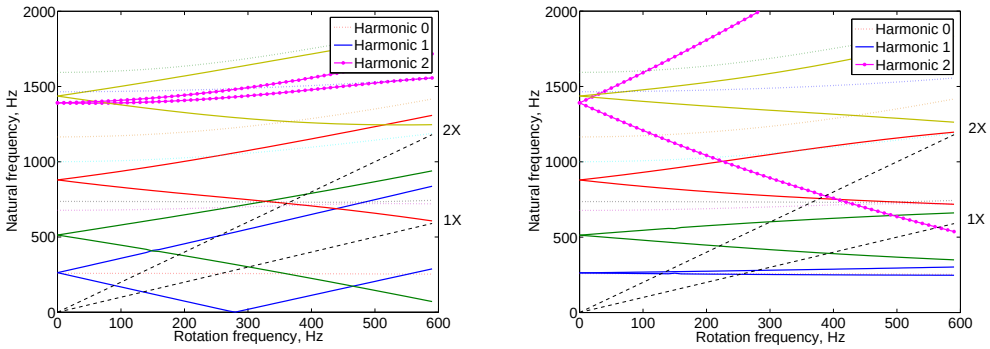

(a) (b)

Figure 4.3 Evolution of natural frequencies of the nominal system with rotating speed in rotating frame (a), transformed to inertial frame (b). Synchronous whirl is marked as dashed line.

dashed lines. The first critical speed in rotating frame occurs at about $\Omega = 130$ Hz corresponding to a forward whirl global bending mode. However, the first critical speed in inertial frame is observed at about $\Omega = 280$ Hz, which corresponds to the cancelation of the apparent static stiffness in the rotating frame [75].

4.3.1 Effect of misalignment on eigenmodes and system response

First we investigate the effects of stacked disks misalignment on eigenmodes of the system. A misalignment scenario was introduced through a set of tilt angles and offsets presented in Tab. 4.1 applied to a full FE reference model and a set of lowest frequency complex eigenmodes was computed.

Figs. 4.4(a) and 4.4(b) present the difference between nominal and perturbed imaginary and real parts of complex eigenvalues calculated at $\Omega = 200$ Hz. It should be noted that eigenvalues are not significantly affected by the misalignment, with maximum difference less than 0.3 percent for the lowest frequency mode. The observation strongly correlates with experimental data indicating that the resonance peaks at critical speeds can be reliably predicted by the Campbell diagram built from a nominal model. Eigenvectors of the nominal and perturbed systems are compared in Fig. 4.5 in terms of complex MAC values. It appears that the eigenspace is af-

Table 4.1 Misalignment parameters

Stage number	$\theta_x, ^\circ$	$\theta_y, ^\circ$	$\Delta x, mm$	$\Delta y, mm$
1	0.01	0.015	1	-0.95
2	-0.05	-0.09	0.3	0.05
3	-0.06	-0.045	-0.75	-2.8
4	0.0443	0.0225	0.85	0.57
5	0.08	-0.095	-0.39	-0.45

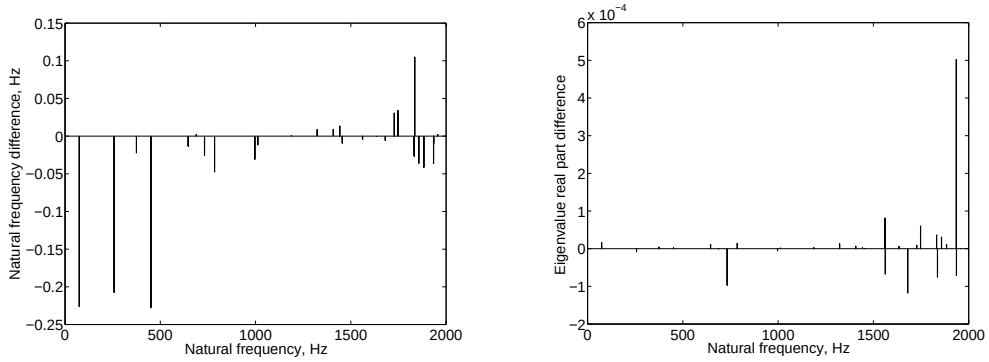

(a) (b)

Figure 4.4 Difference between nominal and perturbed imaginary (a) and real (b) parts of complex eigenvalues calculated at $\Omega = 200$ Hz.

fected more seriously by the effect of misalignment as reflected by low MAC values. Clearly, the mode distortion is the major reason why nominal eigenvectors cannot be used in modal projection based model reduction technique. It can also be seen in Fig. 4.5 that in general, harmonic one modes seem to be less stable under perturbation featuring lower MAC coefficients, whereas the modes of zero and second harmonic are strongly correlated with their original unperturbed counterparts. In order to gain better understanding of the effect of perturbation on eigenvectors we calculate the harmonic content of real and imaginary parts of the first bending and the next in spectrum zero nodal diameter modes at $\Omega = 200$ Hz, depicted in Figs. 4.6

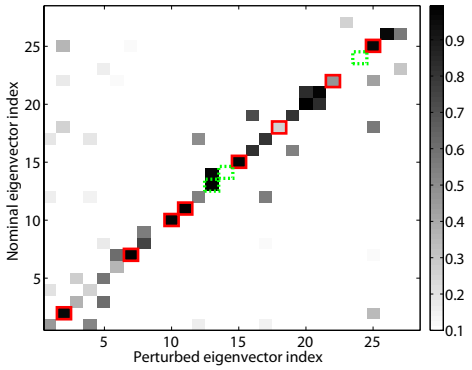

Figure 4.5 MAC value between nominal and perturbed complex eigenvectors calculated at $\Omega = 200$ Hz. Harmonic 0 and 2 modes are highlighted with red solid and green dashed boxes respectively.

and 4.7 correspondingly. Examination of the harmonic content of the modes yields significant insight. Both perturbed harmonic zero and harmonic one modes become contaminated mainly by the closest neighboring harmonics, and display other harmonic components to a lesser extent. The observation is consistent with the banded non-zero structure of the perturbed system matrices in Fourier domain - the amount of harmonic contamination is proportional to the norm of harmonic coupling blocks introduced by perturbation. The acquired additional harmonic content is most discernible in case of 257 Hz perturbed harmonic zero mode. The norm of harmonic one content in the imaginary part of eigenvector is higher than the one of the original harmonic zero content (see Fig. 4.7(d)), which can also be visualized using FE model in Fig. 4.8.

Next, we examine the effects of disk misalignment on static response. The response to centrifugal forcing for both nominal and misaligned system calculated at $\Omega = 200$ Hz is depicted in Fig. 4.9. While the nominal response is a pure harmonic zero displacement field, one can notice the dominance of harmonic one component in the response of the perturbed system. Fig. 4.10 shows the contribution of first four harmonics to the misaligned system unbalance response in 0-600 Hz frequency range. The harmonic decomposition is consistent with [87]. General perception is that both 1X and 2X (two times the rotation speed) components should be present

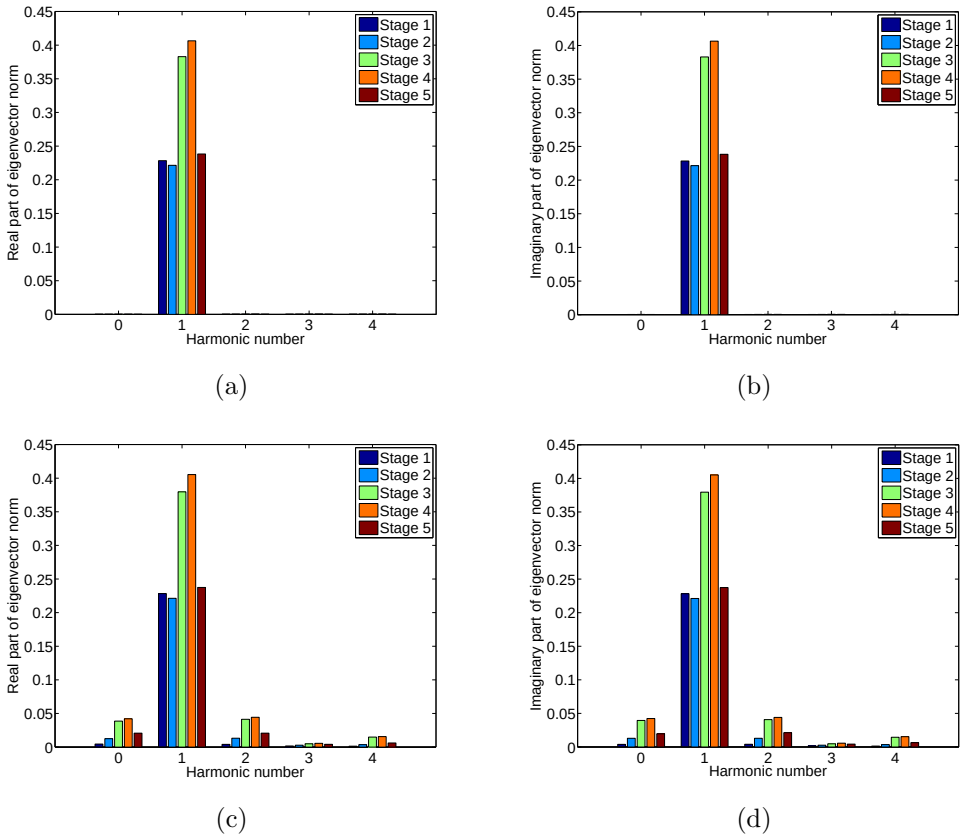

Figure 4.6 Harmonic content of the first bending mode corresponding to 74 Hz natural frequency at $\Omega = 200$ Hz and expressed in terms of norms of each individual stage. Norm of real part of nominal eigenvector (a), imaginary part (b), norm of real part of perturbed eigenvector (c) and imaginary part(d).

in the response of a misaligned system with 1X being dominant, whereas the contribution of 2X vibration grows with severity of misalignment. The physical source of these effects is identified as a rotor bow and rotor asymmetry, respectively. Clearly, the magnitude of the response will be affected by the mode distortion phenomena discussed earlier that characterize misalignment. Thus, 257 Hz harmonic zero mode distorted by harmonic one component may be excited by misaligned system centrifugal forcing dominated by both engine orders, zero and one, contributing significantly

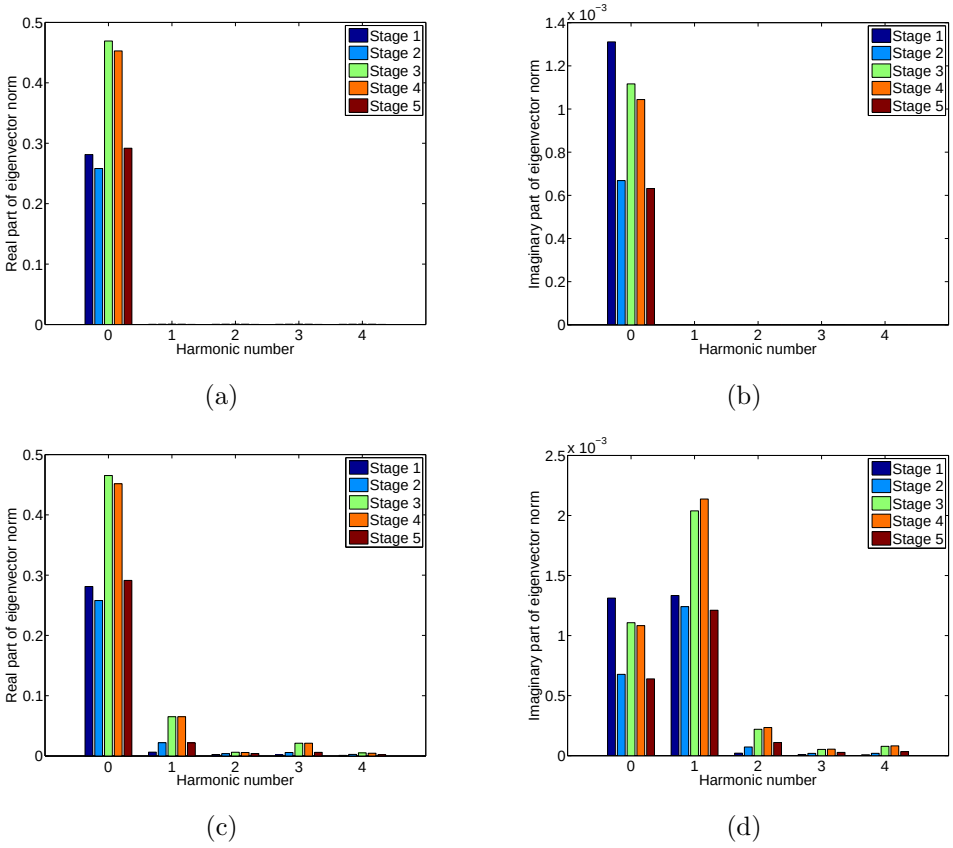

Figure 4.7 Harmonic content of zero nodal diameter mode corresponding to 257 Hz natural frequency at $\Omega = 200$ Hz and expressed in terms of norms of each individual stage. Norm of real part of nominal eigenvector (a), imaginary part (b), norm of real part of perturbed eigenvector (c) and imaginary part(d).

to 1X response magnification.

The effect of disk misalignment on harmonic response of the system excited by EO1 and EO2 forward traveling wave applied to bearing support nodes is shown in Fig. 4.11. It can be seen that the coupling between harmonic blocks introduced by perturbation, the reason of harmonic contamination of mode shapes, can cause significant response amplification, additional resonance peaks not observable in the nominal response as well as extra harmonic content other than the one of excitation.

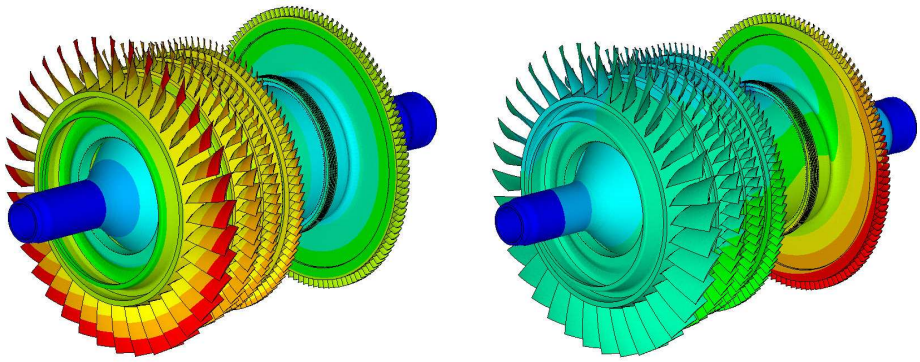

(a) (b)

Figure 4.8 Perturbed harmonic zero modeshape corresponding to 257 Hz natural frequency at $\Omega = 200$ Hz rotational speed: real part (a) and imaginary part (b). The imaginary part of the modeshape is dominated by harmonic one component showing the effect misalignment.

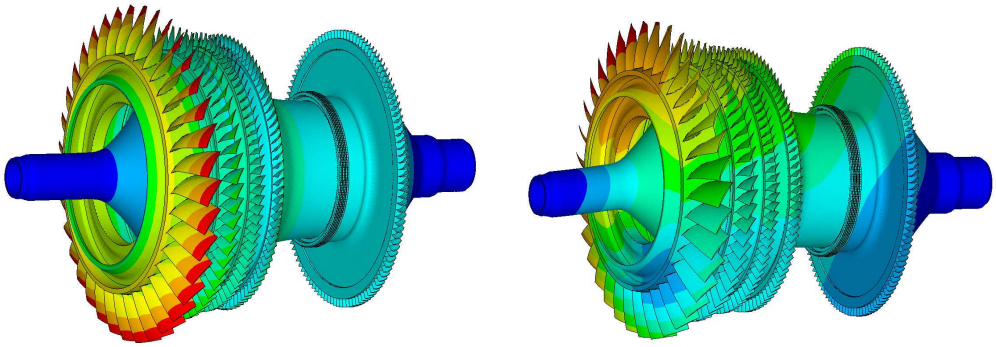

(a) (b)

Figure 4.9 Nominal (a) and misaligned (b) system response under centrifugal forcing.

Observe that the misaligned system response to EO1 excitation is dominated by harmonic 0 component, whereas EO2 forcing brings about significant harmonic 1 response.

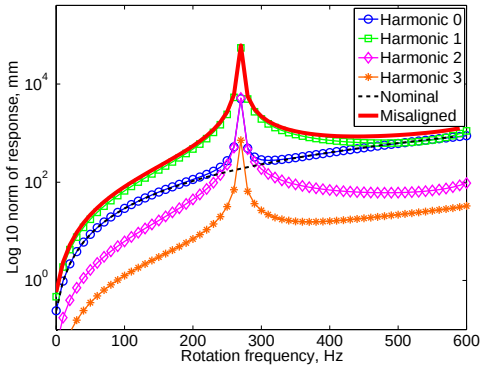

Figure 4.10 Comparison of nominal and misaligned systems unbalance response, the latter is shown decomposed into four harmonic components.

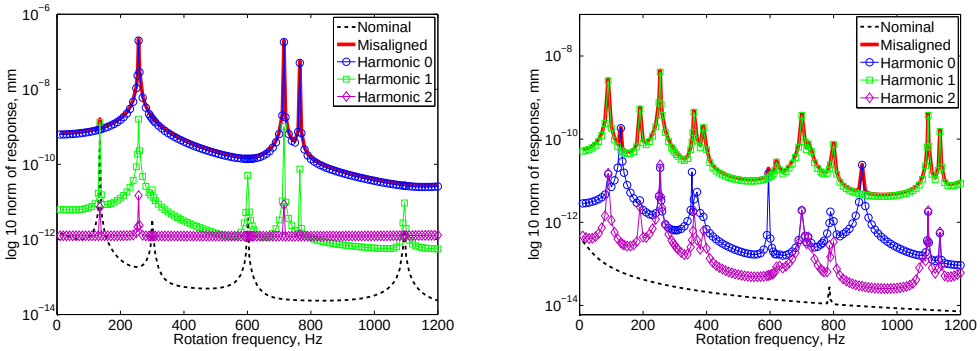

(a) (b)

Figure 4.11 Comparison of nominal and misaligned system dynamic response under synchronous harmonic 1 (a) and 2X harmonic 2 (b) forward traveling wave excitation. The misaligned system response is shown along with its dominant harmonic components.

4.3.2 Accuracy of the proposed method

In the following example the proposed reduction technique is applied to form a reduced order model. To show its effectiveness the unbalance response is compared against the results calculated with full (360°) misaligned rotor-bearing system. Fig. 4.12(a) shows ROM accuracy in terms of norm of global response, same results are compared in Fig. 4.12(b) in terms of MAC correlation coefficients. Obviously,

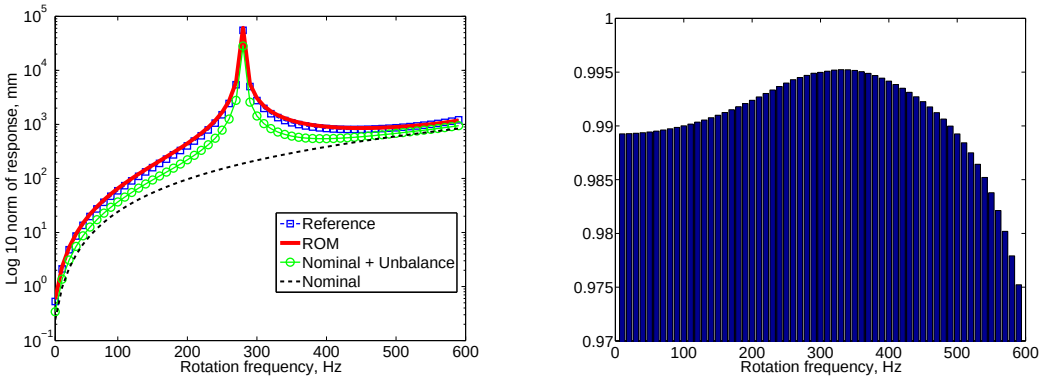

(a) (b)

Figure 4.12 Norm of the unbalance response calculated with ROM, full (360°) FE and unperturbed model excited by the unbalance forcing (a). Note that the latter consistently underestimates the response. MAC values of the unbalance response between ROM and reference FE model (b).

the ROM has been shown to accurately represent the centrifugal effects over the entire range of operating speeds in both sub- and super-critical regions. It slightly over-predicts the magnitude of response compared to the reference model. The MAC value is consistently over 0.97 showing the effect of deteriorating accuracy as rotation speed increases due to geometrical stiffness approximation. The response of nominal system excited by same unbalance forces is presented for comparison. It is evident that modeling of misalignment only with equivalent forces consistently underestimates the global response due to unmodeled effect of harmonic coupling and equivalently modal distortion.

4.3.3 Statistical analysis example

In this example, we consider a baseline model of the multi-stage rotor assembly introduced above (see Fig. 4.2). The reduced order model is constructed by projection, retaining first three Fourier harmonics, which results in a ROM of order 56,820 DOF. Owing to the fact that the most significant cause of excessive rotor vibration is rotor mass unbalance, which manifests itself as severe 1X vibration, the dynamic charac-

teristic of primary interest is steady rotation speed unbalance response. Therefore, in Monte-Carlo simulations we carry out a static analysis under centrifugal loading measuring the deflection at bearing nodes. For simplicity, the nominal model is first perturbed by a set of misalignment parameters $\theta_x^s, \theta_y^s, \Delta x^s, \Delta y^s$ generated as statistically independent Gaussian random variables with zero mean and a standard deviation (0.1°, 0.1 mm). The random realizations of the amplitude of unbalance response at both bearing locations are shown in Fig. 4.13 along with the ensemble mean and percentiles. Observe, that the unbalance response levels at 99^{th} percentile

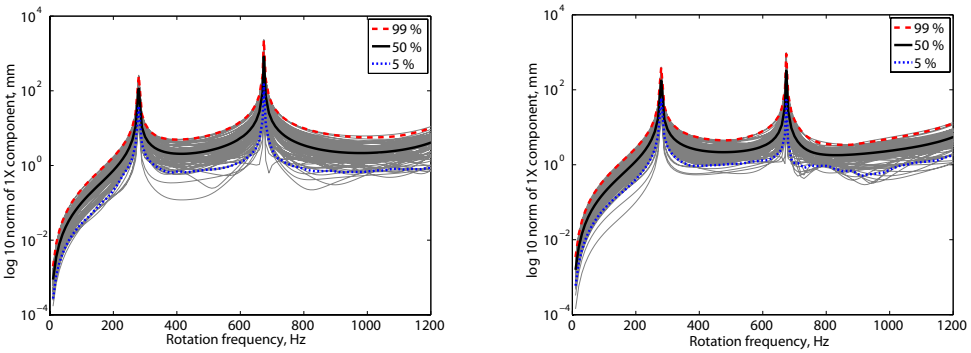

Figure 4.13 Direct Monte-Carlo simulation of the unbalance response with random misalignment parameters generated as statistically independent zero mean, (0.1°, 0.1 mm) standard deviation Gaussian random variables. Norm of 1X harmonic content of the unbalance response for 100 realizations, 99%, 50% and 5% of points at bearings 1 and 2 are shown in (a) and (b) correspondingly.

can reach from 7, between critical speeds, up to 20, at a critical speed, times of those at 5^{th} percentile.

Next, MCS with a sample size 2000 is carried out to test the convergence of the response statistics. Fig. 4.14 displays ensemble mean and variance with respect to the number of samples; a sample size 1000 is found to be adequate for accurate analysis. Fig. 4.15 shows the pdf obtained from 1000 Monte-Carlo runs for three selected rotation frequencies, namely in the sub-critical region, at first critical speed and in the area close to the second critical speed. The observable differences in pdf shapes of

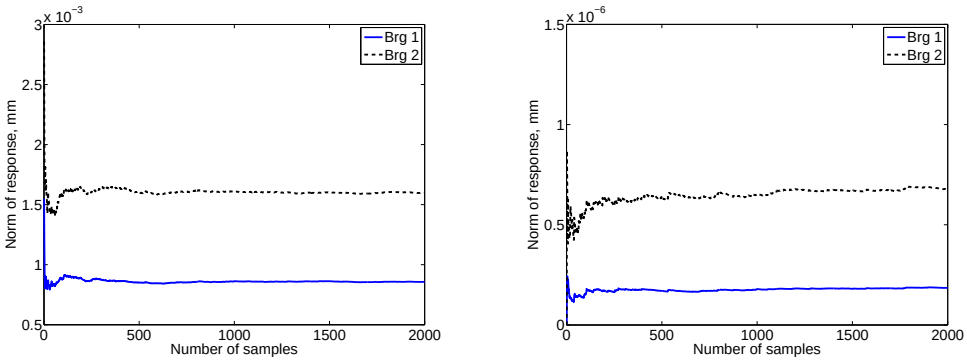

(a) (b)

Figure 4.14 Evolution of the population mean (a) and variance (b) with the number of samples. Each iteration we calculate norm of 1X content of the unbalance response at two bearings at $\Omega = 10$ Hz.

two bearings at three rotation speeds are consistent with the corresponding bending modeshapes: larger variation is expected for a modeshape dominated by motion of that part of structure.

The statistically quantified levels of unbalance response are of importance while selecting robust designs and manufacturing tolerances to avoid large amplitude response within the operating range. An important ramification of imbalance induced excessive 1X vibration, the passage through a critical speed, is illustrated in the following example. The 99^{th} percentile of the unbalance response norm is computed at first critical speed $\Omega = 280$ Hz with two standard deviation values of misalignment parameters (0.5°, 0.5 mm) and (1°, 1 mm) for each stage separately, while those of other disks are kept at (0.1°, 0.1 mm) level. Assuming a typical industrial situation where an optimized stacking orientation for each stage of the rotor assembly is a function of all individual disks random geometries, we introduce a simple decreasing statistical dependence between misalignment parameters $\theta_x^s, \theta_y^s, \Delta x^s, \Delta y^s$ of different stages $s = 1, \ldots 5$. Thus, the selected correlation coefficients are $\rho_{s,s\pm1} = 0.9$, $\rho_{s,s\pm2} = 0.7$, $\rho_{s,s\pm3} = 0.4$ and $\rho_{s,s\pm4} = 0.1$. Fig. 4.16 shows the influence of the amplitude or random geometry variation of each individual stage on the variation of global response calculated for two bearings at first critical speed. The observed

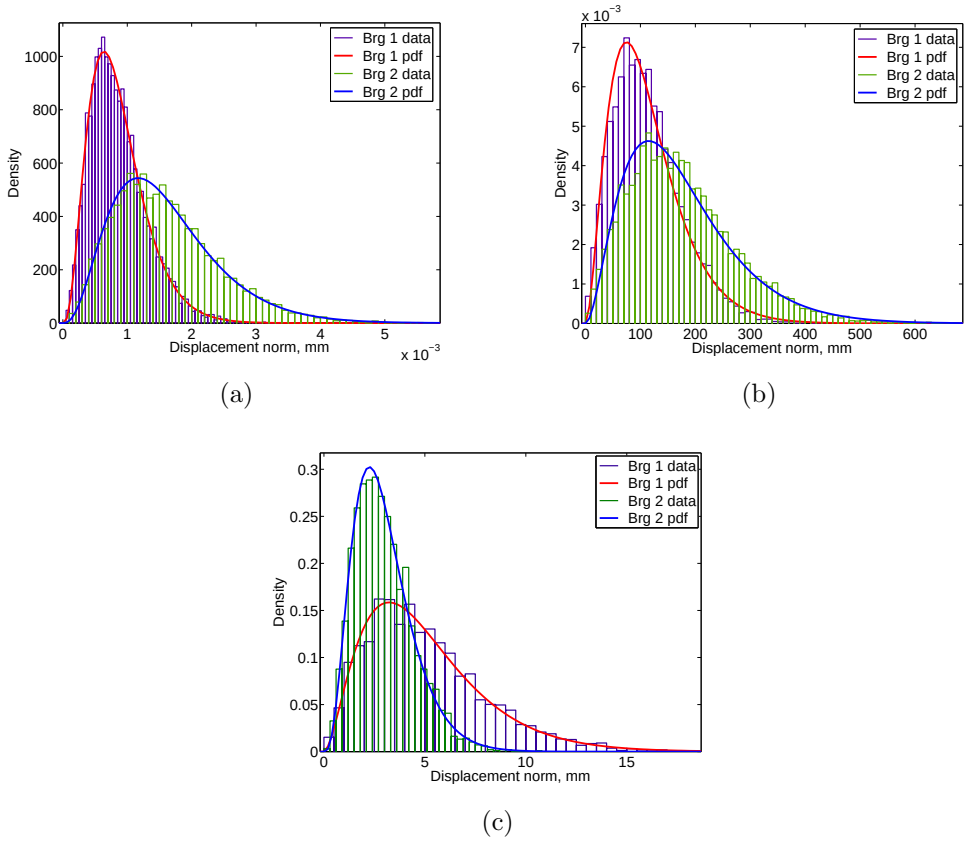

Figure 4.15 Probability density functions of the static response at two bearings (1X component) obtained at $\Omega = 10$ Hz (a), $\Omega = 280$ Hz (b) and $\Omega = 590$ Hz (c). Note larger variation in response at second bearing in the subcritical region and at first critical speed. As we approach the second critical speed, the distribution at first bearing grows wider consistent with the first and second bending modeshapes.

changes in 99^{th} percentile of the response level with the additional uncertainty at one stage agree with the physical intuition. It can be observed that the relative importance of the manufacturing uncertainties in the geometry of the first and the last interfaces outweighs the ones of the middle stages suggesting tighter tolerances to ensure a reliable performance.

All the numerical experiments were conducted on an Intel Xeon Quad-Core 2.66 GHz workstation, coded in FORTRAN employing PARDISO direct sparse

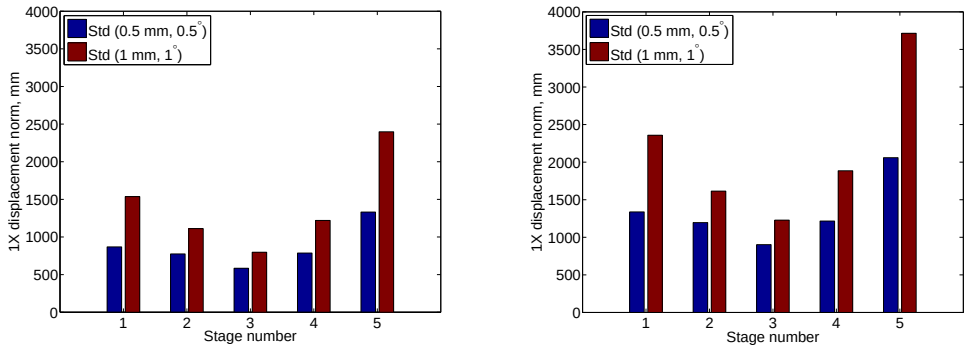

Figure 4.16 99^{th} percentile of the unbalance response norm calculated at $\Omega = 280$ Hz resonance frequency at bearing 1 (a) and bearing 2 (b) obtained by increasing standard deviation of random input parameters to (0.5°, 0.5 mm) and (1°, 1 mm) for each stage separately, while those of others are kept at (0.1°, 0.1 mm).

solver. For comparison, one iteration of MCS with the ROM featuring 56,820 DOF requires 0.5 G of RAM taking approximately 5 s counting both reduced order model update and static analysis. An equivalent accuracy full order model has 929,160 DOF requiring 4 min for static analysis and 17 G of memory (in-core version), whereas a realistic introduction of disk misalignment into the full model would require FE reanalysis.

4.4 Summary

In this chapter we have introduced a computational technique for vibration analysis of misaligned disk rotor assemblies using 3D FE formulation. The reduced model has been obtained after truncation of higher order harmonics in Fourier domain. The problem was greatly simplified by assuming symmetry of individual stages and small parameters variations. Under these assumptions the disks misalignment has been introduced as multiplicative perturbations to system matrices, upon which individual stages were coupled with multi-stage cyclic symmetry approach. We have demonstrated computationally that the proposed algorithm gives outstanding performance

due to reliance on sparse matrix linear algebra and sampling of small parametric space. Of particular interest is the ability to repetitively introduce variation in geometry where the modal projection based methods usually fail or numerically ineffective. It is therefore advantageous in design optimization or uncertain parameter space exploration, specifically for light flexible rotors in supercritical regions. The accuracy of the technique has been illustrated with representative simulation examples, the results have been shown to match reference system over a practical range of geometrical parameter variations and rotational speeds. The development was also instrumental in understanding of the inaccuracy of traditional analysis methods. It was shown numerically that the non-isotropic stiffness variation introduced as sparse blocks coupling neighboring harmonics is the origin of additional 1X and 2X content in the response of misaligned system.

Chapter 5

Conclusion and Future Research Directions

Stochastic analysis of large-scale models stretched traditional computational resources and algorithmic capabilities to the limit. In this dissertation we have addressed two difficult problems, which solution is highly nonlinear in the uncertain input parameters for which less expensive probabilistic techniques proved to be inaccurate or ineffective leaving Monte-Carlo simulation analysis the only feasible means to assess the variability of the response. The general outcome of this work is a systematic approach to design of accurate and computationally inexpensive predictive numerical tools for uncertainty propagation within the stochastic simulation framework. This is achieved by way of:

- Reduction of probabilistic parametric space to "important" and measurable parameters
- Projection based reduced order modeling with a reasonable effort of computing the basis vectors
- Low cost of reduced order model analysis and update for a change in random parameters

5.1 Contributions and findings

The Static Mode Compensation method for inexpensive computation of projection basis vectors of geometrically modified bladed disks has been extended to accommodate multiple mistuned blades and effectively implemented in industrial FORTRAN code. The accuracy, efficiency and scalability of the algorithm has been analyzed on a FE model featuring realistic geometry. Through a number of numerical experiments the method has been shown to provide reliable approximation of perturbed eigenpairs for narrow clustered areas of spectrum displaying lower accuracy in the modal interaction zones. The source of inaccuracy has been identified as poorer preconditioning by revealing that the SMC technique is closely related to the generalized Davidson method for eigenvalue problem. To address those deficiencies a new method based on the Jacobi-Davidson algorithm for eigenvalue problem has been proposed implementing a number of preconditioning techniques and simple heuristic strategies taking advantage of the block-circulant structure of the nominal system and assumptions on perturbation. Numerical experiments have been conducted on an industrial bladed disk FE model demonstrating its accuracy in both areas of spectrum.

The problem of statistical quantification of random mistuning effects on geometrically modified bladed disk vibration response has been confronted by proposing a hybrid approach, which involves relatively infrequent computation of a compact set of projection basis vectors corrected for each geometry change using Chapter 2 development. The projection subspace is exploited repeatedly to build a compact reduced order model suitable for Monte-Carlo analysis for each change of random parameters in blade properties introduced in component modal subspace. The effectiveness and precision of FORTRAN implementation of the technique have been demonstrated through a series of numerical examples on realistic FE model of an industrial bladed disk whose blades featured significant geometry change due to practical damage patterns. The results have shown that in the majority of the analyzed situations large geometric mistuning has not led to significant additional response magnification beyond very low levels of random mistuning. The worst case has been identified in the

high modal density area where "rogue" blade resonance peaks found to be dominant. The situations where deterministic damage effects dominate the dynamic response have been identified to be largely responsible for considerable additive magnification factors beyond low levels of random mistuning as compared to the nominal case, at the same time exhibiting lower sensitivity to additional random mistuning.

For statistical analysis of the effects of uncertainties in the inter-stage geometry of misaligned stacked disk rotor assemblies a novel algorithm has been proposed and effectively implemented in industrial FORTRAN code. The reduced model has been obtained from high fidelity 3D FE models of elementary sectors after truncation of higher order harmonics in Fourier domain. The problem has been greatly simplified by assuming symmetry of individual stages and small parameter variations. Under these assumptions the disks misalignment has been introduced as multiplicative perturbations to system matrices, upon which individual stages were coupled with multi-stage cyclic symmetry approach. It has been demonstrated computationally that the proposed algorithm gives outstanding performance due to reliance on the state-of-the-art direct parallel linear solver, sparse matrix linear algebra and sampling of reduced parametric space. Of particular interest is the ability of the algorithm to repeatedly introduce variation in inter-stage geometry where the traditional modal projection based methods has been ineffective. The accuracy and numerical efficiency of FORTRAN implementation has been illustrated with representative stochastic simulation examples, the results have been shown to match reference system over a practical range of geometrical parameter variations and rotational speeds. The development, in turn, has also provided important insight on the source of inaccuracy of traditional analysis methods. It has been shown that the non-isotropic stiffness variation introduced as sparse blocks coupling neighboring harmonics is the origin of additional 1X and 2X content in the response of misaligned system.

5.2 Future research directions

Beyond the issues and topics treated directly in this dissertation, there are certain open questions, extensions and classes of problems that can potentially benefit from further research effort. The following is a categorized list of suggestions for future work.

5.2.1 Extensions

The extensions, which could be applied to the methods presented in Chapter 2, include an accurate stochastic modeling of random geometric uncertainties as discretized random fields. Consequent reduction of probabilistic space should be aimed to match available high-resolution measurement data. The algorithms presented in Chapter 2 are limited by the assumption of high magnitude low rank perturbation assumption. Inclusion of high rank low magnitude perturbations would call for additional research on efficient algorithms to calculate projection matrices and to decrease the computational effort of repeated analysis, by exploiting extended bases, parametric approaches with interpolation and/or switching.

A natural and logical extension of the techniques and investigations reported in Chapters 2 and 3 would be to perform a global probabilistic analysis of the entire rotor assembly, featuring both large geometry modification and small random parameter variation by employing multi-stage cyclic symmetry approach.

5.2.2 Methodology

There are a number of potential refinements to the preconditioned iterative technique presented in Chapter 2 that could lead to accelerated convergence. First, application of block Krylov sparse linear solvers with multiple right-hand sides to solution of the linear Jacobi-Davidson equation could decrease overall computational time; typically these methods converge in fewer iterations than their single right-hand side versions. Future work should also aim at computation of invariant subspaces that has received a lot of attention in the numerical linear algebra literature; new algo-

rithms and practical implementations have been reported. The problem of invariant subspace approximation frequently appearing in scientific computing applications requires a solution of an algebraic Riccati equation, which can be viewed as a block-generalization of the iterative Jacobi-Davidson technique. Instead of approximating individual eigenvectors one by one, a block procedure would seek to approximate an invariant subspace spanned by the perturbed members of a selected fundamental family of modes. Investigation of alternative preconditioning techniques can also contribute to the reduction of computational time.

Throughout the dissertation, a direct Monte Carlo approach has been used to estimate the statistics of functions of random variables. As a potential step to improve computational efficiency, the most recent developments in spectral Galerkin based stochastic FEM methods can be investigated by capitalizing upon problem structure and exploring alternative basis functions. Examples of such functions include wavelets, which has been found to be more effective for problems involving non-linearities, discontinuities and sharp changes than the traditional spectral FEM approach.

5.2.3 Applications

The concept of intentional mistuning can be fully exploited with accurate and efficient reduced order modeling of geometrically mistuned bladed disks. As indicated in the literature, the nominal blade shape modifications can contribute significantly to the reduction of maximum magnitude and variability of forced response. However great majority of prior research considered small parameter variations. A more general multi-objective optimization tool can be implemented for parametric studies and probabilistic design space exploration.

The techniques developed in Chapters 2 and 3 of this dissertation or their variants could also provide a convenient means to assess the impact of blade geometric mistuning in a multidisciplinary aeroelastic analysis context.

Appendix A

Selected MATLAB Implementations

A.1 Implementation of the Jacobi-Davidson technique

```
function [Uout, Lout]=JDbldisk(T, Nblades, Fs, Fe, actblktol, MaxOuter_It, ...
    Available_Prec, Outer_Tol, No_blocks, N_Restarts, Inner_Tol, MaxInner_It)

%  JDbldisk computes an approximation of perturbed eigenmodes using a sparse
%  iterative preconditioned technique
%  Inputs
%  T             = data structure containing nominal matrices, perturbation
%                  terms and nominal eigenpairs
%  Nblades       = number of elementary sectors
%  Fs            = lowest frequency, Hz
%  Fe            = highest frequency, Hz
%  actblktol     = blocking tolerance (to avoid solving ill-conditioned
%                  system), Hz
%  MaxOuter_It   = maximum number of outer interations
%  Available_Prec = vector of available preconditioners (named by natural
%                  frequencies)
%  Outer_Tol     = outer iteration residual tolerance
%  No_blocks     = flag to turn off blocking in outer iterations
%           GMRES solver settings
%  N_Restarts    = number of restarts
%  Inner_Tol     = inner solver residual tolerance
%  MaxInner_It   = maximum number of inner iterations
%
%  Outputs
```

```
%
%  Uout             = perturbed eigenvectors
%  Lout             = perturbed eigenvalues

T.dK = (T.dK'+T.dK)*0.5;
T.dM = (T.dM'+T.dM)*0.5;

NDofs                = size(T.Phi,1);
nmodes               = size(T.Phi,2);
NSectorDOFs          = NDofs/Nblades;
Even                 = (mod(Nblades, 2) == 0);
MaxDia               = floor(Nblades/2);
Correction_Is_Over = 0;

% initialize residual vector
for gs=0:Nblades-1
  for nn=1:nmodes
    Resid(nn, gs+1) = norm(T.dK*T.Phi(rot(gs),nn)-T.Lambda(nn).*T.dM*T.Phi(rot(gs),
        nn));
  end
end

indxP       = zeros(nmodes);
indxIP      = zeros(nmodes);
indxrotall = zeros(nmodes);
poss        = zeros(nmodes);
mn          = zeros(nmodes);

% form index vector of eigenvectors to correct
k          = 1;
Singlet    = 0;
nsinglets = 0;
for nn=1:nmodes-1
   if( abs(T.Lambda(nn)- T.Lambda(nn+1)) < 0.01 && xor(Singlet,mod(nn,2)))
      Singlet           = ~Singlet;
      indxP(k)          = nn;
      indxIP(k)         = nn+1;
      indxrotall(nn)    = 0;
      k                 = k+1;
      nsinglets         = nsinglets + 1;
   else
     [mn(nn),      poss(nn)] = min(Resid(nn,:));
     [mn(nn+1), poss(nn+1)] = min(Resid(nn+1,:));
     if(mn(nn)< mn(nn+1))
      indxP(k)          = nn;
      indxIP(k)         = nn+1;
      indxrotall(nn)    = poss(nn)-1;
```

```
        indxrotall(nn+1) = poss(nn)-1;
        k = k+1;
       else
        indxP(k)         = nn+1;
        indxIP(k)        = nn;
        indxrotall(nn)   = poss(nn+1)-1;
        indxrotall(nn+1) = poss(nn+1)-1;
         k = k+1;
       end
    end
end

addit_vec = (nmodes - nsinglets)/2 + nsinglets;


% apply minimum residual spatial orientation to nominal eigenvectors
for nn=1:nmodes
 T.Phi(:,nn) = T.Phi(rot(indxrotall(nn)), nn);
end



A                = sparse(NDofs, NDofs);
Fo               = FourierReal(Nblades);
scaling_offset   = 0.0;
Xit              = zeros(NDofs,NinnerIt);
Rnorm            = zeros(addit_vec, 1);

%=========================================================
%==== First Outer Iteration (block correction)=========
%=========================================================
m = 1;
fprintf('%17s: %i\n','Outer Iteration',m)


% M-orthonormalize the projection vectors
Qp  =  T.Phi(:,indxP);
GQ =  Qp'*Qp;
GQ = (GQ' + GQ)*0.5;
[GQ, cholflag] = chol(GQ);
if cholflag == 0
 Qp = Qp/GQ;
else
 warning('MATLAB: JDbldisk', 'The set of normal modes is not full rank.')
end
Qm      = (T.M+T.dM)*Qp;
```

```
% compute current projected residual
r       = T.dK*T.Phi(:,indxP)-T.dM*T.Phi(:,indxP)*diag(T.Lambda(indxP));
r       = -r+Qm*(Qp'*r);

Comp33P = zeros(NDofs, nmodes);
scaling = zeros(nmodes);
dummy = 0;

for nn=1:addit_vec

      in = indxP(nn);
      LmbdA     = T.Lambda(in);

      % block-diagonal SPAI preconditioner in Fourier space
      tm1    = abs(LmbdA-Available_Prec(1));
      pos =1;
      for qq=2:size(Available_Prec)
          tm2 = abs(LmbdA-Available_Prec(qq));
          if(tm2 < tm1)
              pos =qq;
              tm1 = tm2;
          end
      end
      LmbdPrec = Available_Prec(pos);

      % load the preconditioner
      if(LmbdPrec ~= dummy)
         for harm = 1:MaxDia+1
            fname = strcat('Prec', '_', num2str(harm), '_', num2str(LmbdPrec), '.mat'
                );
            PREC(harm).P.P = load(fname);
         end
      end

      % starting guess
      Guess       = (T.Phi(:,indxIP(nn))-Qp*(Qm'*T.Phi(:,indxIP(nn))));
      xxx          = prec(r(:,nn));
      yyy          = prec(afun(Guess));
      scaling(nn) = (yyy'*xxx)/(yyy'*yyy);
      Guess        = scaling(nn)*Guess;


      [Comp33P(:,nn), flag1,relres1(1,nn),iter1,vec1]  =  gmres(@afun,r(:,nn),
          MaxInner_It,Inner_Tol, N_Restarts, @prec, [], Guess);
      resvec1(1,1:size(vec1),nn) = vec1;
```

```
      % make the correction M-orthogonal to the current subspace
      Comp33P(:,nn)      = Comp33P(:,nn)-Qp*(Qm'*Comp33P(:,nn));
      dummy = LmbdPrec;
      fprintf('%17s: %i\n','Inner Iteration',nn)
end

% Rayleigh-Ritz procedure
V = [T.Phi Comp33P];
V = ortha((T.M+T.dM), V);
W = (T.K+T.dK)*V;
H = V'*W;
H =(H+H')*0.5;
[Umam,Lmam]=eig(H);
Lout = diag(Lmam);
Freq=sqrt(Lout)/2./pi;
Uout=V*Umam;

% select Ritz pairs within the frequency band of interest [Fs,Fe]
pos1 =1;
ji   = size(V, 2);
for qq=1:ji
  if(Freq(qq) > Fs)
     pos1 = qq;
     break;
  end;
end;
pos2 = ji;
for qq=1:ji
  if(Freq(qq) > Fe)
    pos2 = qq-1;
    break;
  end;
end;

% Verify if any more outer iterations are needed, residual convergence test
FreqHist(1:pos2-pos1+1, 1) = Freq(pos1:pos2);
r = W*Umam(:,pos1:pos2) - (T.M+T.dM)*Uout(:,pos1:pos2)*diag(Lout(pos1:pos2));

conv       =   0;
keep       =   0;
convind    =  [];
keepind    =  [];
keepres    =  [];
tt         =   1;
normmin    = Inf;

for jj=pos1:pos2
```

```
  Nr(1,tt)        = norm(r(:,tt));
% perform selection for correction to solve for the next outer iteration
  if(Nr(1,tt) < Outer_Tol)
    conv            = conv+1;
    convind(conv)   = jj;
  else
    if(normmin >  Nr(1,tt))
        normmin = Nr(1,tt);
        Indin=jj;
        Indinr=tt;
    end;
    keep            = keep+1;
    keepind(keep)   = jj;
    keepres(keep)   = tt;
  end
  tt=tt+1;
end

ki       = 0;
LmamROM = zeros(nmodes, 1);
if(conv ~= 0)
  LmamROM(ki+1:ki+conv)        = Lout     (convind(1:conv));
  Q     (:,ki+1:ki+conv)       = Uout   (:,convind(1:conv));
 % keep all non-converged Ritz vectors in the test subspace
  V = [Uout(:,1:pos1-1) Uout(:,keepind(1:keep)) Uout(:,pos2+1:ji)];
  ki                           = ki + conv;
end

% print statistics
fprintf('Kept Ritz values \n')
sqrt(Lmam(keepind(1:keep)))/2/pi
fprintf('Their respective residual norms \n')
Nr(1,keepind(1:keep)-pos1+1)
fprintf('Converged Ritz values \n')
sqrt(Lmam(convind(1:conv)))/2/pi
fprintf('Currently selected for correction Ritz value \n')
sqrt(Lmam(Indin))/2/pi

%=================================================
%==== Outer Iteration Loop in case of non-convergence
%=================================================
for m=2:MaxOuter_It
   Comp33P = zeros(NDofs, nmodes);
   if(ki == nmodes)
       break;
   end
   % blocking for inner solutions to avoid solving ill-conditioned systems
```

```
  block = [];
  prev  =  1;
  for tt=1:keep-1
       IN(tt).block = [];
       block = [block keepind(tt)];
       if((Freq(keepind(tt+1))-Freq(keepind(tt))) < actblktol)
         continue;
       else
% initialize all previous
         for jj=prev:tt
           IN(jj).block = block;
         end
         prev  = tt+1;
         block = [];
       end
  end
  IN(keep).block = [];
  block = [block keepind(keep)];
  for jj=prev:keep
     IN(jj).block = block;
  end

  if(No_blocks)
    addit_vec                       = 1;
  else
    addit_vec                       = keep;
  end

  dummy = 0;
  avoid_reloading_preconditioner = 0;

  for nn=1:addit_vec

      if(No_blocks)
        in  = Indin;
        inr = Indinr;
      else
        in  = keepind(nn);
        inr = keepres(nn);
      end

      % M-orthonormalize the projection vectors
      Qp  =  [Q Uout(:,IN(nn).block)];
      GQ =  Qp'*Qp;
      GQ = (GQ' + GQ)*0.5;
      [GQ, cholflag] = chol(GQ);
      if cholflag == 0
```

```
        Qp = Qp/GQ;
    else
        warning('MATLAB:JDbldisk', 'The set of normal modes is not full rank.')
    end
    Qm    = (T.M+T.dM)*Qp;
    R     = -r(:,inr)+Qm*(Qp'*r(:,inr));


  % select nearest preconditioner
    tm1   = abs(Lmam(in)-Available_Prec(1));
    pos =1;
    for qq=2:size(Available_Prec)
      tm2 = abs(Lmam(in)-Available_Prec(qq));
      if(tm2 < tm1)
          pos =qq;
          tm1 = tm2;
      end
    end
    LmbdPrec = Available_Prec(pos);
    LmbdA    = Lmam(in);


  % block-diagonal SPAI preconditioner in cyclic domain based on tuned system
  if(LmbdPrec ~= dummy || avoid_reloading_preconditioner ~= LmbdPrec)
    avoid_reloading_preconditioner = LmbdPrec;
    for harm = 1:MaxDia+1
        fname = strcat('Prec', '_', num2str(harm), '_', num2str(LmbdPrec), '.mat'
            );
        PREC(harm).P.P = load(fname);
    end
  end

  % starting guess
  Guess = [];
  [Comp33P(:,nn), flag1,relres1(m,nn),iter1,vec1]  =  gmres(@afun,R,MaxInner_It,
      Inner_Tol, N_Restarts, @prec, [], Guess);
  % make the correction M-orthogonal to the current subspace
  resvec1(m,1:size(vec1),nn) = vec1;
  Comp33P(:,nn)     = Comp33P(:,nn)-Qp*(Qm'*Comp33P(:,nn));
  dummy = LmbdPrec;
  fprintf('%17s: %i\n','Inner Iteration',nn)
end

% make decision whether to expand or to correct the test subspace
if(keep == 1 || No_blocks)
 %   No_blocks = 1;
    V = [V Comp33P];
```

```
    else
        V(:,pos1:pos1+keep-1) =  V(:,pos1:pos1+keep-1) + Comp33P;
    end
    % orthonormalization relative to (T.M+T.dM)
    V = ortha((T.M+T.dM), V);
    W = (T.K+T.dK)*V;
    H = V'*W;
    H =(H+H')*0.5;
    [Umam,Lmam]=eig(H);
    Lout = diag(Lmam);
    Freq=sqrt(Lout)/2./pi;
    Uout=V*Umam;

% select Ritz vectors within frequency band of interest (i.e. closest to
% some target value tau)
    pos1 =1;
    ji    = size(V, 2);
    for qq=1:ji
      if(Freq(qq) > Fs)
          pos1 = qq;
          break;
      end;
    end;
    pos2 = ji;
    for qq=1:ji
      if(Freq(qq) > Fe)
          pos2 = qq-1;
          break;
      end;
    end;
% Compute the residuals

    FreqHist(1:pos2-pos1+1, m)    = Freq(pos1:pos2);
    r                             = W*Umam(:,pos1:pos2) - (T.M+T.dM)*Uout(:,pos1:pos2)
        *diag(Lout(pos1:pos2));

% test residuals for convergence
    conv      =    0;
    keep      =    0;
    convind   =   [];
    keepind   =   [];
    keepres   =   [];
    tt = 1;
    normmin = Inf;

    for jj=pos1:pos2
      Nr(m,tt)        = norm(r(:,tt));
```

```
% perform selection for correction to solve for the next outer iteration
      if(Nr(m,tt) < Outer_Tol)
        conv            = conv+1;
        convind(conv)   = jj;
      else
        if(normmin >  Nr(m,tt)) normmin = Nr(m,tt); Indin=jj; Indinr=tt; end;
        keep            = keep+1;
        keepind(keep)   = jj;
        keepres(keep)   = tt;
      end
      tt=tt+1;
    end

    if(conv ~= 0)
      LmamROM(ki+1:ki+conv)        = Lout   (convind(1:conv));
      Q     (:,ki+1:ki+conv)       = Uout(:,convind(1:conv));
   % keep all nonconverged Ritz vectors in the test subspace
      V = [Uout(:,1:pos1-1) Uout(:,keepind(1:keep)) Uout(:,pos2+1:ji)]; % start with
          smaller residuals
      ki                           = ki + conv;
    end


    fprintf('%17s: %i\n','Outer Iteration',m)
    fprintf('Kept Ritz values   \n')
    sqrt(Lout(keepind(1:keep)))/2/pi
    fprintf('Their respective residual norms   \n')
    Nr(m,keepind(1:keep)-pos1+1)
    fprintf('Converged Ritz values   \n')
    sqrt(Lout(convind(1:conv)))/2/pi
    fprintf('Currently selected for correction Ritz value   \n')
    sqrt(Lout(Indin))/2/pi

end

[Lout,pos]    = sort(LmamROM);
Uout          = Q(:,pos);


% spatial phase rotation of nominal eigenvectors
function y = rot(shift)
 y(shift*NSectorDOFs+1:NDofs) = 1:(Nblades-shift)*NSectorDOFs;
 y(1:shift*NSectorDOFs)       =   (Nblades-shift)*NSectorDOFs+1:NDofs;
end

% sparse matrix vector multiplication with M-orthonormalization
function y = afun(x, trans)
```

```
    tmp1 = A*x;
    y=tmp1-Qm*(Qp'*tmp1);
end

% DFT-SPAI Preconditioner
function y = prec(x, trans)

    Dummy = zeros(NDofs,size(x, 2));
    y     = zeros(NDofs,size(x, 2));

    i1 = 1;
    k  = 1;
    for i=1:Nblades
      i2=(NSectorDOFs)*(i-1)+1;
      i3=(NSectorDOFs)*i;
      for j=1:Nblades
         j1=(NSectorDOFs)*(j-1)+1;
         j2=(NSectorDOFs)*j;
         Dummy(i2:i3,:)= Dummy(i2:i3,:)+ Fo(j,i).*x(j1:j2,:);
      end
      % multiplication of first, every other and last blocks
      if(mod(i,2) || (i==Nblades && Even))
          Dummy(i1:i3,:) = PREC(k).P.P*Dummy(i1:i3,:);
          k = k + 1;
      end
      i1 = i2;
      if(i==Nblades && Even)
         i1 = i3 + 1;
      end
    end
   % inverse DFT transform
    for i=1:Nblades
      i1=(NSectorDOFs)*(i-1)+1;
      i2=(NSectorDOFs)*i;
         for j=1:Nblades
            j1=(NSectorDOFs)*(j-1)+1;
            j2=(NSectorDOFs)*j;
            y(i1:i2,:)= y(i1:i2,:)+ Fo(i,j).*Dummy(j1:j2,:);
         end
    end
    y = y - Qk*((Qk'*Qm)\(Qm'*y));
end

end
```

Bibliography

[1] D. Moens and D. Vanderpitte, "A survey of non-probabilistic uncertainty treatment in finite element analysis," *Computer Methods in Applied Mechanics and Engineering*, vol. 194, pp. 1527–1555, 2005.

[2] G. Stefanou, "The stochastic finite element method: past, present and future," *Computer Methods in Applied Mechanics and Engineering*, vol. 198, pp. 1031–1051, 2009.

[3] R. Ghanem and P. Spanos, *Stochastic finite elements: a spectral approach*. New York NY: Springer, 1991.

[4] F. Dohnal, B. Mace, and N. Ferguson, "Joint uncertainty propagation in linear structural dynamics using stochastic reduced basis methods," *AIAA Journal*, vol. 47(4), pp. 961–969, 2009.

[5] G. Schueller and H. Pradlwarter, "Uncertainty analysis of complex structural systems," *International Journal for Numerical Methods in Engineering*, vol. 80, pp. 881–913, 2009.

[6] B. de Lima and N. Ebecken, "A comparison of models for uncertainty analysis by the finite element method," *Finite Elements in Analysis and Design*, vol. 34, pp. 211–232, 2000.

[7] B. Mace and P. Shorter, "A local modal/perturbation method for estimating frequency response statistics of built-uo structures with uncertain properties," *Journal of Sound and Vibration*, vol. 242(5), pp. 793–811, 2001.

[8] B. Van den Nieuwenhof and J. Coyette, "Modal approaches for the stochastic finite element analysis of structures with material and geometric uncertainties," *Computer Methods in Applied Mechanics and Engineering*, vol. 192, pp. 3705–3729, 2003.

[9] G. Schueller, "Computational stochastic mechanics - recent advances," *Computers and Structures*, vol. 79, pp. 2225–2234, 2001.

[10] G. Schueller, "On the treatment of uncertainties in structural mechanics and analysis," *Computers and Structures*, vol. 85, pp. 235–243, 2007.

[11] L. Hinke, F. Dohnal, B. Mace, T. Waters, and N. Ferguson, "Component mode synthesis as a framework for uncertainty analysis," *Journal of Sound and Vibration*, vol. 324(1–2), pp. 161–178, 2009.

[12] A. Antoulas, D. Sorensen, and S. Gugercin, "A survey of model order reduction methods for large-scale systems," *Contemporary Mathematics*, vol. 280, pp. 193–219, 2001.

[13] Y. Halevi, "Projection properties of L_2 optimal reduced order model," *International Journal of Control*, vol. 79(4), pp. 298–310, 2006.

[14] W. Gawronski, *Advanced structural dynamics and active control of structures*. New York NY: Springer, 2004.

[15] Y. Chahlaoui, D. Lemonnier, A. Vandendorpe, and P. Van Dooren, "Second order balanced truncation," *Linear Algebra and its Applications*, vol. 415, pp. 373–384, 2006.

[16] Z.-Q. Qu, *Model order reduction techniques: with applications in finite element analysis*. London: Springer, 2004.

[17] D. Thomas, "Dynamics of rotationally periodic structures," *International Journal for Numerical Methods in Engineering*, vol. 14, pp. 81–102, 1979.

[18] A. Bunse-Gerstner, B. Salimbahrami, R. Grotmaack, and B. Lohmann, "Existence and computation of second order reduced systems using Krylov subspace methods," in *Proceedings of 16th Symp. on the Mathematical Theory of Networks and Systems*, (Katholieke Universiteit Leuven, Belgium), 2004.

[19] Y. Chahlaoui, D. Lemonnier, K. Meerbergen, A. Vandendorpe, and P. Van Dooren, "Model reduction of second order systems," in *Proceedings International Symposium Mathematical Theory of Networks and Systems*, (University of Notre Dame, Belgium), 2002.

[20] C. A. Beattie and S. Gugercin, "Krylov-based model reduction of second-order systems with proportional damping," in *Proc. 44th CDC/ECC*, (Seville, Spain), pp. 2278–2283, 2005.

[21] B. Salimbahrami and B. Lohmann, "Order reduction of large scale second order systems using Krylov subspace methods," *Linear Algebra and its Applications*, vol. 415(23), pp. 385–405, 2006.

[22] R. Eid, B. Salimbahrami, and B. Lohmann, "Parametric order reduction of proportionally damped second-order systems," *Journal of Sensors and Materials*, vol. 19(3), pp. 149–164, 2007.

[23] J. M. S. Silva, J. Villena, P. Flores, and L. Silveira, *Outstanding issues in model order reduction. Scientific computing in electrical engineering.* Berlin Heidelberg, Germany: Springer, 2007.

[24] G. Shi, B. Hu, and C. J. Shi, "On symbolic model order reduction," *IEEE Transactions on computer-aided design of integrated circuits and systems*, vol. 25(7), pp. 1257–1272, 2006.

[25] G. W. Allen and K. Maute, "Application of reduced order models for the stochastic design optimization of dynamic systems," in *10th AIAA/ISSMO Multidisciplinary Analysis and Optimization Conference*, (Albany, NY), 2004.

[26] G. Weickum, M. Eldred, and K. Maute, "Multi-point extended reduced order modeling for design optimization and uncertainty analysis," in *2nd AIAA Multidisciplinary Design Optimization Specialist Conference*, (Newport, RI), 2006.

[27] L. Daniel, O. Siong, L. Chay, L. K., and J. White, "Multiparameter moment matching model reduction approach for generating geometrically parameterized interconnect performance models," *IEEE Transactions on computer-aided design of integrated circuits and systems*, vol. 23(5), pp. 678–693, 2004.

[28] A. Leung and R. Khazaka, "Parametric model order reduction technique for design optimization," in *IEEE Proc. Intl. Symp. Circuits Syst.*, (Kobe, Japan), pp. 1290–1293, 2005.

[29] X. Li, L. Peng, and L. Pileggi, "Parameterized interconnect order reduction with explicit-and-implicit multi-parameter moment matching for inter/intra-die variations," in *IEEE International Conference on Computer Aided Design*, (San Jose, USA), pp. 806–812, 2005.

[30] B. Lohmann and R. Eid, "A new framework for order reduction of parametric models by superposition of locally reduced ones," in *Workshop on Model Reduction of Parametrized Systems*, (Munster, Germany), 2009.

[31] B. Lohmann and R. Eid, *Efficient order reduction of parametric and nonlinear models by superposition of locally reduced models*. Aachen: Shaker Verlag, 2009.

[32] D. Amsallem, J. Cortial, K. Carlberg, and C. Farhat, "A method for interpolating on manifolds structural dynamics reduced-order models," *International Journal for Numerical Methods in Engineering*, vol. 80(9), pp. 1241–1258, 2009.

[33] V. Ganine, M. Legrand, H. Michalska, and C. Pierre, "A reduction technique for mistuned bladed disks with superposition of large geometric mistuning and small model uncertainties," in *The 12-th International Symposium on Transport Phenomena and Dynamics of Rotating Machinery, paper 2008-20158*, (Honolulu, Hawaii, USA), 2008.

[34] V. Ganine, M. Legrand, H. Michalska, and C. Pierre, "A sparse preconditioned iterative method for vibration analysis of geometrically mistuned bladed disks," *Computers and Structures*, vol. 87, pp. 342–354, 2009.

[35] V. Ganine, H. Michalska, and C. Pierre, "Statistical quantification of the effects of blade geometry modification on mistuned disks vibration," *Journal of Computational and Nonlinear Dynamics*, Submitted.

[36] V. Ganine, D. Laxalde, H. Michalska, and C. Pierre, "Parameterized reduced order modeling of misaligned stacked disks rotor assemblies," *Journal of Sound and Vibration*, Submitted.

[37] S. Wei and C. Pierre, "Localization phenomena in mistuned assemblies with cyclic symmetry part 1: Free vibrations," *Journal of Vibration, Acoustics, Stress, and Reliability*, vol. 110, no. 4, pp. 429–438, 1988.

[38] S. Wei and C. Pierre, "Localization phenomena in mistuned assemblies with cyclic symmetry part 2: Forced vibrations," *Journal of Vibration, Acoustics, Stress, and Reliability*, vol. 110, no. 4, pp. 439–449, 1988.

[39] M. Castanier and C. Pierre, "Modeling and analysis of mistuned bladed disk vibration: Status and emerging directions," *Journal of Propulsion and Power*, vol. 22, no. 2, pp. 2285–2298, 2006.

[40] M. Castanier, G. Ottarsson, and C. Pierre, "A reduced-order modeling technique for mistuned bladed disks," *Journal of Vibration and Accustics*, vol. 119(3), pp. 439–447, 1997.

[41] M. Yang and J. Griffin, "A reduced order model of mistuning using a subset of nominal system modes," *ASME Journal of Engineering for Gas Turbines and Power*, vol. 123, pp. 893–900, 2001.

[42] R. Bladh, M. Castanier, and C. Pierre, "Component-mode-based reduced order modeling techniques for mistuned bladed disks - part 1: Theoretical models," *ASME Journal of Engineering for Gas Turbines and Power*, vol. 123, no. 1, pp. 89–99, 2001.

[43] R. Bladh, M. Castanier, and C. Pierre, "Component-mode-based reduced order modeling techniques for mistuned bladed disks - part 2: Applicaiton," *ASME Journal of Engineering for Gas Turbines and Power*, vol. 123, no. 1, pp. 100–108, 2001.

[44] D. Feiner and J. Griffin, "A fundamental model of mistuning for a single family of modes," *Journal of Turbomachinery*, vol. 124, pp. 597–605, 2002.

[45] R. Bladh, M. Castanier, C. Pierre, and M. Kruse, "Dynamic response predictions for a mistuned industrial turbomachinery rotor using reduced order modeling," *ASME Journal of Engineering for Gas Turbines and Power*, vol. 124, no. 2, pp. 311–324, 2002.

[46] S. Lim, R. Bladh, M. Castanier, and C. Pierre, "A compact, generalized component mode mistuning representation for modeling bladed disk vibration," *AIAA Journal*, vol. 45, no. 9, pp. 2285–2298, 2007.

[47] J. Brown, *Reduced Order Modeling Methods for Turbomachinery Design*. PhD thesis, Wright State University, 2008.

[48] D. Tran, "Component mode synthesis methods using partial interface modes: Application to tuned and mistuned structures with cyclic symmetry," *Computers and Structures*, vol. 87, pp. 1141–1153, 2009.

[49] A. Sinha, "Reduced-order model of a bladed rotor with geometric mistuning," *Journal of Turbomachinery*, vol. 131, pp. 031007–1–031007–7, 2009.

[50] E. Petrov, K. Sanliturk, and D. Ewins, "A new method for dynamic analysis of mistuned bladed disks based on the exact relationship between tuned and mistuned systems," *ASME Journal of Engineering for Gas Turbines and Power*, vol. 124, pp. 586–597, 2002.

[51] S. Lim, M. Castanier, and C. Pierre, "Vibration modeling of bladed disks subject to geometric mistuning and design changes," in *Proceedings of the 45-th AIAA/ASME/ASCE/AHS/ASC Structures, Structural Dynamics and Material Conference, paper 2004–1686*, (Palm Springs, California, USA), 2004.

[52] G. Sleijpen, A. Booten, and D. Fokkema, "Jacobi-Davidson type methods for generalized eigenproblems and polynomial eigenproblems," *BIT Numerical Mathematics*, vol. 36(3), pp. 595–633, 1996.

[53] A. Sameh and Z. Tong, "The trace minimization method for the symmetric generalized eigenvalue problem," *SIAM Journal of Computational and Applied Mathematics*, vol. 123, pp. 155–175, 2000.

[54] M. Akgun, "A new family of mode-superposition methods for response calculations," *Journal of Sound and Vibration*, vol. 167(2), pp. 289–302, 1993.

[55] A. Stathopoulos, "Nearly optimal preconditioned methods for hermitian eigenproblems under limited memory. Part I: Seeking one eigenvalue," *SIAM Journal on Scientific Computing*, vol. 29(2), pp. 481–514, 2007.

[56] J. Lombard, J. Dupeux, C. Dupont, F. Garcin, and S. Baumhauer, "Mistuning phenomena on bladed disk: Industrial methods and applications," in *Proceedings of ASME Turbo Expo 2006: Power for Land, Sea and Air, paper GT2006-90205*, (Barcelona, Spain), 2006.

[57] O. Bendiksen, "Localization phenomena in structural dynamics," *Chaos, Solutions and Fractals*, vol. 11(10), pp. 1621–1660, 2000.

[58] M. Kim, J. Moon, and J. Wickert, "Spatial modulation of repeated vibration modes in rotationally periodic structures," *ASME Journal of Vibration and Acoustics*, vol. 122, no. 1, pp. 62–68, 2000.

[59] D. Fokkema, L. Sleijpen, and H. Van der Vorst, "Jacobi-Davidson style QR and QZ algorithms for the reduction of matrix pencils," *SIAM Journal on Scientific Computing*, vol. 20(1), pp. 94–125, 1998.

[60] G. Stewart and J. Sun, *Matrux perturbation theory*. San Diego CA: Academic Press, 1990.

[61] T. Zhang, G. Golub, and K. Law, "Subspace iterative methods for eigenvalue problems," *Linear Algebra and its Applications*, vol. 294, pp. 239–258, 1999.

[62] M. Yang and J. Griffin, "A normalized modal eigenvalue approach for resolving modal interation," *ASME Journal of Engineering for Gas Turbines and Power*, vol. 119, pp. 647–650, 1997.

[63] G. Sleijpen, H. Van Der Vorst, and E. Meijerink, "Efficient expansion of subspaces in the Jacobi-Davidson methods for standard and generalized eigenproblems," *Electronic Transactions on Numerical Analysis*, vol. 7, pp. 75–89, 1998.

[64] C. Edmond and Y. Saad, "Experimental study of ILU preconditioners for indefinite matrices," *SIAM Journal of Computational and Applied Mathematics*, vol. 86, pp. 387–414, 1997.

[65] M. Grote and T. Huckle, "Parallel preconditioning with sparse approximate inverses," *SIAM Journal on Scientific Computing*, vol. 18, pp. 838–853, 1997.

[66] M. Castanier and C. Pierre, "Investigation of the combined effects of intentional and random mistuning on the forced response of bladed disks," in *Proceedings of 34th Joint AIAA/ASME/SAE/ASEE Propulsion Conference and Exhibit, paper AIAA-98-3720*, (Cleveland, OH, USA), 1998.

[67] M. Castanier and C. Pierre, "Using intentional mistuning in the design of turbomachinery rotors," *AIAA Journal*, vol. 40, no. 10, pp. 2077–2086, 2002.

[68] B. Choi, A. Lentz, A. Rivas-Guerra, and M. Mignolet, "Optimization of intentional mistuning patterns for the reduction of the forced response effects of unintentional mistuning: Formulation and assessment," *ASME Journal of Engineering for Gas Turbines and Power*, vol. 125, no. 1, pp. 442–454, 2003.

[69] J. Hou and C. Cross, "Minimizing blade dynamic response in a bladed disk through design optimization," *AIAA Journal*, vol. 43, no. 2, pp. 406–412, 2005.

[70] K. Jones, "Minimizing maximum modal force in mistuned bladed disk forced response," *Journal of Turbomachinery*, vol. 130, pp. 011011–1–011011–11, 2008.

[71] M. Nikolic, E. Petrov, and D. Ewins, "Robust strategies for forced response reduction of bladed disks on large mistuning concept," *ASME Journal of Engineering for Gas Turbines and Power*, vol. 130, pp. 022501.1–022501.11, 2008.

[72] G. Jacquet-Richardet, G. Ferraris, and P. Rieutord, "Frequencies and modes of rotating flexible bladed disc-shaft assemblies: a global cyclic symmetry approach," *Journal of Sound and Vibration*, vol. 191(5), pp. 901–915, 1996.

[73] H. Irretier, G. Jacquet-Richardet, and F. Reuter, "A three dimensional modeling of the dynamic behavior of composite rotors," *International Journal of Rotating Machinery*, vol. 5(4), pp. 263–271, 1999.

[74] G. Genta, *Dynamics of rotating systems*. New York NY: Springer, 2005.

[75] D. Combescure and A. Lazarus, "Refined finite element modeling for the vibration analysis of large rotating machines: Application to the gas turbine modular helium reactor power conversion unit," *Journal of Sound and Vibration*, vol. 318, pp. 1262–1280, 2002.

[76] R. Stephenson and K. Rouch, "Modeling rotaing shafts using axisymmetric solid finite elements with matrix reduction," *Journal of Vibration and Acoustics*, vol. 115, pp. 484–489, 1993.

[77] E. Chatelet, D. Lornage, and G. Jacquet-Richardet, "A three dimensional modeling of the dynamic behavior of composite rotors," *International Journal of Rotating Machinery*, vol. 8(3), pp. 185–192, 2002.

[78] J. Sawicki and W. Gawronski, "Balanced model reduction and control of rotor-bearing systems," *Journal of Engineering for Gas Turbines and Power*, vol. 119, pp. 456–463, 1997.

[79] M. Friswell and D. Inman, "Reduced-order models of structures with viscoelastic components," *AIAA Journal*, vol. 37(10), pp. 1318–1325, 1999.

[80] Y. Khulief and M. Mohiuddin, "On the dynamic analysis of rotors using modal reduction," *Finite Elements in Analysis and Design*, vol. 26(1), pp. 41–55, 1997.

[81] D. Kammer, "Test-analysis-model development using exact model reduction," *The International Journal of Analytical and Experimental Modal Analysis*, vol. 2(4), pp. 174–179, 1987.

[82] M. Friswell, J. Penny, and S. Garvey, "Model reduction for structures with damping and gyroscopic effects," in *Proceedings of ISMA-25*, (Leuven, Belgium), September 2000.

[83] A. Das and J. Dat, "Reduced model of a rotor-shaft system using modified serep," *Mechanics Research Communications*, vol. 35, pp. 398–407, 2008.

[84] S. Edwards, A. Lees, and M. Friswell, "Experimental identification of excitation and support parameters of a flexible rotor-bearing-foundation system from a single run-down," *Journal of Sound and Vibration*, vol. 235(5), pp. 963–992, 2000.

[85] R. Markert, R. Platz, and M. Seidler, "Model based fault identification in rotor systems by least squares fitting," *International Journal of Rotating Machinery*, vol. 7(5), pp. 311–321, 2001.

[86] N. Bachschmid, P. Pennacchi, and A. Vania, "Identification of multiple faults in rotor systems," *Journal of Sound and Vibration*, vol. 254(2), pp. 327–366, 2000.

[87] J. Sinha, A. Lees, and M. Friswell, "Estimating unbalance and misalignment of a flexible rotorating machine from a single run-down," *Journal of Sound and Vibration*, vol. 272(3-5), pp. 967–989, 2004.

[88] P. Pennacchi, N. Bachschmid, A. Vania, G. Zanetta, and L. Gregori, "Use of modal representation for the supporting structure in model-based fault identification of large rotating machinery," *Mechanical Systems and Signal Processing*, vol. 20, pp. 662–681, 2006.

[89] D. Laxalde, J. Lombard, and F. Thouverez, "Dynamics of multi-stage bladed disks systems," *Journal of Engineering for Gas Turbines and Power*, vol. 129(4), pp. 1058–1064, 2007.

[90] J. Shortle and M. Mendel, "Predicting dynamic imbalance in rotors," *Probabilistic Engineering Mechanics*, vol. 11, pp. 31–35, 1996.

[91] L. G. Maqueda, O. Bauchau, and A. Shabana, "Effect of centrifugal forces on the finite element eigenvalue solution of a rotating blade: a comparative study," *Multibody System Dynamics*, vol. 19, pp. 281–302, 2008.

[92] D. Sundararajan, *The discrete Fourier transform. Theory, algorithms and applications*. Singapore: World Scientific, 2001.